Characterization of erythrocyte-derived extracellular vesicles produced during *Plasmodium falciparum in vitro* infection and identification of variations engendered by current analytical tools

KUCYKOWICZ, Stephanie

Parasitology

McGill University, Montreal

December 2018

A thesis submitted to McGill University in partial fulfillment of the requirement of the degree of Master's of Science

Table of contents

Acknowledgments

I would like to thank Dr. Petra Rohrbach for giving me the chance to work on this exciting project and for her mentorship and guidance all throughout my Master's degree. The work presented here was supported by grants from NSERC. I would also like to thank my advisory committee member, Dr. Elias Georges, for his insightful advice, feedback and guidance. I also appreciate all the support and help from all the present and past members of the Rohrbach laboratory. I am very grateful for our collaboration with Dr. Neta Regev-Rudzki's laboratory at the Weizmann Institute of Science (Rehovot, Israel). The help from all the members of her laboratory, particularly by Anna Rivkin, was instrumental in helping launch this new project in our laboratory, mainly in establishing the EV isolation method and in permitting me to familiarize myself with this new field. I am also very thankful for being granted the Graduate Mobility Award by McGill's Macdonald campus that supported my two-month stay at the Weizmann Institute. I thank Youssef Chebli for providing essential technical support for the SEM analysis and sample preparation. I thank Dr. Darwin Lyew and Yvan Gariepy from the Bioresource Engineering department at McGill and Dr. Nanci's laboratory from Université de Montreal for their help with the higher magnification SEM as well. I also appreciate all the companies that set extended demos that permitted us to test multiple instruments and obtain comparative results, namely ParticleMetrix and Malvern for NTA demos and Beckman Coulter for the CytoFLEX demo. I acknowledge the work executed by the proteomics platform from the "Centre de recherche du CHU du Québec" for the proteomic analysis of my EV samples. I thank the MR4 for providing us with a great variety of *P. falciparum*-specific antibodies used for immunoblotting. I also appreciate all the help from Dr. Nina Simon and thank her for sharing valuable advice and many protocols specific to *P. falciparum* work. Lastly, I would like to highlight the support from everyone, students and professors alike, at the Institute of Parasitology and thank them for creating a welcoming workplace. I would like to single out Fadi Baakdah's help for answering all my questions and fostering thoughtful conversations with me.

Contribution of authors

All parts of this manuscript were written by Stephanie Kucykowicz. Revisions and corrections were provided by supervisor Dr. Petra Rohrbach.

All experiments presented in this manuscript were performed by Stephanie Kucykowicz with the exception of some Western blots that were carried out by undergraduate student Jennifer Huxham (presented in Figure 7 of the manuscript). All the protocols used were designed and established in Dr. Rohrbach's laboratory.

List of abbreviations

ATM	atomic force microscopy
Cryo-EM	electron cryomicroscopy
DPBS	Dulbecco's phosphate-buffered saline
ELVs	exosome-like vesicles
EVs	extracellular vesicles
FACS	fluorescence activated cell sorting
LC-MS/MS	liquid chromatography-tandem mass spectrometry
MPs	microparticles
miRNA	microRNA
mRNA	messenger RNA
NTA	nanoparticle tracking analysis
PBS	phosphate-buffered saline
PfEMP1	*Plasmodium falciparum* erythrocyte membrane protein 1
PfPTP2	PfEMP1 trafficking protein 2
RBCs	red blood cells
uRBCs	uninfected RBCs
uRBC-EV	EVs collected from an uninfected red blood cell culture
iRBCs	*Plasmodium falciparum* infected RBCs
iRBC-EV	EVs collected from a *P. falciparum*-infected red blood cell culture
RESA	ring-infected erythrocyte surface antigen

RMVs	RBC-derived microvesicles
SBP1	skeleton binding protein 1
SDS-PAGE	sodium dodecyl sulfate polyacrylamide gel electrophoresis
SEM	scanning electron microscopy
STEVOR	subtelomeric variable open reading frame
STING	stimulator of interferon genes
TBS	tris-buffered saline
TBSM	tris-buffered saline with 0.5% milk
TBSM-Tween	TBSM with 0.05% Tween
TCA	tricarboxcyclic acid cycle
TEM	transmission electron microscopy
TNF	tumor necrosis factor
TRBP	TAR RNA binding protein

List of figures

List of tables

Abstract

The complexity of the infection mechanisms developed by *P. falciparum* restricts our current progress of eradication strategies. The erythrocyte-bound parasites maintain cell to cell communication through the release and uptake of extracellular vesicles (EVs). As central to the pathogenesis of several diseases, this cooperative behaviour has been associated with modulation of gametocytogenesis and of the host's immune response during malaria infections. A lack of consistency in the literature led us to further characterize EVs secreted during *P. falciparum in vitro* infections using various standard analytical techniques. The isolation of EVs was achieved through sequential differential centrifugation and filtration of consumed media collected from 3D7-infectected and uninfected red blood cell (RBC) cultures. Nanoparticle tracking analysis (NTA), and scanning electron microscopy (SEM) analysis identified the release of a heterogenous EV population averaging 100-130nm from iRBCs and uRBCs, with a slightly smaller size average from iRBCs. Particle size and concentration were found to be affected by the parasite's life stage at the time of release and by the sample's storage conditions. Moreover, iRBC-EVs and uRBC-EVs were perceived as structurally similar, spherical lipid-rich particles which allowed labelling of the EVs with lipophilic dyes, DiO and SP-DiO, and visualization by fluorescent NTA. Fluorescent labelling for RBC-specific marker band 3 allowed RBC-EV identification by fluorescent NTA and fluorescence triggered flow cytometry, although low labelling efficiency was measured. In addition, spectrin, another host cell-derived marker, was found to be carried by all RBC-EVs, while the presence of a few parasite-specific markers such as plasmepsin II and HAP was also identified uniquely in iRBC-EVs by Western blotting. More in-depth proteomic profiling highlighted poor sample purification levels, identifying albumin as the major contaminant. Adequate purification levels were achieved by means of a density-based assay using sucrose gradient centrifugation. Taken together, we are beginning to better understand the unique features of *P. falciparum*-derived EVs. These experiments highlight the need for the establishment of novel technologies and the combinatorial use of current strategies for the analysis of downstream roles of EVs as potential therapeutic strategies.

Résumé

La complexité des mécanismes d'infection développés par *P. falciparum* restreint le progrès actuel des stratégies d'éradication. Les parasites qui résident dans les érythrocytes maintiennent une forme de communication de cellule à cellule par la décharge et l'assimilation de vésicules extracellulaires (VEs). Tel qu'essentiel dans la pathogénie de plusieurs maladies, ce comportement coopératif a été associé avec la modulation de la gamétocytogénèse et la modulation de la réponse immunitaire de l'hôte pendant des infections palustres. Cependant, le manque d'un consensus scientifique à cet égard nous a menés à caractériser davantage les VEs sécrétées pendant une infection *in vitro* avec *P. falciparum* en utilisant diverses techniques analytiques considérées standards. L'isolement des VEs a été accompli au moyen de centrifugations séquentielles et différentielles et de filtrations du milieu de culture de globules rouges infectés ou non par la souche 3D7 de *P. falciparum* après son usage en culture. Une analyse du suivi individuel de particules (NTA) par NanoSight et ZetaView, ainsi qu'une analyse par microscopie électronique à balayage (SEM) ont révélé la décharge d'une population de VEs hétérogène d'une taille moyenne de 100-130nm à partir des cultures non infectées et infectées. Ces dernières démontrent par ailleurs une taille moyenne légèrement plus petite. La taille et concentration des particules ont été affectées par le stade de vie du parasite au moment de la production des VEs et par les conditions de conservation des échantillons. En outre, des particules riches en lipides avec des structures similaires et sphériques ont été observées pour les VEs des cultures infectées et non infectées ce qui a permis le marquage des VEs avec des colorants lipophiles, DiO et SP-DiO, et leur visualisation au moyen du mode fluorescent du NTA. Le marquage fluorescent utilisant « band 3 », un marqueur spécifique aux globules rouges, a permis l'identification des VEs produites par les globules rouges par le biais de NTA en mode fluorescent et de la cytométrie en flux avec un déclencheur fluorescent malgré la faible efficacité du marquage. De plus, la spectrine, un autre marqueur dérivé des globules rouges, a été vue être transportée par tous les VEs produites par les globules rouges que nous avons étudiées. À contrario, la présence de quelques marqueurs spécifiques au parasite telles que la plasmepsine II et la protéase histoaspartique ont été identifiées par immunobuvardage de type Western uniquement dans les VEs provenant des globules rouges infectés. Un profilage protéomique plus détaillé a souligné le faible niveau de purification atteint et a identifié l'albumine comme contaminant principal. Des niveaux adéquats de purification ont

été atteints via un essai à base de densité utilisant un gradient de sucrose durant la centrifugation. Collectivement, nous avons seulement commencé à comprendre les caractéristiques uniques aux VEs produites par les globules rouges infectés par *P. falciparum*. Ces expériences soulignent le besoin d'établir des nouvelles technologies et de combiner les stratégies actuelles pour l'analyse des rôles ultérieurs des VEs comme potentielles stratégies thérapeutiques.

1. Introduction

1.1. Malaria: a well-adapted killer

Despite countless global initiatives, malaria still threatens the life of almost half the world's population. The parasitic disease caused by an infection with a *Plasmodium* parasite led to 445,000 deaths in 2016 alone (1). The highest proportion of these cases are concentrated in Sub-Saharan Africa and continue to have a great impact on the socioeconomic situation of the affected countries (1). The parasite is transmitted to humans by infected female mosquitoes belonging to the *Anopheles* genus, *Plasmodium*'s definitive host, which currently maintain continuous transmission in 91 countries (1).

Plasmodium parasites belong to the *Apicomplexa* phylum, attributable to the presence of three organelles on their apical end: rhoptries, micronemes and dense granules (1). Five species of the *Plasmodium* parasite are responsible for causing clinical disease in humans: *P. vivax*, *P. falciparum*, *P. ovale*, *P. malariae* and *P. knowlesi*, although much rarer for the latter, which was not originally discovered in humans (1, 2). Following inoculation with the sporozoites that developed in the salivary glands of infected mosquitoes, all *Plasmodium* species initially infect liver cells of the human host, as detailed in the parasite's life cycle in figure 1 (2, 3). Once mature, they release merozoites into circulation that are free to infect red blood cells (RBCs), establishing the erythrocytic replication cycle of the parasite. During this asexual replication cycle, the parasite will move through the ring, trophozoite and schizont stages. The latter will eventually undergo segmentation followed by rupture to release merozoites that will invade new RBCs. Some merozoites will develop into gametocytes following RBC invasion. This is the sexual stage of the parasite that will undergo the sexual replication cycle in the mosquito vector following uptake during a blood meal.

P. vivax and *P. falciparum* can cause life-threatening malaria, despite their infection mechanisms differing in many ways (2). *P. vivax* has a restrictive invasion strategy as it solely targets Duffy positive reticulocytes to establish its asexual replication cycle (2). Infections with *P. vivax* and also *P. ovale* can remain quiescent once in the liver and can cause later relapses following new RBC invasions (2). *P. falciparum* infection prevails as the deadliest as it invades most RBCs in circulation and subsequently prompts the modification of its host cell, allowing its own proliferation. The RBC's membrane is altered by the addition of the parasite-derived *Plasmodium*

falciparum-erythrocyte-membrane-protein-1 (PfEMP1), considered the parasite's primary virulence factor (4). Its protrusion from the host cell's membrane permits *P. falciparum* to avoid splenic clearance, the process used to filter out aged RBCs, by adhering to the host's vascular endothelium (4). PfEMP1 also allows the parasite to evade the host's immune system through antigenic variation of the *var* genes encoding for PfEMP1 (4-7). Therefore, this *P. falciparum* specific RBC modification allows it to establish a successful infection in humans. Moreover, PfEMP1 is responsible for many of the complications seen during *P. falciparum* infections such as anemia and cerebral malaria to name a few.

Onset of symptoms is observed once the intra-erythrocytic proliferation cycle is successfully established (2). Diagnosis of malaria is challenging, as the disease presents itself as a febrile episode with other non-specific symptoms, including headaches, chills and vomiting, occurring at least 7 days following infection (1, 2). Therefore, early infections can remain unnoticed or cannot be initially associated with malaria, which delays drug treatment. Severe illness and death can ensue in a short period of time if left untreated. At-risk groups, namely children under the age of 5, pregnant women, and immunocompromised patients (e.g. HIV positive patients), can develop life-threatening symptoms such as severe anemia, respiratory distress or cerebral malaria, particularly following *P. falciparum* infection (1). Treatment relies on antimalarial drugs, artemisinin-based combination therapy (ACT) being the current first-line treatment following the rise in chloroquine resistance (1). ACT combines artemisinin or a derivative, a fast acting and efficient drug, with another drug that has a longer half-life. The most efficient combinations being used are: artesunate-mefloquine, artemether-lumefantrine, dihydroartemisinin-piperaquine, artesunate-sulfadoxine-pyrimethamine and artesunate-amodiaquine (8). However, resistance towards all available drugs is on the rise and constitutes a real challenge (1, 2).

Malaria prevention currently focuses on vector control by means of long-lasting insecticide-treated bed nets (LLINs) and indoor residual spraying (IRS) (1, 2). Despite their positive impact, insufficient knowledge on the correct use of these techniques leads to inefficient use of vector control methods (9). However, to drive control to the point of disease elimination, vector control alone will not suffice. Although the expansion of control activities and more accessible prevention methods led to a 21% decrease in malaria incidence and a 29% decrease in mortality between 2010 and 2015, malaria remains one of the top 3 killers worldwide (1). Unfortunately, the development

of efficient vaccines against malaria is still lagging. It is restricted by our limited knowledge of *P. falciparum*'s complex life cycle, of its overall biology and of the host's protective immune responses against the parasite (10-12). By clarifying the mechanisms that modulate the progression of the parasite's life cycle, it will be possible to discover and further develop new ways to block disease progression and transmission.

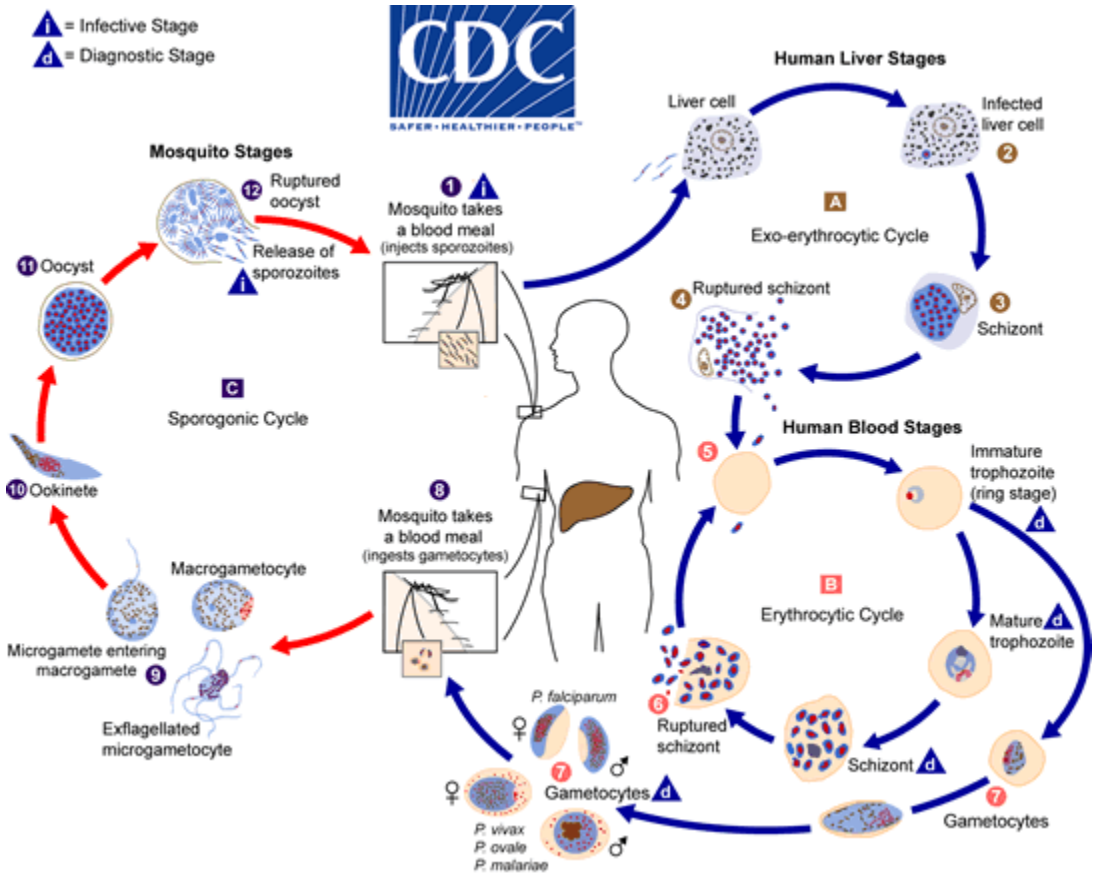

Figure 1. *Plasmodium* parasite life cycle. Detailed diagram of the progression of the malaria parasite's asexual (#1-8) and sexual i.e. sporogonic (#8-12) replication cycles within its two hosts: humans and *Anopheles spp.* mosquitoes respectively. In humans, the parasite undergoes a first round of replication in liver cells known as the exo-erythrocytic cycle (A) and then establishes the erythrocytic cycle within the red blood cells in circulation (B). (3)

1.2. Previously uncharacterized diffusible molecules stimulate malaria transmission

Mechanisms triggering sexual commitment of the intra-erythrocytic *Plasmodium* have been sparking interest due to its importance in perpetuating malaria transmission but are still, to this

day, poorly characterized. Predominantly, causal links between gametocytogenesis and factors such as the host's immune status, lymphocyte production or parasitemia, were initially hypothesized on the basis of simple observations (13, 14). Stress inducing factors have since been repeatedly associated with gametocytogenesis induction, promoting the hypothesis that the parasite's sexual commitment results from the stimulation of survival mechanisms when faced with unfavorable growth environments (15). Certain stressful conditions have been gradually found to enhance the conversion to sexual forms and are currently used in combination in gametocytogenesis protocols (16, 17). These include introducing chloroquine in culture media (18), reducing the hematocrit levels (19), increasing the percentage of reticulocytes in blood (20), or the addition of hemolysis products to the parasite culture (21). In some cases, it was noted that the specific factors studied cannot alone drive sexual differentiation; Schneweis *et al.* clearly acknowledge the role of another unknown factor in triggering this process (21), supporting the belief that several processes are needed *simultaneously* to induce gametocytogenesis (22). More recently, the focus has shifted towards the identification of specific genes and on the understanding of gene modulation mechanisms implicated in the transition to sexual forms, yielding some interesting results such as the discovery of the "sexual development cluster" found through transcriptomic studies (23-26). The expression pattern of approximately 246 genes was specifically associated with gametocyte production (24). Genes ranging from TCA cycle enzymes, proteases, and hypothetical genes were identified and have the potential to become targets of antimalarial drugs that aim to block transmission of the parasite. Overall, the slow turn-over of *in vitro* studies of sexual differentiation can be explained by restrictions such as the overall low percentage of sexually committed parasites produced in culture and the parasite's predisposition to lower its gametocyte production as its time in culture increases (27, 28).

Some early experiments that looked at understanding the rate of gametocyte production proposed that changes in environmental factors in culture are responsible for fluctuations in the production of the transmission stages of the parasite (13). It was observed that gametocytogenesis decreased when different *P. falciparum* cultures were subcultured *in vitro* in fresh RBCs but that gametocyte production rose after a few days of continuous culture. The authors suggest that some unidentified environmental factors repress gametocyte production when the parasite is diluted in a new culture but after a few days promote gametocytogenesis. In agreement with these conclusions, sexual

commitment was shown to be triggered when *P. falciparum* was cultured in parasite-conditioned media, i.e. in used media that has been recovered from a culture in which the parasite was previously grown (29). Being essentially depleted media, culture supernatant was collected from the same flask for 5-6 days, centrifuged and filtered to eliminate any RBCs or small debris that could remain in the culture media. A greater number of gametocytes were produced when conditioned media was introduced in *P. falciparum* infected erythrocyte monolayers than when the parasite was grown in fresh culture media. Thus, it was confirmed that one or multiple soluble factors found in the culture media are modifying the parasite's environment in such a manner as to induce gametocytogenesis *in vitro*. Further evidence was provided by Dyer and Day following the study of malaria parasite's asexual replication using a co-culture system that allows diffusion of small molecules through semi-permeable membranes (30). They determined that sexual differentiation is repressed by means of diffusible molecules contained in culture media when growth conditions are optimal. However, they showed that sexual development is restored when asexual growth is being compromised, for example when maximum parasitemia is reached, i.e. when the maximum amount of parasites present in RBCs is reached (30). Furthermore, they suggest that the transition from the asexual to the sexual stages is achieved through a parasite density-dependent mechanism. A test parasite, a strain known as 3D7, was co-cultured with varying concentrations of another 3D7 parasite culture, ranging from 0 to 2%, to study the impact of the presence of an asexually replicating parasite on the growth of the test culture. It is ultimately shown that the presence of greater amounts of asexually replicating parasites will inhibit the development of sexual stages through the release of diffusible molecules. Currently, these findings are being successfully applied in protocols to increase *in vitro* production of gametocytes (31). Indeed, the use of parasite-conditioned media is used in combination with other methodologies to trigger gametocytogeneis. Nonetheless, the origin, nature or mode of action of these diffusible factors found in culture media remained unknown. It is essential to understand the molecular mechanism(s) implicated in the decision to trigger gametocytogenesis during malaria infection. The key to comprehending sexual commitment is thought to lie, at least partially, in these poorly characterized diffusible factors. There is a need to elucidate the specific roles of these molecules.

1.3. Diffusible vesicles play a role in disease progression during malaria infection

Similar small soluble factors that induce gametocyte production during *P. falciparum* infection have been alternatively described to stimulate specific responses from their host cells in other infection models. For example, factors identified as microparticles (MPs) and isolated from *P. berghei* infected mice (species infecting only mice and used for *in vivo* models) were shown to have the ability to prompt innate inflammatory responses. Indeed, they have been observed to induce pro-inflammatory responses from macrophages *in vitro* such as CD40 upregulation and induce increased cytokine expression (TNF), confirming their role in the development of pathogenesis (32). It was successfully shown that MPs derived from infected RBCs (iRBCs) also possess the ability to induce a similar pro-inflammatory response from macrophages: CD40 upregulation and TNF expression (32). Importantly, it was also noted that these identified MPs differ from previously characterized inflammation-induced MPs since these MPs were not released when an inflammation environment was induced in mice. It can thus be concluded that these vesicles released during various infections, notably malaria infection, are immunomodulatory within the host and not induced by inflammation. Moreover, small vesicles identified as exosomes that were purified from mice infected with *P. yoelii* 17X, a model for *P. vivax* infection in mice, were found to carry malaria antigens and were thought to have immunomodulatory properties as well (33). Indeed, this paper suggests that these exosomes induce an IgG driven humoral response when reintroduced in mice. Thus, there seems to be multiple vesicle subtypes that get released in *in vivo* malaria models that can modulate the host's immune response.

The relevance of *in vitro* and *in vivo* findings was confirmed in patients suffering from malaria, since their blood concentrations of RBC-derived MPs increased in comparison to healthy individuals (34). This can be explained by the increased production of MPs by *infected* RBCs, which were discriminated from *uninfected* RBC-derived MPs by the presence of RESA (ring-infected erythrocyte surface antigen) that is solely on the membrane of iRBC-derived MPs. Interestingly, a correlation between the severity of symptoms and the blood levels of RBC-derived MPs has been repeatedly observed (34). Indeed, a greater number of RBC-derived MPs was detected in patients infected by the deadly *P. falciparum* species than in patients with milder *P. vivax* and *P. malariae* infections. When comparing severe with uncomplicated *P. falciparum*, a greater MP release was detected during more severe infections. Therefore, there seems to exist a

relationship between MP release and disease severity. Moreover, the administration of antimalarials to infected patients resulted in decreased MP blood levels regardless of the *Plasmodium* species causing the infection (34).

Although the severity of *Plasmodium* infections has been related to plasma-derived MP concentrations, circulating platelet-derived MPs also impact disease outcome in an important manner (35-37). Persistence of symptoms during *P. vivax* infections and increased RBC cytoadherence in brain tissues during *P. falciparum* infections, leading to cerebral malaria, are linked to platelet-derived MP blood concentrations. Similarly, in mouse models, an impaired ability to produce platelet-derived MPs or even macrophage-derived vesicles, in turn leads to protection from cerebral malaria complications (38). Indeed, there is a lessened upregulation of adhesion molecules within the brain vasculature and thus a reduced sequestration of cells in this tissue when the activity of the ATP-binding cassette transporter 1 gene is undermined (38). In other words, when the regulation of membrane composition is altered, MP production is weakened, leading to a heightened protection against cerebral malaria.

This demonstrates that diverse subtypes of host cell-derived vesicles are contributing to the development of disease by regulating the host's immune response and by regulating sexual commitment. This emphasizes the need to elucidate their biological significance, their biogenesis and characterize their contents to understand their mechanisms of action.

1.4. Extracellular vesicles: a universal vehicle for cell-cell communication

Initially viewed as cellular excretory by-products, technological advances have permitted further understanding of the biological relevance of the different components of the cell's secretome (39). Extracellular vesicles are membrane-enclosed vesicles secreted by most cell types, from prokaryotes to eukaryotes. They have also been isolated from many biological fluids and were observed to have multiple physiological functions, ranging initially from reticulocyte maturation and later expanded to antigen presentation, coagulation, immunomodulation, and signaling, to name a few (40). Their secretion and their role are in part determined by the specific micro-environments and the cell type from which they originate (Figure 1) (41-43). This has complicated the association of each EV subtype with specific characteristic functions. As their membrane

composition, surface markers, and contents are quite heterogenous, the two main subtypes of EVs are differentiated mainly by size and biogenesis (41). There is overlap in composition between the two main subtypes of EVs, as they both have the ability to carry proteins, RNA, microRNAs (miRNAs), DNA and lipids, and both display membranes enriched in cholesterol and sphingomyelin (41). Interestingly, all EV phospholipid bilayer membranes also display higher resistance to environmental changes and enzymatic activity, making them safe compartments to store information. Exosomes are secreted when multivesicular bodies fuse with the plasma membrane, thus, are of endocytic origin and range between 30-100nm (Figure 2) (41). Microvesicles, also known as microparticles or ectosomes, simply bud off the plasma membrane and are 100-1000nm in size (Figure 2) (41). Despite these differences, the isolates from different experiments display unwanted heterogeneity. The latter is explained by the lack of good isolation methods and characterization techniques, mostly limited by their detection thresholds that cannot cover the entire size range of EVs (44). Nonetheless, a number of markers have been associated

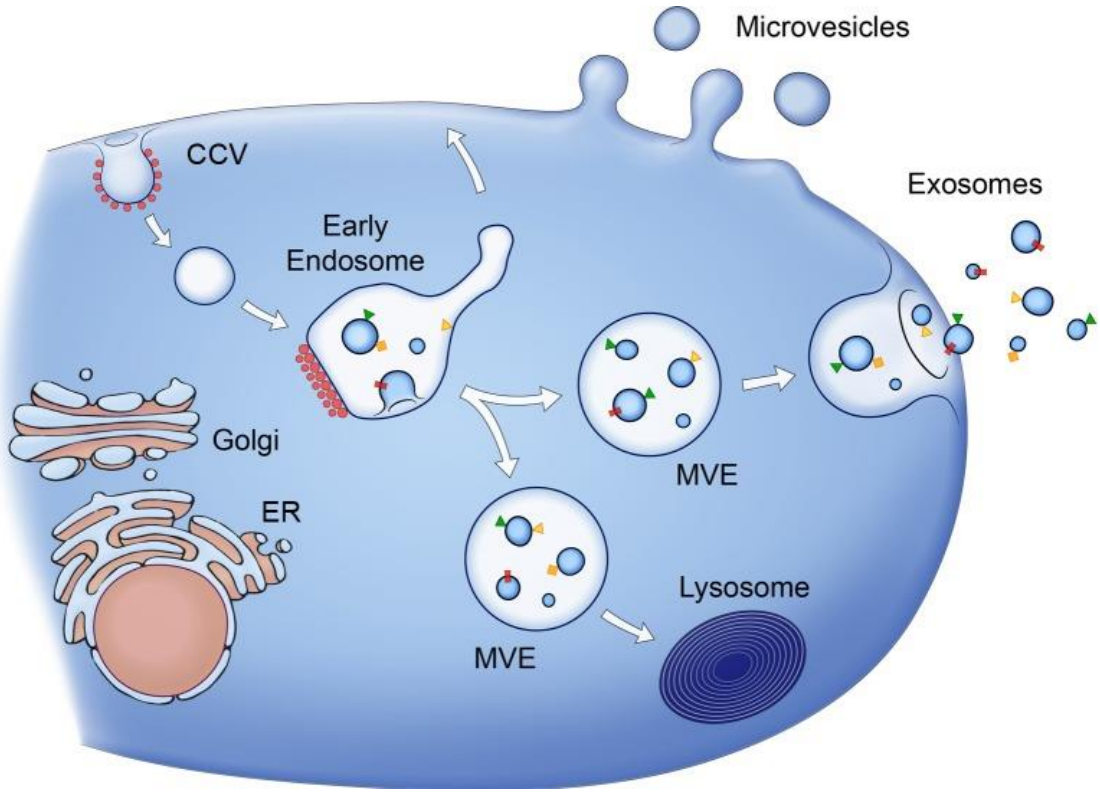

Figure 2. Biogenesis of EV subtypes. The two main subtypes of EVs (microvesicles and exosomes) are currently differentiated by size and biogenesis, as depicted above. MVE: multivesicular endosome, CCV: Clathrin-coated vesicle. Figure modified from original source (136).

with exosomal membranes, such as CD63, ceramide, and various Rab proteins involved in endosome trafficking and recycling (e.g. Rab11, Rab27, Rb35) (41). However, since secretion mechanisms are dynamic, these markers are not universal to all exosomes. Despite the lack of characterization of these messengers, there is overwhelming evidence that EVs play an important role in cell-to-cell communication and can modulate the recipient cell's behaviour (45, 46). Elucidating the specific processes of EV-mediated communication during homeostasis and improving the techniques that allow the study the role of EVs will allow us to find ways to manipulate them in the context of disease (47).

The ability of EVs to relay information can also be detrimental to the host (41). EVs have been described to contribute to the pathogenesis of many diseases, such as many types of cancer and viral infections (41, 48). For instance, EVs are strategically manipulated by Epstein-Barr virus to downregulate cytokine expression in their target cells, the uninfected dendritic cells, by means of viral miRNA delivery (49). Furthermore, MPs allow the transfer of information between cancerous cells, leading to the propagation of multidrug resistance in the population and worse prognosis (50). Hence, understanding the mechanisms of secretion and uptake (dependent on ligand-receptor interactions) of these EVs has the potential to yield new drug targets to fight diseases as well as to elucidate new disease biomarkers (10-12). Furthermore, intercellular communication by means of EVs has not only be described in the context of cancer and viral infections but also during parasitic infections.

1.5. EVs and homeostasis: Human red blood cells release extracellular vesicles under various physiological conditions

At stable physiological state, a basal level of vesicles is found in the human blood. Different types of cells contribute to the varying origin of these vesicles: platelets, RBCs, leukocytes and endothelial cells continuously release these microparticles into the extracellular milieu (51). Indeed, they are necessary for the modulation of different processes required for maintenance of homeostasis such as angiogenesis, cell differentiation, immunomodulation, senescence and as a response to stressful changes in the environment (51, 52).

RBCs contribute the largest amount of EVs in blood. These cells specialize in oxygen and carbon dioxide transport through tissues owing to their hemoglobin content. In turn, this results in a lack of a nucleus, loss of the capacity to conduct *de novo* protein synthesis and restricts their repair mechanisms (53). Nonetheless, despite their enucleate nature, it is believed that RBCs undergo a similar process of programmed cell death equivalent to apoptosis, termed eryptosis, that leads to the production of apoptotic bodies (51). This constitutes a protective response to oxidative stress or other processes allowing the elimination of intracellular toxic molecules to extend the RBCs' lifespan in the bloodstream (54). Similarly, as a protection mechanism, RBCs can produce a second type of vesicle known as microvesicles (51, 55). The latter are the predominant subtype found in circulation and pinched off the plasma membrane as a result of the normal process of aging, also known as senescence. Throughout their lifespan, RBCs lose a considerable area of their membranes through the multiple vesiculation processes. Moreover, the same process of microvesiculation as a result of aging is observed in RBCs during storage conditions in blood banks (53). Lesions that negatively impact RBC membrane integrity, deformability and their capacity to transport oxygen occur during storage and lead to microvesicle release. Better characterization and understanding of this process is necessary since the implications of the presence of these microvesicles is significant for patients as they can prime neutrophils ultimately leading to undesired immune responses. Lastly, RBCs have been shown to possess the ability to produce all three types of extracellular vesicles as they have been shown to also release exosomes, although solely during their early developmental stages in the bone marrow (56).

Two distinct mechanisms have been shown to contribute to the dynamic formation of microvesicles from RBCs. An increase in intracellular calcium levels or the activation of protein kinase C have both been associated with the redistribution of phospholipids at the cell's surface, the ensued loss of asymmetry in RBC membrane lipid constitution and thus microvesicle formation (55, 56). In fact, intracellular calcium is responsible for the loss of lipid membrane asymmetry through the inhibition of flippase and the activation of enzymes responsible for internalizing phosphatildylserine: flappase and scramblase. Furthermore, cytoskeleton-cleaving proteins also get switched on, increasing membrane deformability. Thus, RBC vesiculation is directed by a combination of these two processes. Furthermore, the formation and release of microvesicles was also described in various studies following diverse treatments of the RBCs. The addition of

lipoprotein A, para-methoxyamphetamine or the ionophore A23187 in presence of extracellular calcium directs an increased unveiling of phosphatidylserine on the extracellular side of the RBC lipid bilayer ultimately increasing symmetry and microvesicle release (55, 57). ATP depletion has also been shown to increase microvesicle production as it essentially accelerates RBC senescence by decreasing the activity at the plasma membrane thus lowering calcium ion pumping and ultimately increasing the intracellular calcium concentration (58).

The human RBC-derived microvesicle populations characterized by multiple groups have analogous size ranges and composition. A first group identified two main populations of sizes 205.8 ± 51.4nm and 125.6 ± 31.4nm (55) whereas another group had observed earlier the release of microvesicles of 185 ± 23nm (58). The former group observed the microvesicles by scanning electron microscopy and described their typical spherical shape and confirmed the same size range. As for their protein profile, all groups identified transmembrane protein band 3 as the most prevalent protein on the microvesicle membranes. Hemoglobin has also been found to be carried by RBC-derived EVs. Indeed, it is estimated that RBCs lose about 20% of their hemoglobin through vesicle production in their lifespan (59). The presence of glycophorins, blood group antigens, and CD47 on their membranes has been highlighted by diverse groups while most of the other integral membrane proteins, spectrin and cytoskeletal proteins have not been found to be carried by these microvesicles (51). Moreover, these EVs are enriched in phospholipids, phosphatidylserine and lipids associated specifically with lipid raft domains.

Many roles have been attributed to RBC-derived EVs beyond their contribution to homeostasis. Evidence of pro-inflammatory and procoagulant responses from endothelial cells have been provided as a direct consequence of the interaction of RBC-derived EVs with monocytes in circulation (60). In fact, the EVs are phagocytosed by monocytes sequentially activating them leading to cell adhesion upregulation in endothelial cells. The presence of these extracellular vesicles in blood is also being closely investigated in the context of various blood-related diseases. For instance, EV release has been associated with tumor cells, hemolytic anemia, sickle cell anemia, thalassemia, and with infections with external agents, specifically during malaria infections (51, 61, 62).

1.6. EVs and parasitic pathogenesis: not a new concept

EVs participate in host-parasite interactions and in parasite-to-parasite communication during infections established by protozoan parasites and helminths. Secretion of EVs to establish successful infection in humans has been observed for protozoan species such as *Trichomonas vaginalis* (63) and *Giardia duodenalis* (64) and for different species of flatworms and nematodes (39, 65, 66). For species belonging to the *Apicomplexa* phylum, EV secretion has been described from host cells harboring *Toxoplasma gondii* and *Cryptosporidium parvum* infections. The former parasite increases antigen presentation, whereas the latter leads to the secretion of antimicrobial peptides (67). Also, the release of EVs has been extensively studied in kinetoplastids. In the cases of *Trypanosoma brucei* and *Trypanosoma cruzi*, the causative agents of African sleeping sickness and Chagas disease respectively, EV secretion has been associated with immunomodulatory potential, as EV secretion overwhelms the host's immune system through a heightened secretion of epitopes, ultimately leading to increased survival of the parasites (68). For *T. cruzi* specifically, proteomic studies following transmission electron microscopy (TEM) visualization of EV shedding have permitted the identification of parasite-derived proteins from which some have been linked to virulence (69, 70). Moreover, upon stimulation from a *T. cruzi* infection, red blood cells will release microvesicles that have the ability to bind complement C3 convertase. The C3 and EVs will together form a complex on the parasite's surface that inhibits C3-dependent catalysis, ultimately promoting the parasite's survival (71). In a similar fashion, *Leishmania spp.*, causative agent of Leishmaniasis, can use EVs to shed virulence factors (72). These EVs can also modulate the immune system, which is achieved in human monocytes by inhibiting pro-inflammatory cytokine production and stimulating the production of an immunosuppressive environment, and by preventing CD4+ T cell differentiation (73). Therefore, EVs from these two intracellular protozoan parasites promote interactions between the parasite and the host's cells. Since their invasion mechanisms have similarities with *Plasmodium* parasites, and since research has suggested the potential role of microparticles or other soluble factors in malaria infection progression and transmission, it is postulated that similar processes are mirrored in *Plasmodium* infections (48). It therefore comes as no surprise that EVs have been recently characterized in *Plasmodium* infections and that multiple roles have been already associated with their release.

1.7. EVs are actively involved in host-parasite and parasite-to-parasite communication during malaria infections

EVs were isolated from human plasma and shown to play specific roles during homeostasis, such as reticulocyte maturation and coagulation (41). Disturbances in these environmental conditions were seen to influence release and uptake of EVs and can have an impact at many levels of the infection by altering the interactions between the parasite with itself and between its host. Indeed, during *P. falciparum* infection at the blood stages, EV production is observed to impact the parasite as well as the host's immune cells.

As reported in other parasitic infections, phenotypically distinct EVs derived from *P. falciparum*-iRBCs are released, as shown by two independent research groups. Mantel *et al*. isolated vesicles ranging from 100-400nm from culture media that they described as RBC-derived microvesicles (RMVs) (74). By means of proteomic profiling and immunoblotting, they showed the presence of both RBC proteins and parasite antigens within the RMVs and identified two specific markers: RESA and SBP1. Following characterization, they showed that RMVs can modulate the host immune response through different processes and that RMVs specifically derived from *infected* RBCs have a greater capacity to stimulate such responses. Incubation with isolated RMVs from iRBCs was shown to lead to activation of multiple immune cells: (i) activation markers were upregulated in monocytes and B cells, (ii) pro and anti-inflammatory cytokine secretion was observed from macrophages, and (iii) increased migration of neutrophils was quantified. Interestingly, the source of the RMVs differentially effect host cells: the RMVs shed from iRBCs activate neutrophils, inducing movement, and also get internalized by other circulating RBCs more efficiently than uRBC-derived RMVs, even though the actual mechanism of uptake is still under study. Furthermore, when actin polymerization, a required process for EV uptake, was inhibited in human macrophages, the recipient cells, the mRNA levels of pro- and anti-inflammatory cytokines decreased in these cells. This suggests that the activated phenotype seen in macrophages is dependent of EV uptake.

Similarly, Regev-Rudzki *et al.* also note that inhibiting the action of actin and microtubules halted parasite-to-parasite communication during malaria infection (75). They went further and identified a parasite-specific protein located on the Maurer's cleft, that allows EVs to bud off, PfEMP1 trafficking protein 2 (PfPTP2). However, by means of transmission electron microscopy and

atomic-force microscopy, this group characterized their isolated EV population purified from *P. falciparum*-conditioned culture media. Due to their average size being of approx. 70nm, these EVs were referred to as exosome-like vesicles (ELVs), which differ from the ones isolated by Mantel *et al.*(74). These ELVs were indirectly shown to serve as messengers by means of plasmid transfer between different strains and by their ability to induce gametocyte production (explained later), thus confirming their role in cell-to-cell communication. EVLs are also speculated to possess the ability to carry and potentially transfer DNA following the successful transfer of DNA between parasites without physical contact, which had been described in cancer cells previously (50).

More recently, direct immunomodulatory properties have been associated exclusively with the DNA cargo of the EVs released from the iRBCs. Indeed, by image flow cytometry, a group demonstrated that the EV's DNA gets transferred into monocytes and disseminates within their cytosol (76). By accessing this intracellular space, the DNA triggers the cytosolic DNA-sensing pathway known as the STING-dependent signaling pathway that induces type I interferon responses. As the STING pathway is important in malaria parasites' development within the RBCs, it is not surprising that the parasite has established a mechanism to adjust the host's response. Overall, this study confirms only one of the many pathways the EVs and their cargo have the ability to regulate.

Overall, even though different roles were described for EVs by Mantel *et al.*, Regev-Rudzki *et al.* and Sisquella X. *et al.*, all three agree that EVs are required for cell-to-cell communication during malaria infection, whether it is to communicate with the host or amongst parasites (74-76).

1.8. EVs derived from *P. falciparum* infected RBCs mediate gametocytogenesis

Strikingly, Mantel *et al.* and Regev-Rudzki *et al.* described a common role for *P. falciparum*-infected RBC-derived EVs that was in agreement with previous findings about the relationship between soluble factors from parasite-conditioned medium and sexual differentiation (74, 75). A strong correlation between EV release and gametocytogenesis during malaria *in vitro* infection was observed (74, 75). Mantel *et al.* show that RMVs play a direct role in gametocytogenesis (74). For this, a 3D7 strain was grown in control media, media conditioned by early stage parasites and

media conditioned by late stage parasites. Gametocyte counts under the microscope revealed an increased production of gametocytes in both types of conditioned media compared to control medium, but still an even greater production when the late stage conditioned media was added to the culture. This experiment confirms much of the previously presented data but also reveals that parasite life stage plays a role in modulating EV release, hinting that the parasite's schizont stage stimulates EV release at a higher extent. Furthermore, gametocyte production increased in a dose-dependent manner following addition of different concentrations of RMVs isolated from iRBCs, while RMVs derived from uRBCs could not induce the same levels of sexual commitment. Parasitemia remained unaffected by the addition of RMVs in culture. This is strong evidence that EVs can *directly* modulate communication between erythrocytic stages of the parasite. Mantel *et al.* also postulate that these results suggest that the parasite is able to use EVs to estimate its own population density and modulate the gametocyte production accordingly.

Regev-Rudzki *et al.* also make a strong case for the need of parasite-to-parasite communication in triggering gametocytogenesis (75). The co-culture of two parasitic strains in presence of a drug lead to a 17-fold increase in gametocyte production than when grown individually in the same conditions, as seen by microscopy and flow cytometry. This suggests that communication between parasites increases sexual commitment following environmental changes. Through this experiment and other conducted in their study, it is suggested that sexual differentiation is prompted as a survival mechanism in response to detection of a stressful environment, here triggered by drug pressure.

Although a clear correlation between the presence of EVs and gametocytogenesis has been described by both groups, there is a great need for (i) more supporting data, (ii) determining the factors modulating EV release, and (iii) the different pathways they trigger to support the proposed role of EVs in cell-to-cell communication. Thus, it is clear that the study of the EVs' function in the context of a malaria infection has to be supplemented by a greater understanding of the composition and the cargo of these vesicles to identify the active biomolecules that lead to their importance in circulation.

1.9. Characterization of RBC- derived EVs during homeostasis and during malaria infection: proteomics and lipidomics

Most of the characterization focus was initially turned into identifying the different proteins and lipids that made up the lipid bilayer of the EVs derived from *P. falciparum*-infected RBCs to better grasp their similarities in composition to RBC-derived EVs and known EV markers. The protein and lipid composition of RBC-EVs, which are known to be almost solely microvesicles, is still not entirely decoded. It has been noted that while the phospholipid composition of microvesicles released by RBCs mirrors the one of the original cell's membrane, the protein diversity on the RBC-derived microvesicles is much more restricted than on the RBC's membranes (55). In fact, most integral membrane and cytoskeletal proteins were not detected on the microvesicles (51). As presented earlier, all studies agree on the abundant presence of band 3, with differences in aggregation, and on the absence of spectrin from RBC-MVs (51, 55, 58, 77). The presence of other proteins such as glycophorins, blood group antigens, stomatin, CD47, lipid raft proteins and hemoglobin overlaps amongst reports whilst the presence of other proteins such as actin is still disputed (51, 55, 77).

Subsequently, when looking at the impact of a malaria infection on protein and lipid composition of the EVs released by RBCs, a specific core content of RBC-associated proteins was identified in EVs from both origins by means of mass spectrometry (74). The latter included lipid raft-associated proteins: band 3, stomatin and carbonic anhydrases. However, unlike previous reports on RBC-EVs, spectrin was visible, although partly depleted, on both types of EVs (74). Although, the lipid composition of the released EVs was not studied in detail, the presence of phosphatidylserine was detected by Annexin V staining which also aligns with earlier findings on RBC-EV lipid profiles (51, 55, 74). Thus, not only are these observations mostly consistent with previous studies that profiled the protein and lipid contents of EVs derived from RBCs but also confirms that EVs produced from iRBCs maintain the same RBC-related proteins. Furthermore, the EVs released from the iRBCs carried about 30 different *P. falciparum*-specific proteins (74). The latter were either proteins classically associated with the host cell's membrane, such as Maurer's clefts or with the parasitophorous membrane or proteins that play a role during invasion such as rhoptry proteins. The same proteomic profile was described for EVs isolated from *in vitro*

cultures of 2 different *P. falciparum* strains implying the packaging of these proteins is not a random process.

Nevertheless, as laboratory strains have not been subjected to the pressures of living inside a human host for a long period of time, the parasite might have adapted its EV release process in consequence. For this purpose, Adbi *et al.* carried out the first thorough proteomic analysis of EVs isolated from the blood of *P. falciparum* infected patients from Kenya (78). Their research yielded results that are comparable to the observations provided by Mantel *et al.*, confirming the existence of a fixed set of released bioactive molecules. There was an overlap of 53 distinct proteins between the two studies while Abdi *et al.* identified another 100 proteins solely present in their isolates, totaling about 184 different proteins identified when combining both reports (78). Also, some virulence factors such as PfEMP1 or STEVOR were not found within the EVs, supporting the findings from Mantel. *et al.* Despite the absence of these proteins, Abdi *et al.* revealed proof of increased presence of other proteins associated with virulence in their samples; proteins that work to remodel the RBC's surface and proteins that play a role during RBC invasion such as Maurer's clefts, rhoptry-associated or microneme-associated proteins (78). Interestingly, they noted that the amount of proteins found in EVs varies with the parasite's different life stages at which they are produced: almost all the proteins present at the ring stage were also found in the late developmental stages but about 100 other proteins were identified from the second half of the parasite intra-erythrocytic cycle (78). Overall, their analysis identified proteins associated with the extracellular membrane and parasitophorous membrane to be present with the most abundance whereas merozoite antigens from the parasite's apical end followed in abundance which again aligns nicely with the observations from Mantel *et al.*

Additionally, another group performed a proteomic analysis of the microparticles found in the blood of infected patients. Antwi-Baffour *et al.* show that EVs released into the blood of malaria infected patients carried greater quantities of hemoglobin than their counterparts implying a correlation between the lower levels of hemoglobin seen in malaria infected patients and RBC vesiculation (79). Additionally, they identified increased levels of certain *P. falciparum* proteins such as enolase, heat shock 70 kDa protein and L-lactate dehydrogenase that had not been singled out in the other studies and they pinpointed a few other proteins that were only seen in a limited amount of the infected samples (79).

1.10. Characterization of RBC- derived EVs during homeostasis and during malaria infection: nucleic acids

RNAs have long been identified in circulation and have been at the center of research for their potential as disease biomarkers (80, 81). However, it is some years later that the first evidence of the ability of EVs to shuttle small RNAs between cells was provided by Valadi H. *et al.* (82). Working with exosomes from mouse and human mast cell lines, the group revealed the presence of intact mRNA from around 1300 different genes in these vesicles and showed that the abundancy of these transcripts varied from their parent cells. These mRNA transcripts retain their functionality as they can be used to produce polypeptides in the presence of the required machinery. To greater extent, they provided proof of the ability of EVs to also carry miRNAs and their ability to transfer them between cells, leading to believe that the latter can communicate by means of gene modulation (82).

Despite their inability to sustain *de novo* protein synthesis and modulation mechanisms, RBCs were shown to carry endogenous miRNA machinery to carry out gene silencing by means of microRNA deep sequencing and mass spectrometry (83). 197 different miRNAs were identified, including predominantly miR-451a and others such as miR-144/145 and miR-144-3p. Additionally, despite the absence of two components of the RNA-induced silencing complex Dicer and TRBP, the presence of Argonaute 2 and its ability to bind a variety of cofactors was confirmed in the same study (83). Thus, these observations suggest that RBCs possess the ability to use miRNAs to regulate certain processes.

In agreement with these findings, in a recent study conducted to identify the specific RBC-derived EV contents responsible for the immunomodulation of host cells in the context of an *in vitro* malaria infection, both host-derived and parasite-derived small RNAs were characterized (76). The RNA contents of uRBC-EVs and iRBC-EVs differ, particularly regarding their amounts, iRBC-EVs carrying at least twice as much (76). Subjecting the isolated EVs to small RNA deep sequencing revealed that uRBC-derived EVs carry a higher proportion of microRNA reads compared to iRBC-derived EVs but still share about 218 out of 229 total human microRNAs detected, with has-miR-451a predominating in both EV types (76). Furthermore, by means of GO enrichment analysis, a positive bias of miRNA targets associated with cell adhesion gene regulation was revealed. They include many PfEMP1 adhesion targets from the host such as

platelet endothelial cell adhesion molecule-1 (PCAM-1), vascular cell adhesion molecule-1 (VCAM-1) and intercellular adhesion molecule-1 (ICAM-1), to name a few (76). It is thus hypothesized that adhesion mechanisms of iRBCs can be regulated by EV-derived microRNAs in host endothelial cells.

In the same study, genomic DNA, apicoplast and mitochondrial DNA derived from the malaria parasite was also identified within iRBC-derived EVs (76). This DNA packaging process seems to be limited solely to *P. falciparum* early developmental stages. In fact, the DNA was also shown to play an immunomodulatory role as it gets transferred into host monocytes and subsequently activates the STING signaling pathway as presented earlier (76).

Although there seems to be an increased consensus regarding the different components of RBC-EVs and *P. falciparum*-infected RBC-EVs with time, many inconsistencies are still observed. To strengthen the evidence, there is first a need to eliminate the bias and skewing of results that is created by the heterogeneity of methodologies used for isolation and characterization, not only in the context of malaria EV research but also in the whole field of extracellular vesicles.

1.11. The drawbacks and limitations of the young field of extracellular vesicles

As it is still being highlighted in any research paper published in the field and in numerous reviews, the biggest challenge in the field of extracellular vesicles remains to find consistency and achieve reproducibility between studies. There are no set standards yet. Consequently, result interpretation is highly sensitive to the variations in nomenclature and the different isolation techniques available. Although there have been efforts to combine over 350 studies into a single database called Vesiclepedia, the lack of established methodologies is noticeable and made more obvious by the ever-growing sensitivity of molecular techniques (84).

Initial efforts focused on establishing specific characteristics to each EV subtype, based on size restrictions, biogenesis processes, surface markers, cargo and downstream function. Over the years, this was proven to be harder than initially expected, as many of the isolations yielded heterogenous EV populations. To further complicate matters, many standard exosome markers were later found to be carried by microvesicles just as commonly, as was the case for tetraspanins (84). Moreover, a single cell can produce EVs that differ in size, in cargo and even in biogenesis

adding another level of complexity to profiling the secretome of different cell types. This was demonstrated in a study that obtained 2 different subtypes of EV populations using the same isolation method of sequential centrifugal ultrafiltration to collect the EVs produced by a human colon cancer cell line (85). A first population was heterogenous and displayed a large size range whereas the second population was described as homogenous, had a much smaller size range and carried many of the traditional EV markers. Interestingly, their downstream ability to invade cells was also different between EV subtypes (85). Nonetheless, as awareness about the lack of consensus in the field rises, more researchers are focusing their efforts into standardizing the differences between EV subtypes (86).

It has become clear that the methodologies used for sample collection, processing and isolation can also impact the characterization outcomes and are dependent on the biofluid studied (87). For instance, ultracentrifugation has been considered the gold standard of isolation methods in this field. However, there are increasing reports regarding the negative impact of this technique on the structural integrity of the extracellular vesicles, which in turn can affect their active properties (88). The EV cargo can be modified as a consequence of the damage enforced onto the EV membranes by the high force exerted on them by the centrifugation. Incomplete sedimentation and pelleting of other materials other than the EVs of interest are also growing concerns in the field. Co-sedimentation of undesired materials such as lipoproteins and protein aggregates are not uncommon sights (87, 89). Moreover, it was shown that many factors can introduce variation in pelleting efficiency between studies such as the viscosity of the biofluid of interest or the rotor type and angle to name a few (90). Other less widely used isolation methods include size exclusion chromatography, density gradient centrifugation and filtration to name a few. Each of these techniques comes with their own set of restraints.

Disparities between investigations is also introduced during the analysis of isolates. For instance, when comparing some methods used for size determination and the visualization of the EV's morphologies such as scanning electron microscopy, nanoparticle tracking analysis and atomic force microscopy, there is variability between studies. Some other techniques are already known to be less suited for similar studies such as dynamic light scattering and flow cytometry (87). Moreover, storage and handling practices are also seen to influence results (87).

Thus, to produce reliable results, to identify specific markers for EV subtypes and study their biogenesis and downstream effects, there exists a clear need to improve the current isolation methods. This is followed by a need to find better markers for different EV subtypes and a need to develop good controls for the different techniques used. The lack of consistency and the inability to establish standard protocols continues to emphasize the gaps in knowledge in the field of extracellular vesicles. These challenges are seen across different contexts and particularly in the context of a malaria infection, as research in this area is in its infancy. The lack of understanding of the malaria parasite's complete biology contributes to the difficulty of establishing standard methodologies and consensus amongst scientists.

2. Project Overview

2.1. Rationale and Hypothesis

Circulating microparticles have recently been recognized to play significant roles during malaria infections. Multiple roles have already been attributed to the presence of *P. falciparum*-infected RBCs derived EVs from immunomodulation to gametocytogenesis regulation. Indeed, a significant amount of studies have shown evidence of the capacity of the parasite to use the EVs for exchanging information, for communication. However, being a young research field, EV isolation procedures have not been standardized and do not yield homogenous vesicle populations. This has led to variations between the conclusions reported by different studies and lack of reproducibility. In turn, the inability to differentiate EV subtypes prevents the establishment of widely accepted methodologies. In this context, before investigating the roles of the EVs in culture, in our laboratory, we turn our attention to confirming previous findings from other groups and to then expand upon established knowledge. We hypothesize that the EV population produced during *P. falciparum* infection of RBCs differs in content from the EVs shed by RBCs at homeostasis to include parasite-specific information to allow communication between parasites within the host. We seek to establish robust protocols that will allow consistent isolation and characterization of iRBC-derived EVs. We then propose to further characterize the EVs from infected cultures and investigate the differences with EVs shed by RBCs as their unique features will allow the understanding of mechanisms of biogenesis and mechanisms of action during a *P. falciparum* infection. The identification of parasite-specific markers and parasite-specific contents in iRBC-EVs by a combination of different methods is the basis of any future research looking to reveal specific pathways involved in EV release, uptake and survival. This can ultimately contribute to the discovery of new vaccine targets or new drug targets that aim to interfere with the parasite-to-parasite communication.

2.2. Specific Aims

To test this hypothesis, we address the following specific aims:

I. Isolation, purification and characterization of the EV population collected from *P. falciparum*-infected RBCs *in vitro* culture

II. Determine specific markers for the identification of RBC-derived EVs and parasite-infected-RBC EVs

III. Investigate the differential composition of the information enclosed in uRBC-EVs and iRBC-EVs

To this end, we will conduct our study of EV populations following the collection of conditioned media from the *in vitro* model of *P. falciparum*-infected RBC cultures. A range of analytical methods will be applied throughout the study seeking to combine multiple widely accepted technologies in the EV field to validate our conclusions. The use of complementary methods remains the gold standard as each has their own limitations created by the size of the particles.

3. Methodology

3.1. *Plasmodium falciparum in vitro* culture

Parasites of the *P. falciparum* reference strain 3D7 were used for this study. Parasites were maintained in culture at 5% hematocrit in complete RPMI 1640 media (Wisent Bioproducts). RPMI media was supplemented with L-glutamine (300mg/L), HEPES (25mM), sodium bicarbonate (200mg/L), hypoxanthine (1mM) and gentamicin (50mg/mL) (Wisent Bioproducts). As serum substitute, bovine serum albumin was added to the culture media prepared from AlbuMAX I (Invitrogen) to reach a final concentration of 0.5% (w/v). Parasites were kept in fresh human red blood cells of type A+ received as packed red blood cells (Interstate blood bank, Memphis, Tennessee, US). Upon arrival, blood was washed with incomplete RPMI and stored at 4ºC at 50% hematocrit in incomplete RPMI media supplemented with gentamicin (50mg/mL) for no longer than 4-5 weeks. *P. falciparum* cultures were kept at controlled atmospheric conditions of 5% CO_2, 3% O_2 and 92% N and at constant 37ºC. For maintenance, parasitemia was sustained between 3-5% but was elevated to 5%-8% when cultures were used to produce EVs for isolation. 10mm^2 culture dishes were used for maintaining cultures whereas 650 mL flasks were used for growing bigger cultures to collect greater amounts of EVs from the culture media. To calculate parasitemia, thin blood smears were prepared by spreading a drop of blood on a microscope slide. The smears were shortly dipped in methanol and when completely dried, they were stained in 5-10% Giemsa solution.

To grow synchronized cultures, the parasite cultures were treated by sorbitol lysis. After confirming high parasitemia with high percentage of ring stage parasites by thin-blood smears, the iRBC suspensions were incubated for 10 minutes with a 5% D-sorbitol solution (Thermo Scientific). The RBCs were then washed once with incomplete RPMI to thoroughly remove the sorbitol and put back in culture in complete RPMI.

For uRBC cultures used to collect uRBC-derived EVs for control purposes, RBCs were maintained in the same way as iRBC cultures i.e. at 5% hematocrit in the same volume of complete RPMI media and in flasks. These cultures were synchronized in the same fashion as infected cultures.

3.2. Isolation of extracellular vesicles

P. falciparum-infected RBC cultures maintained in T175 flasks at 5% parasitemia or higher were first synchronized by sorbitol treatment. Synchronization of the culture is important to avoid collecting media from a parasite culture where egress had started to take place to prevent the collection of merozoites or other by-products of similar size to vesicles but of different nature. The culture supernatant was collected at different time points post-synchronization. For ring stage-specific EVs, the media was collected about 24h after the synchronization and for EVs derived from the late blood stages, the media was collected from the period between 24h to 40h post-synchronization. When the life stage was not important for the experiments or for optimizations, the consumed media was collected from the flasks directly 30-40 hours after the initial synchronization. To collect the culture supernatant, the cell suspensions were sequentially centrifuged at increasing speeds to eliminate any cells and debris from the media of interest. First centrifugations were carried out in Sorvall ST16R (Thermo Scientific) with rotor T5003629, starting with two centrifugations at 1900 rpm and for 5 minutes and followed by two centrifugations at 3,000 rpm for 10 minutes. The cell suspensions were then centrifuged at 17,000 xg for 1 hour at 4ºC using rotor JLA16.250 (Beckman Coulter). The media was filtered through a 0.45µm filter (Nalgene) to get rid of other protein aggregates and more debris. To concentrate the media and as to reduce its volume, the filtrated media was passed through a VivaCell 100 PES centrifugal concentrator (Sartorius) that possesses a 100kDa molecular weight cut off. VivaCells with media were centrifuged at 3,000 rpm at 4ºC until media was concentrated to desired point. A final ultracentrifugation step was done to pellet out the EVs from the concentrated media. Two variations of this last step were used in this study. The concentrated media was transferred to thickwall polypropylene 32 mL tubes (Beckman Coulter) and centrifuged at 150,000 xg with 50.2Ti rotor at 4ºC for 12-16 hours. Alternatively, the concentrated media was transferred to centrifuge polycarbonate 10.4 mL bottles with cap assemblies (Beckman Coulter) and centrifuged at 150,000 xg (i.e. 40 500 rpm) with 70.1Ti rotor (Beckman Coulter) at 4ºC for 12-16 hours. The EV pellets were resuspended in DPBS (Gibco). The EV suspensions were then analyzed by nanoparticle tracking analysis or Western blot. If not used immediately after isolation, EV suspensions were stored at -80ºC for longer periods. Furthermore, to obtain uRBC-derived EVs to be used as controls and to carry out comparisons, the same protocol was followed.

3.3. Sucrose gradient purification and albumin depletion

Sucrose solutions of different densities were prepared by mixing the adequate mass of sucrose, following the mass to volume ratio desired, with 1.4g of Tris in 50ml of water. The solutions were first equilibrated to pH 7.2-7.4 and then filtered simultaneously through a 0.22µm filter (Corning) and a reusable anion membrane absorber 15cm^2 Sartobind Q15 (Sartorius). Sucrose solutions were stored at 4ºC. The gradients were prepared in thickwall polypropylene 32mL ultracentrifuge tubes (Beckman Coulter). The nonlinear gradients were composed of three 5mL layers of different densities; the denser layer was placed at the bottom of the tube and the decreasingly lighter layers were layered on top of each other very slowly with the help of a syringe with a 20G needle (BD), to disturb the layering as little as possible. Here, gradients of 40% - 35% - 30% and 50% - 45% - 40% were prepared. Alternatively, as part of the optimization steps, a sucrose cushion of 40% sucrose was also tested. It was prepared by adding a single 5 mL layer of 40% sucrose solution to the ultracentrifuge tube. Following the gradient or cushion preparation, the concentrated media obtained after multiple centrifugation rounds with the molecular weight cut off was carefully layered on the sucrose gradient or cushion. The gradients were centrifuged for 18 hours at 25,000 rpm (approx. 100,000 xg) and at 4ºC using the SW-28 rotor (Beckman Coulter). Individual fractions were collected from each sucrose layer and washed twice with DPBS to eliminate as much of the sucrose as possible. For the first wash, each fraction was placed in a new 32 mL ultracentrifuge tube and spun down for 2 hours at 27,500 rpm (approx. 136,000 xg), at 4ºC in the SW-28 rotor (Beckman Coulter). For the second wash, only 5 mL recovered from the bottom of each tube were placed in a new thinwall polypropylene 12 mL ultracentrifuge tube (Beckman Coulter) and centrifuged for 2 hours at 28,000 rpm (approx. 134,000 xg), at 4ºC in the SW-41 rotor (Beckman Coulter). For the final step of the EV collection, only 1 mL was recovered from the bottom of the previous tube and placed in a 1.5 mL microfuge tube (Beckman Coulter). These were centrifuged for 1h30 at 50,000 rpm (approx. 100,000 xg) at 4ºC in the TLA 100.3 rotor (Beckman Coulter). The final pellet was resuspended in ~100µL of DPBS. For protocol optimization, all the fractions obtained were analyzed by Western blot and by Coomassie brilliant blue staining to verify the purity of the isolations. If not needed for further use, the EV suspension in DPBS was flash frozen and stored at -80ºC.

For further purification by albumin depletion, the Pierce albumin depletion kit (ThermoScientific) was tested on our EV isolations. The instructions were followed as outlined in the kit. One slight modification was done to the protocol to accommodate the type of albumin that will be bound to the resin in the column. The binding/wash buffer, a low-salt alternative composed of 25mM Tris and 25mM NaCl, was prepared and set at pH 7.5. About 25-50µL of the DPBS diluted samples were passed through the column twice and the flow-through was collected. The flow-through of several washes to the column were also collected and all collections were pooled together. Their protein profile was analyzed by Coomassie brilliant blue staining following separation of the proteins by SDS-PAGE.

3.4. Isolation of extracellular vesicles from enriched iRBC cultures

Enrichment for iRBC was achieved by removing the greatest amount possible of uRBCs from the culture based on differences in cell density, as iRBCs are expected to have a bigger mass than uRBCs. About 24 hours following synchronization of the iRBC cultures, when all the parasites have reached the trophozoite stage, the RBC pellet from one flask containing all RBCs from one culture was resuspended in incomplete RPMI media and layered on top of a Percoll (GE Healthcare) or Easycoll (Millipore Sigma) layer. For the Easycoll layer, a 15 mL layer at a concentration of 75% of the 1.124g/mL Easycoll solution was prepared with incomplete RPMI media. For the Percoll, a 10 mL layer at a concentration of 68% of the 1.130g/mL Percoll solution was prepared with 1X PBS. Both separating layers can be used interchangeably, and both resulted in similar separation efficiency. Not more than 2.5 mL of RBCs was placed at the top of each separation column, i.e. 2 columns were used for each flask of culture. Columns were centrifuged at 1,500 xg for 20 min to separate the iRBCs from the uRBCS. Slower acceleration and deceleration speeds were used to not disturb the separations at the beginning and the end of the centrifugation. The uRBC pellet was found below the separation layer whereas the heavier iRBCs were found at the top the layer. The top layer was collected and washed twice with incomplete RPMI media at 800 xg for 2 minutes. The final enriched iRBC pellet was introduced back into the flask with the same initial amount of media i.e. 100 mL, by consequence lowering the hematocrit of the culture. Thin-blood smears of the culture were prepared and stained with Giemsa to count parasitemia, to confirm that the enrichment was successful. As small volumes of iRBCs are

generally recovered, since this is restricted by the parasitemia of the culture, more flasks of culture were used in this EV isolation process, usually about 4 x T175 flasks (each with 100 ml of 5% hematocrit cultures at a parasitemia ranging between 5-10%), to increase the amount of EVs collected at the end of the process. The culture supernatants were collected, as previously explained, approx. 7 hours after the enrichment process, or just before schizonts start undergoing egress. Thin-blood smears were prepared again to examine the stages of the parasites in culture at this time point. EVs were isolated from the collected media as previously outlined. For protocol optimization, all isolations obtained were analyzed by Western blot to verify the purity of the isolations.

3.5. EV enumeration and EV size distribution analysis

3.5.1. Nanoparticle Tracking Analysis

Extracellular vesicles were isolated as described above through differential ultracentrifugation steps from iRBCs and uRBCs and the final pellet was resuspended in ~200µL DPBS. For the purpose of this study, analysis was done directly on freshly isolated EVs, i.e. EVs that had just been resuspended in DPBS, or on EVs that had been stored as particle suspensions in DPBS for different periods of time at -80ºC following isolation, here referred to as frozen samples. Nanoparticle tracking analysis (NTA) was performed with the NanoSight NS300 (Malvern Panalytical) and with the ZetaView (ParticleMetrix). The EV samples were diluted by 10,000 and 100,000 fold in DPBS to get more accurate reads on these machines. For some settings used for the NanoSight, the slider shutter was set between 1200-1300, the slider gain was set to approx. 500 and the camera level to approx. 16. For the ZetaView, the ZNTA filter was used to measure the size and concentration of the particles and the shutter was set to 100, the sensitivity ranged from 90-95 and the gain was set to approx. 33. The settings were optimized for each instrument and remained unchanged between samples. Instruments captured video recordings, 3 x 1 minute videos for the NanoSight and 9 x 10 second videos for the ZetaView, and analyzed them. The analysis was presented by each machines' software as a size distribution graph, supplemented with a report containing results such as the mean and median particle sizes and short videos of the particles in solution.

3.5.2. Fluorescence triggered flow cytometry

Extracellular vesicles were isolated as described above through differential ultracentrifugation steps from iRBCs and uRBCs and the final pellet was resuspended in ~200µL DPBS. EV enumeration was performed with the CytoFLEX (Beckman Coulter). The EV samples were diluted 10,000-fold in DPBS to reach a final sample volume of 1 mL to reduce abort rates. The side scatter measurements were done using the 405 nm violet laser. A bead mix was used to set up the instrument detection limit for microparticles (APOGEE and Beckman Coulter). Dot plots were produced with the CytoFLEX analysis software, CytExpert (Beckman Coulter). DPBS alone was used as control.

3.6. Scanning electron microscopy of purified extracellular vesicles

Prior to sample preparation, the surface used to hold the specimen of interest were bathed for 20-30 minutes in 100% ethanol solution on a shaker to remove all debris. Both glass coverslips (30mm round, Warner Instruments) and polished titanium disks (provided by Dr. Nanci's laboratory at the Université de Montréal) were used as mounting substrates in this study. The latter were dipped several times in filtered water and then placed in a 0.01% poly-L-lysine bath for 20 minutes at room temperature. Following this incubation, the coverslips and disks were rinsed with filtered water and left to dry overnight at room temperature. As a test, the disks not coated with poly-L-lysine were left to dry right after the first wash with filtered water was done. Samples of interest were the EVs isolated from uRBC and the EVs isolated from enriched iRBC cultures. They were fixed in 3.7% formaldehyde solution dissolved in DPBS. Approx. 40 volumes of fixing solution were added per sample into 1.5 mL microcentrifuge tubes (Beckman Coulter). Samples were incubated overnight at 4ºC. The fixed samples were then centrifuged for 30 minutes at 50,000 rpm (approx. 100,000 xg) at 4ºC in rotor TLA100.3 (Beckman Coulter). EV pellets were resuspended in ~200µL DPBS. Pre-warmed glass coverslips were coated with ~100µL of resuspended EV samples while ~50µL of resuspended EV samples were spread over the surface of pre-warmed titanium disks due to their smaller surface. These mounted surfaces were incubated for 2 hours at 37ºC in a humid chamber. Coverslips and disks were washed 3 times for 15 minutes with filtered DPBS on a rocking plate, before starting the sample dehydration process. Then, they were bathed

for 15 minutes in increasingly concentrated ethanol solutions: 30%, 50%, 70% and 90% ethanol solutions. All solutions were filtered through a 0.22µm filter (Corning) prior to use to eliminate all debris and dust particles. Lastly, the mounted surfaces were placed in a 100% ethanol bath until the next step was performed (ranging from 24 to 72 hours). Complete dehydration of the samples was achieved by critical point drying. The latter was done with CO_2 in a critical point dryer (Leica EM CPD). A slow CO_2 entry into the chamber was used to reduce the disturbance of the vesicles on the slides. 20 cycles of CO_2 exchange cycles were used to remove all the ethanol. The pressure was also slowly released to not disturb the samples. Lastly, samples were coated with 5nm of gold and palladium by means of a sputter coater (Leica EM ACE200). Samples were first imaged with 2 different tabletop scanning electron microscopes; they were imaged at 10,000 x (Hitachi TM-1000) and up to 30,000 x (Hitachi TM-3000). Samples were also imaged at higher magnifications with JSM-7400F electron microscope (Jeol) at ~20µA and 2-3kV. For the latter, conductive carbon tape was placed on stage and the edges of the titanium disks were painted with a carbon paint to help with the conduction to obtain sharper images.

3.7. Protein extraction and protein concentration assessment

For protein extraction from EVs, both iRBC- and uRBC-derived EVs, lysis buffer was directly added to the EV suspension in DPBS. For 200µL of EV suspension, ~200µL of lysis buffer was used. Two variations of RIPA buffer were used for protein extraction in this study. RIPA buffer 1 was composed of 50mM Tris-HCl (pH 7.8), 5mM EDTA, 50mM NaF, 0.1%SDS, 1% Triton X-100 and a fresh supplement of 1mM DTT. RIPA buffer 2 constitutes of 50mM Tris-HCl (pH 7.4), 1% NP40 and 0.2% sodium deoxycholate. Both lysis buffers were completed with the addition of protease inhibitor cocktail at 1:100 dilution (Halt™ Protease inhibitor single-use cocktail 100x, Thermo Scientific). The extraction was incubated on ice for 20-30 minutes on ice. To aid with the protein extraction, a vortex mixer was used for mechanical disruption of the samples. Samples can then be stored at -80ºC at this point. Otherwise, following the incubation, samples were centrifuged at 13,000 rpm (approx. 16,000 xg) for 1 minute. As controls, proteins were also extracted from uRBCs and from parasite infected cultures of at least 5% parasitemia. First, to release the RBC contents in both preparations, RBC membranes were lysed using saponin. The blood pellets were resuspended in 40mL of 0.025% saponin dissolved in incomplete RPMI media. The reaction was

incubated on ice for 10 minutes. Samples were centrifuged for 15 minutes at 5,000 rpm (approx. 4,700 xg) and deceleration 5. Keeping the same centrifugation settings, pellets were washed twice with DPBS. iRBC and uRBC pellets were resuspended in lysis buffer following the same procedure as for the EV suspensions.

Protein concentration of all samples was measured by means of BCA protein concentration assay as instructed in the Pierce BCA protein assay kit (Thermo Scientific). Serial dilutions of each sample were prepared for more accurate readings. Following a 30 minute incubation at 37ºC, the absorption was read at 562nm in the Synergy H4 hybrid reader (BioTek). Standard curves were generated by plotting the average of blank-corrected measurements for each standard against the protein concentration (in µg/mL) on Microsoft Excel. The standard curve was used to calculate the protein concentration of the unknown lysed samples.

3.8. SDS-PAGE (polyacrylamide gel electrophoresis), Coomassie Brilliant Blue stain and immunoblot analysis

Proteins were separated on a 10% polyacrylamide gel. The amount of proteins loaded on the gel varied between 4µg to 60µg of proteins depending on the concentration of the sample used, as only about 30µL of sample can be loaded per well. This information will be indicated in the respective figures. The calculated amount of protein was first mixed with 5 x SDS loading buffer, heated to 95ºC for 5 minutes, mixed with a few slow pulses on the vortex mixer and centrifuged down shortly prior to loading of the gel. Gel electrophoresis was run at 120V or alternatively at 45-50 milliampers for approximately 1.25 or 1.5 hours. For Coomassie brilliant blue staining, at the end of the gel electrophoresis, the gel was first washed with water for 30 minutes. The gel was sometimes briefly dipped in methanol prior to washings to reduce the chances of the gel breaking when handling it. The gel was incubated for 1 hour with 50 mL of Bio-Safe Coomassie G-250 stain solution (BioRad) at room temperature on a rocker. The gel was destained with water overnight at room temperature. The gel was imaged with Gel Doc XR+ System (BioRad). Alternatively, for immunoblot analysis, the proteins from the polyacrylamide gel were transferred onto a PVDF membrane by means of semi-dry transfer using Pierce semi-dry blotter (Fisher Scientific). Pre-soaked Whattman paper was placed at the top and bottom of the gel and the PVDF

membrane (0.45 µm pore size, Immobilon-P), previously activated in methanol. Transfer was performed for 30 minutes at 25V. For protein detection, membrane was first washed in 1x TBS following transfer, to wash off the transfer buffer. The blocking step was performed with TBS supplemented with 5% milk (TBSM) for 1 hour at room temperature on a rocker. The membrane was incubated with primary antibodies at 4ºC overnight with rocking motion. Primary antibodies throughout this study and their respective working concentrations were: monoclonal anti-band 3 antibody (Clone BIII-136, Sigma Aldrich) at 1:5,000, exosome anti-CD63 mouse monoclonal antibody (Ts63, ThermoFisher Scientific) at 1:1,000, rabbit monoclonal to bovine serum albumin antibody (EPR12774, Abcam) at 1:10,000, monoclonal anti-spectrin (α and β) produced in mouse (SB-SP1, Sigma Aldrich) at 1:5,000, and anti-tubulin antibody (Sigma-Aldrich) at a:1,000. Other primary antibodies used in this study were obtained through the MR4 resource center from BEI Resources and were used at the dilutions indicated on table 1. Primary antibodies were diluted at to the appropriate concentration in TBSM-Tween (TBS + 0.5% milk + 0.05% Tween-20). Following incubation, membranes were washed three times for 10 minutes with TBSM-Tween. The HRP-conjugated secondary antibodies specific for the species of the primary antibody were diluted to the appropriate concentration in TBSM-Tween. Membranes were incubated with secondary antibodies for 1 hour at room temperature on a rocker (Rocker II, Boekel Scientific). Secondary antibodies used in this study were a goat polyclonal secondary Antibody to mouse IgG HRP (ab6789-1MG, Abcam) at a dilution of 1:5,000 and goat polyclonal secondary antibody to rabbit IgG HRP (ab97080-500UG, Abcam) at a dilution of 1:5,000. To remove unbound antibody, membranes were washed three times for 10 minutes with TBS supplemented with 0.05% Tween. Membranes were placed in a developing cassette and immunoreactive bands were detected by activating the HRP enzyme with the addition of Supersignal west pico chemiluminescent substrate (Thermo Scientific) for 5 minutes. Alternatively, when protein expression was too low, the Supersignal west femto maximum sensitivity substrate (ThermoFisher Scientific) was used to detect bands of interest. To image the membrane, a film (Bioflex EconoFilm) was placed over the membrane in the developing cassette in a dark room. The exposure time of the film with the membrane varied between a few seconds to 1 minute when using the femto substrate and between 5 minutes and 1 hour when using the Pico substrate. Exposure times also varied with the antibody's affinity to the proteins. Film was developed with X-OMAT 2000 processor (Kodak).

Table 1. List of parasite-specific antibodies tested by means of Western blot. Antibodies have been grouped based on the functions of their target proteins. The catalog number from the MR4 website is indicated.

Role in parasite	Antibody	Target epitope	Dilution used	Catalog #	Source
Merozoite invasion	anti-EBA-175	region II F1 domain	1:1,000	MRA-712A	BEI Resources
	anti-EBA175	region II F2 domain	1:1,000	MRA-711A	BEI Resources
	anti-AMA-1	Whole protein Grown in N3-2D9 hybridoma	1:250	MRA-479A	BEI Resources
	anti-AMA-1	Whole protein Grown in N3-1D7 hybridoma	1:250	MRA-480A	BEI Resources
	anti-AMA-1	Whole protein Grown in N4-1F6 hybridoma	1:250	MRA-481A	BEI Resources
	anti-AMA-1	Pan-specific	1:500	MRA-897A	BEI Resources
Hemoglobin degradation within digestive vacuole	anti-histoaspartic protease	Whole protein	1:10,000	MRA-811A	BEI Resources
	anti-plasmepsin II	25 amino acid MAP peptide derived from the N-terminus of plasmepsin II (HSHSSNDNIELNDFQNIM FYGDAEV)	1:3,000	MRA-66	BEI Resources
Chaperone; Expressed in ER	anti-PfGRP78-BiP	Antiserum to a synthetic peptide (C-SGDEDVDSDEL)	1:500	MRA-1246	BEI Resources
	anti-PfGRP78-BiP	Antiserum to a synthetic peptide (C-SGDEDVDSDEL)	1:500	MRA-1247	BEI Resources
Sexual developmental stages	anti-Pfs48/45	Antigens found on gametes	1:500	MRA-316A	BEI Resources
	anti-Pfs230	Gamete surface antigen	1:250	MRA-878A	BEI Resources
	anti-Pfs16	Whole Pfs16 protein	1:5,000	MRA-1276	BEI Resources
	anti-Pfg27	Whole Pfg27 protein	1:2,000	MRA-1277	BEI Resources

3.9. Fluorescence and immunofluorescence assays

3.9.1. Fluorescent NTA

EVs were analyzed based on fluorescence by means of the fluorescent NTA mode of the ZetaView (ParticleMetrix). EVs were labelled with lipophilic dyes DiO and SP-DiO from the Lipophilic

Tracer Sample Kit (Life Technologies) and immunolabelled with monoclonal anti-band 3 antibody (Clone BIII-136, Sigma Aldrich) or monoclonal anti-spectrin (α and β) produced in mouse (SB-SP1, Sigma Aldrich) or exosome anti-CD63 mouse monoclonal antibody (Ts63, ThermoFisher Scientific). 50µL of the solutions containing purified EVs from iRBC and uRBC cultures were stained with the appropriate concentration of dyes in 500µL – 1 mL of DPBS in translucent brown microcentrifuge tubes for an initial particle dilution of 1:10 or 1:20. Dyes were both used at a concentration of 500 nM. EVs were incubated with dyes for 30 minutes at 4ºC in constant rotation. Samples were then prepared for analysis with the ZetaView by further diluting the stained samples to the microparticle dilutions established previously in section 3.5. For the immunofluorescent labelling, 50µL of the solutions containing purified EVs from iRBC and uRBC cultures were incubated for 2 hours at 4ºC with primary antibodies in 500 µL DPBS inside translucent brown microcentrifuge tubes. The anti-band 3 antibody was used at a dilution of 1:500 while the anti-spectrin antibody and the anti-CD63 antibody were used at a dilution of 1:1,000. Then, the secondary antibody was directly added to the microcentrifuge tubes to reach the desired concentration of 1:1,000. The secondary antibody used was conjugated to a fluorophore, AlexaFluor 488 F(ab') 2 fragment of goat anti-mouse IgG (H+L) (Molecular Probes). Incubation with the secondary antibody was carried out for 1 hour at 4ºC in constant rotation. Samples were then prepared for analysis with the ZetaView by further diluting the stained samples to the microparticle dilutions established previously in section 3.5. The ZNTA-F filter was used with a 488nm laser for excitation. The sensitivity was increased from 95 – 98, depending on the sample, whereas the shutter was set to 100, as when using the normal NTA filter. Fluorescence controls for the different dyes consisted of DPBS incubated with the same concentration of the dyes and diluted in the same fashion. Fluorescence controls for the immunofluorescence assays consisted of DPBS incubated in the same manner with primary and secondary antibodies or just with secondary antibodies. The analysis done by NTA was presented as a size distribution graph and short videos of the particles in solution. Controls included are DPBS labelled with both antibodies or with the secondary antibody alone.

3.9.2. Fluorescence triggered flow cytometry

EVs in solution from iRBC and uRBC cultures were diluted by a factor of 100 in DPBS for a total volume of 100µL prior to the immunolabelling. The EV dilutions were incubated with monoclonal

anti-band 3 antibody (Clone BIII-136, Sigma Aldrich) at 1:20 dilution for 15 minutes at room temperature. The secondary antibody, AlexaFluor 488 F(ab') 2 fragment of goat anti-mouse IgG (H+L) (2mg/mL; Molecular Probes), was directly added to the EV dilution at 1:33 dilution and incubated for 15 minutes at room temperature. Different amounts of DPBS were then added, depending on desired final EV dilution to be read by the instrument, either a 1:1000 or 1:10,000 final dilution. Analysis of the fluorescently labelled RBCs and EVs was performed by flow cytometry with the CytoFLEX (Beckman Coulter). An important modification done to allow visualization of small particles was the use of the violet filter (405nm) for measuring the side scatter. A bead mix was used to set up the instrument (APOGEE and Beckman Coulter). All the appropriate controls were prepared for the different types of cells and antibodies used and included: EVs labelled with primary antibody alone, EVs labelled with secondary antibody alone, DPBS incubated with both antibodies, DPBS labelled with primary antibody alone and unlabelled DPBS. The same antibody concentrations that were used for the EV samples were also used for the controls.

To find the right primary and secondary antibody concentrations, we performed a titration using different antibody volumes: 1µL, 3µL and 5µL of either the primary or the secondary antibody. We directly labelled 10µL of concentrated RBCs in 100µL DPBS with the antibodies and maintained the same incubations that were outlined earlier. Following labelling, the samples were further diluted with DPBS to reach appropriate cell concentrations to do the flow cytometric analysis with the CytoFLEX.

3.10. Proteomics and data interpretation

EVs from iRBC and uRBC cultures were isolated as described earlier and resuspended in DPBS. 40µg of total protein were separated in a 10% polyacrylamide gel. Gel electrophoresis was run, following the procedure described earlier and until the protein separation had a span of 5 cm. The gel was fixed with methanol. To help remove most of the SDS in the gel and thus reduce the interference with trypsin later, the gel was stained with Coomassie brilliant blue (BioRad) for 1 hour and de-stained with water overnight. Each lane of the gel containing a sample was cut in 5 equal bands of 1 cm with a scalpel and individually stored in microcentrifuge tubes with water.

The bands from each sample were shipped to the Proteomics platform of the CHU de Québec Research Center (Laval University, Canada) that carried out the sample digestion and protein profiling. In-gel digestion of each band was done by tryptic digestion, optimized on their robotic station. Individual bands were injected separately and analyzed for 1 hour by means of LC-MS/MS (TripleTOF 5600+ or Orbitrap Fusion). For the bioinformatics analysis, spectra from all 5 bands were mixed for each sample. Results were expressed in a semi-quantitative way by spectral counting and interpreted by means of a specialized software that will yield statistically validated matches between these spectra and their corresponding peptides. The search was performed on the database *Uniprot complete proteome homo sapiens and plasmodium falciparum*, combining both the human and the *Plasmodium* databases. Results were visualized and validated with Scaffold 4 software (Proteome Software). The criteria used for confirmation of protein identification was the identification of at least 2 unique peptides with a peptide probability of 95% or more for each individual peptide. The number of unique peptide count was maintained at 95% probability for result visualization. All reagents used for these experiments were filtered prior to use to reduce any contamination from sources such as the skin or hair.

4. Results

4.1. A heterogenous population of extracellular vesicles is released from iRBCs and uRBCs

To study the specific role of parasite-derived EVs in the blood, we first need to gain a better understanding of the morphology and composition of the EVs. To analyze these particles, we established a protocol for isolation of EVs from the supernatant of *in vitro* cultures of *P. falciparum* based on the methods from Regev-Rudzki's laboratory. The purification was based on differential centrifugation steps and various filtration steps (Figure 3A). These steps are essential to remove debris, residue and particles of other nature that are bigger or smaller than our EVs of interest. The EV isolations were performed from the culture supernatant collected when a parasitemia of ≥ 5% was reached and collected at different time points ranging from 24h-40h post-synchronization, depending of the parasite's life stage of interest. We collected EVs from uninfected cultures, i.e. a cell suspension of uninfected RBCs, to use as control for the normal EV shedding from RBCs at homeostasis.

To characterize the EVs obtained from these isolations, we first performed analysis by NTA, currently considered the gold standard for the purpose of quantifying particles in this field. This method uses the scattering of light produced by the vesicles and their Brownian motion in a liquid suspension, collected by means of a camera, to calculate the size and concentration of the microparticles. We measured the concentration of EVs in our isolations and the size distribution profile of these populations with two different commercially available NTA instruments: the NanoSight and the ZetaView. Their analysis is performed in the same manner and yields a size distribution curve from which the profile of each population is displayed (Figure 3B and 3C). As seen in the representative graphs from both instruments, there is a simultaneous release of multiple subtypes of EV populations in the EV collections; a main peak representing the most abundant population is always seen and the presence of smaller peaks/populations of higher and lower sizes, the latter representing smaller microvesicles or possibly exosomes if purely based on size, are also identified for all samples. These distributions denote the heterogeneous nature of the EV isolations from *P. falciparum*-infected and uninfected cultures as shown quantitatively in Figure 3D. The heterogenous EV populations freshly isolated were observed to display an average size of 103.5 ± 35.7nm for iRBC-EVs and 112.9 ± 36.4nm for uRBC-EVs with the NanoSight. With the

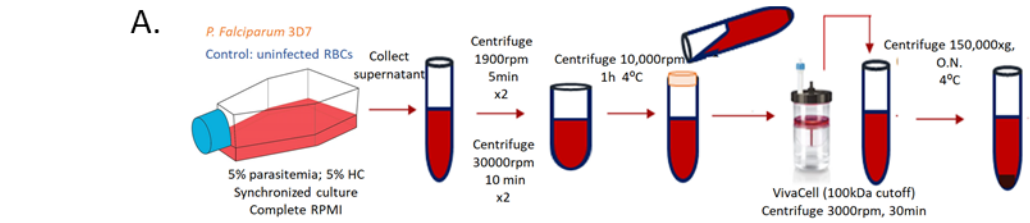

B.

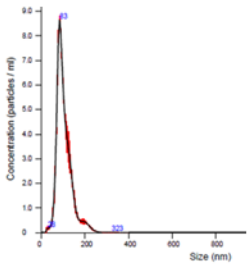

C.

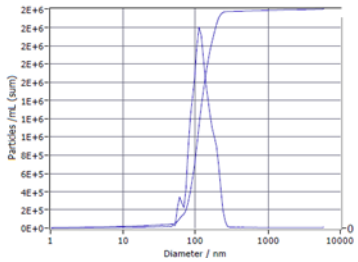

D.

		NanoSight				ZetaView			
	Sample	Concentration (particles/mL)	Mean (nm)	SD (nm)	Mode (nm)	Concentration (particles/mL)	Mean (nm)	SD (nm)	Median (nm)
FRESH	iRBC-EV	--	--	--	--	6.8×10^{12}	125.6	36	111.7
	iRBC-EV early	9.6×10^{12}	103.5	35.7	83	4.67×10^{12}	123.6	35.7	110.3
	iRBC-EV late	--	--	--	--	4.4×10^{12}	130.8	55	114.8
	uRBC-EV	4.16×10^{12}	112.9	36.4	100.4	4.0×10^{12}	127.4	47.9	113.35
FROZEN	iRBC-EV	--	--	--	--	3.67×10^{12}	132.6	55.4	117.3
	iRBC-EV early	2.09×10^{13}	88.6	36.6	76.0	2.97×10^{12}	146	62.3	123.9
	iRBC-EV late	5.02×10^{13}	84.8	38.8	78.1	2.99×10^{12}	145.9	78.3	120.9
	uRBC-EV	9.78×10^{12}	86.5	30.1	79.6	1.6×10^{12}	135.7	135.7	118.2

Figure 3. Initial detection and visualization of EVs isolated from *P. falciparum*- infected red blood cells and uninfected red blood cells *in vitro* cultures by Nanoparticle Tracking Analysis. A. EV isolation protocol based on differential sequential centrifugation and filtration steps and a final ultracentrifugation step. **B.** Example of a particle size distribution profile obtained from NTA analysis with the NanoSight. Curve is produced from averaging the measurements obtained from three 1-minute videos of one sample. This curve shows the particle size distribution of freshly isolated iRBC-derived EVs from the early life stages (0-24h). **C.** Example of a particle size distribution profile obtained from NTA analysis with the ZetaView. Curve is produced from averaging the measurements obtained from ~10seconds readings from 9 chambers. This curve shows the particle size distribution of freshly isolated early stage iRBC-derived EVs (0-24h). **D.** Particle size and particle concentration of iRBC-derived EVs and uRBC-derived EVs measured by NTA. The table compares measurements obtained from the two most commonly used instruments for NTA analysis. The measurements from the NanoSight were obtained from one single EV isolation for each sample. The measurement from the ZetaView are representative of 6 different samples (or only 4 samples in the case of uRBC-EV late). It also compares the impact of storage at -80ºC for different periods of time, denoted as frozen sample, on particle counts and particle sizes to the measurements obtained from freshly isolated EVs. Lastly, measurements were acquired from EV samples isolated at different life stages of *P. falciparum*: early stages (0-24h) and late stages (24-40h).

ZetaView, particles from the iRBC-EV isolation exhibit a mean size of 125.6 ± 36nm while the particles from the uRBC-EV isolation were observed to have a mean size of 127.4 ± 47.9nm. Although the size measurements from both instruments differ, this divergence is less important when considering the standard deviations. Also, measurements do not seem to differ significantly

between iRBC-EVs and uRBC-EVs for each machine, both actually indicating the iRBC-EVs population has a slightly smaller average size. In fact, it is important to note that neither of the instruments can accurately distinguish the different EV subpopulations present in the isolations. However, we can argue that various subpopulations of EVs are likely isolated from both cultures, although the average population size values points to a greater presence of small microvesicles in the isolations. Indeed, this would be expected from EVs derived from RBCs, previously shown to predominantly release microvesicles by analysis using dynamic light scattering methods, SEM and FACS. In fact, found at the midpoint of the size distribution from the ZetaView were microparticles of 111.7nm for iRBC-EV isolations and microparticles of 113.35nm from uRBC-EV isolations. This validates the greater abundance of small microvesicles in the EV isolations. On the other hand, particles of 83nm were perceived the most frequently in the iRBC-EV population and particles of 100.4nm were the most frequently found in the uRBC-EV population with the NanoSight. These measurements agree with the average size of the isolations, indicating that larger particles are released in the uninfected cultures. These indicate a greater presence of smaller EVs, potentially exosomes based on size alone, in the isolations and thus contradicting the conclusions inferred from the measurements with the ZetaView. Additionally, despite the different types of subpopulations observed with these instruments, the total concentration of vesicles isolated from infected and uninfected cultures were very close in range between these samples, as agreed by measurements from both instruments (Figure 3D). This indicates that the collection yield remains somewhat unchanged by the origin of the vesicles, although the results obtained from the ZetaView and mainly from the NanoSight lead us to believe there is likely a greater production of EVs from parasite infected cultures. Thus, we can conclude that microparticles are successfully isolated through the established protocol and that both instruments yield comparable results. Nonetheless, we cannot distinguish the nature of the EV subtypes since we still have no information about the biogenesis of the EVs and size alone cannot be used to identify the nature of the subpopulations.

Subsequently, we investigated the impact of the parasite's life cycle on the release of vesicles as it has previously been described to play a role in timing the release of different EV populations (Figure 3D). The parasite life stages from which originate the EVs seems to lead to a slightly different sized population; a mean size of 123.6 ± 35.7nm and 130.8 ± 55nm was observed for the

EV populations collected from the early parasite stages and the late parasite stages respectively with the ZetaView, while a median particle size of 110.3nm and 114.8nm was measured for the EVs derived from early and late stages respectively. These results suggest that EVs might be more frequently isolated from the early stages of infection and/or larger microparticles are released during the late phase of the parasite's life cycle. These differences are only noticeable in the freshly isolated samples, which reflect more accurately the naturally shed EV populations. Further analysis is required to obtain more conclusive observations.

We were also interested in testing the impact of the storage conditions on both concentration and EV size of our isolations (Figure 3D). EVs are stored at -80ºC in the same buffer in which they are resuspended following ultracentrifugation, i.e. DPBS, with no additions to the medium. With the ZetaView, we saw close to half of the amount of particles compared to fresh isolations measured with the same instrument, whereas we saw an increase in total particle numbers with the NanoSight in both iRBC-EV and uRBC-EV isolations. What remains consistent between measurements taken with both instruments following freezing is that there are higher concentrations of particles collected from the infected cultures, when compared to fresh samples. Thus, storage by freezing clearly affects the perceived concentration of EVs. Both shrinking, and particle fragmentation can provide possible explanations for these changes. In fact, the increase in particle number seen with the NanoSight is accompanied by a decrease in mean size of EVs, which likely indicates possible fragmentation of the particles and consequently justifying the changes in both the mean sizes and the EV concentrations. The mean size was reduced from 103.5 ± 35.7nm to 88.6 ± 36.6nm and 84.8 ± 38.8nm for iRBC-EVs depending on the parasite's life stage and reduced from 112.9 ± 36.4nm to 86.5 ± 30.1nm for uRBC-EVs. The difference in EV size between samples of infected and uninfected origin is also less pronounced following freezing. Interestingly, the opposite is seen with the ZetaView where an increase in mean size is observed following storage in freezer. iRBC-EVs were seen to have a mean size change from 125.6 ± 36nm to 132.6 ± 55.4nm and uRBC-EVs went up from 127.4 ± 47.9nm to 135.7 ± 135.7 nm. However, the median size of the populations remained more closely related to the ones measured from the fresh samples indicating that this increase in size might not be as dramatic as initially indicated by the average population size. Indeed, after a closer look, this increase in size is also accompanied by a big increase in standard deviation which shows that the measurements obtained are not as reliable as they are likely biased

by the presence of new EV subpopulations created as by-products of the storage conditions. Of note, the ZetaView showed overall larger standard deviation values and overall larger particle sizes than the NanoSight which was made more obvious when looking at the frozen isolations, meaning that this instrument seems to be more easily biased by the presence of a small population of very large EVs. The larger average size and mean population sizes described earlier compared to the NanoSight also elude to the possibility of greater bias towards bigger particles. These discrepancies could also indicate that the ZetaView is a more sensitive instrument than the NanoSight which can impact the interpretation of the results.

Then, we corroborated the presence of the heterogenous EV populations in our isolates by flow cytometry to further validate our isolation method. The instrument used has been optimized for the visualization of smaller particles by putting to use many new technologies such as the use of an avalanche photodiode and a violet laser for side scatter measurements. Unlike conventional flow cytometry, this fine-tuned instrument is slowly gaining status in the EV field. With this instrument, we observed a clear increase in total number of particles being acquired in the iRBC-EV and uRBC-EV samples compared to the DPBS control (Figure 4A). There is approx. 10 times more particles in the iRBC-EV sample and approx. a 27-fold increase in total particle number in the uRBC-EV sample compared to the number of particles counted in the DPBS control. The increase in presence of microparticles in the samples is clearly illustrated in the dot plot overlay comparing the number of events quantified for the uRBC-EV sample and control DPBS (Figure 4B). This suggests that more particles of small size are present in the EV isolations and that higher amounts of particles were isolated from the uninfected cultures. Although it is not possible to differentiate our particles of interest from any debris found in the DPBS without specific tagging of the vesicles, these results imply the successful collection of EVs from our *in vitro* cultures. Following background correction, an estimated 1.7×10^9 and 4.7×10^9 EVs are estimated to be found in the iRBC-EV and uRBC-EV samples respectively, which represents a 1,000 to 10,000-fold lower count than what was calculated by NTA (Figure 4C). Since total particle concentration numbers are low in comparison to NTA, it suggests that the instrument's sensitivity diminishes due to the background that hides the smaller particles. In turn, this lack in sensitivity explains why we also counted more particles in the uRBC-EV sample than in the iRBC-EV sample which contradicts the observations from NTA. Furthermore, despite the lack of optimization, we analyzed

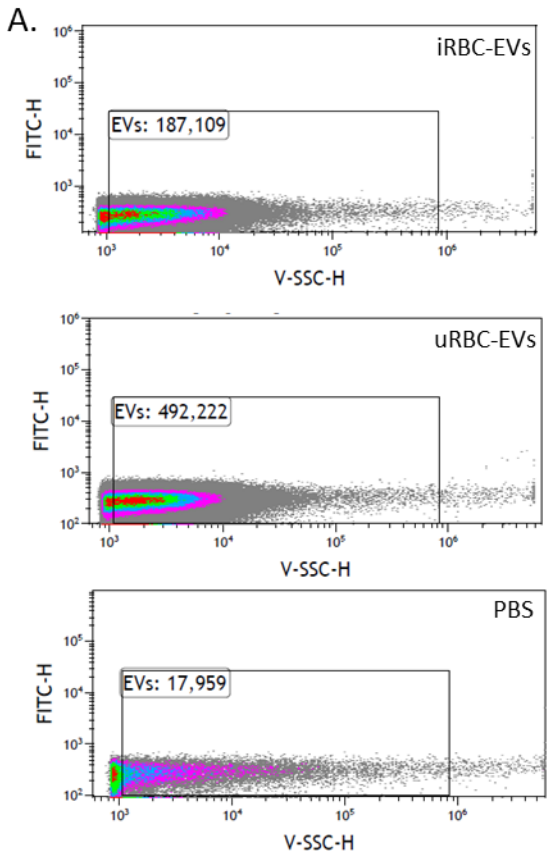

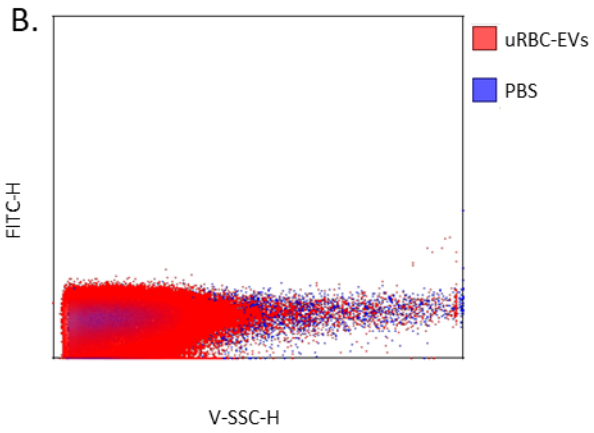

C.

Sample	Particle count 1 : 10000 dilution (particles/mL)	Particle count PBS-corrected 1 : 10000 dilution (particles/mL)	Estimated EV concentration (particles/mL)
iRBC-derived EVs	187 109	169 150	1.7×10^9
uRBC-derived EVs	492 222	474 263	4.7×10^9
PBS	17 959	0	----

Figure 4. Enumeration of EV populations isolated from iRBC and uRBC cultures by flow cytometry. A. Representative flow cytometry plots with gate placed to identify the heterogenous EV population. Sample in top plot: iRBC-derived EVs diluted in DPBS; sample in middle plot: uRBC-derived EVs diluted in DPBS; bottom plot: DPBS, denoted as simply PBS on plot (background). Measurements obtained by using the violet laser for the SSC to increase sensitivity towards microparticles. **B.** Overlay of gated population from flow cytometry plots from iRBC-EVs and DPBS to show the difference in amount of particles read per sample. **C.** Summary table of microparticle count and estimated EV concentration measured by means of flow cytometry for iRBC-EVs and uRBC-EVs. Measurements are representative of one reading.

the size of the EVs. In reference to the polysterene bead mix used for calibration of the instrument, this characterization method points to the presence of microparticles ranging in size from 75-150nm (data not shown).

Collectively, we were able to assess the value of the isolation technique used throughout this study.

4.2. Structurally similar lipid-rich particles are collected from iRBC and uRBC cultures

Since NTA analysis cannot actually visualize the EVs, i.e. it cannot distinguish between non-vesicular particles and EVs as it only infers their presence from the particle's light scattering, we performed scanning electron microscopy (SEM) analysis of our EV isolations to observe the individual morphology of these vesicles and obtain more information on their structure. We imaged the vesicles from iRBC-EV and uRBC-EV samples at various magnifications: 10,000 x, 20,000 x and approx. 30,000 x, the latter being the greatest magnification at which an adequate

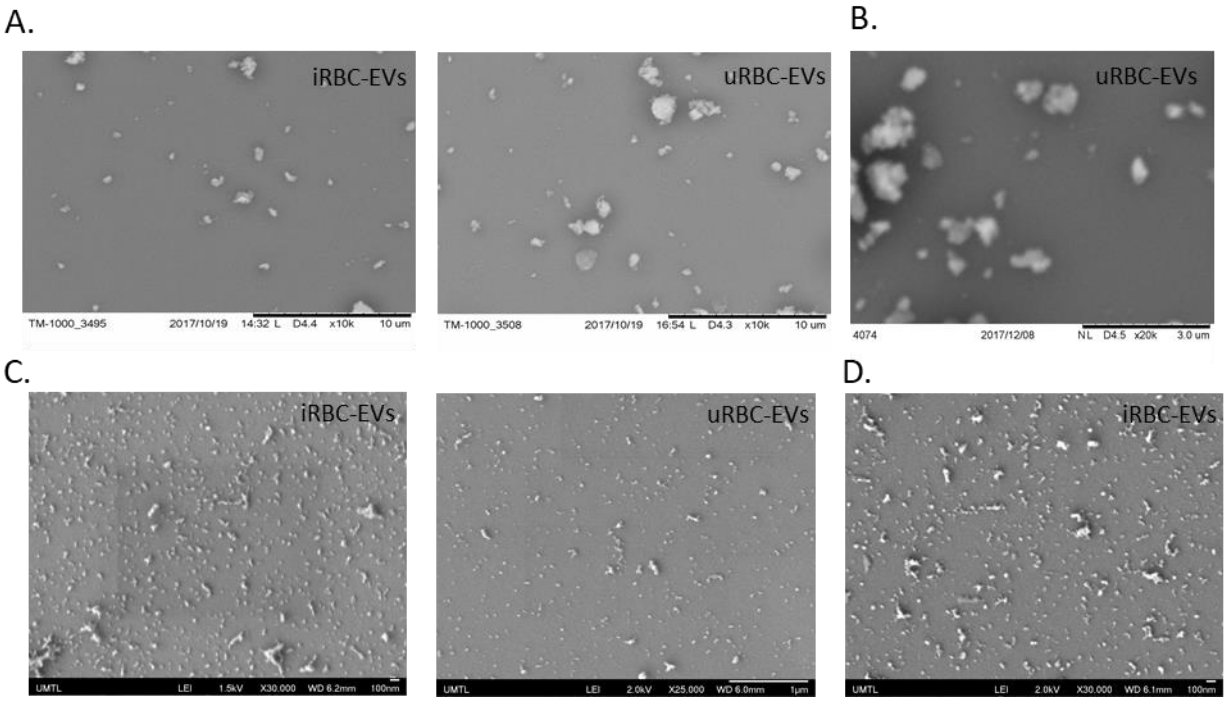

Figure 5. Characterization of morphology and homogeneity of EV isolations from iRBC and uRBC cultures. A. Scanning electron microscopy analysis of iRBC-EVs and uRBC-EVs populations at 10,000x magnification using Hitachi TM-100 SEM. All EVs were freshly isolated before starting the fixation process. Poly-L-lysine coated coverslips were used to mount the EV samples. Scale bar: 10 µm. **B.** Scanning electron microscopy analysis of uRBC-EVs population at 20,000x magnification using Hitachi TM-3000 SEM. EVs were freshly isolated before starting the fixation process. Poly-L-lysine coated coverslips were used to mount the EV samples. Scale bar: 3µm. **C.** Scanning electron microscopy analysis of iRBC-EVs at 30,000x magnification and uRBC-EV populations at 25,000x magnification using JSM-7400F SEM. iRBC-EVs were isolated from a culture that was enriched for iRBCs at the trophozoite stage by means of an Easycoll or Percoll gradient before collection of the media. uRBC-EVs were collected without the enrichment step. Both EV samples were freshly isolated. Poly-L-lysine coated polished titanium disks were used to mount the samples. The scale bar is indicated below each image. **D.** Scanning electron microscopy analysis of EV population from an enriched iRBC culture imaged in the same way as in (C). However, the sample was mounted on an uncoated polished titanium disk.

resolution was still maintained (Figure 5A-D). At the lowest magnification, the same EV profile was revealed in iRBC-EV and uRBC-EV preparations (Figure 5A). Indeed, we observed individual particles of spherical or almost spherical shape and of a size ranging from 100nm to 500nm in diameter. However, these EVs are very small and their morphology is hard to distinguish at this magnification. At 20,000 x, it is still difficult to discern the structure of the microparticles, as demonstrated with the uRBC-EV sample (Figure 5B). The magnification here is so high that it impacts the resolution. At both magnifications, a lot of bigger non-spherical particles were present in these preparations. The majority of these seem to be aggregates of multiple particles, likely aggregates of approx. four to five EVs, and are less than 1µm in size. The rest of the bigger particles of approx. 1-2µm likely demonstrate the presence of cell fragments. Moreover, a greater proportion of these aggregates and cell fragments were seen in the uRBC-EV sample, which speaks more about the challenging sample preparation than the nature of the EV populations. Finally, at the highest magnification, spherical or nearly spherical particles of approx. 100-150nm and of no more than 200nm in size were most frequently seen in both preparations (Figure 5C and D). Particles of diameters below 100nm may be present in these samples but cannot be distinguished at the current magnification. The bigger particles seem to lose their spherical shape the most and look more oval or elongated than their counterparts. Overall, a clear heterogenous population of EVs is denoted in both samples with various subpopulations present. The majority of the EV populations in these preparations are separate particles. Also, the use of poly-L-lysine to cover the disks onto which the EV samples were placed does not seem to impact the EV subpopulations observed, as the particle profile seen without the use of poly-L-lysine is similar to the poly-L-lysine treated samples (Figure 5D). Nonetheless, there are aggregates and cell fragments of an estimated 500nm in diameter found in all preparations, but their numbers are reduced compared to previous samples analyzed at lower magnifications. Interestingly, the presence of these clusters of vesicles speak to their membrane lipid content that makes them stick to each other, which is in fact to be expected due to their nature and their mechanisms of biogenesis.

To further confirm the vesicular nature of the microparticles found in our isolations and evaluate their lipid content denoted by SEM, we performed fluorescent NTA analysis on EVs labelled with two closely related lipophilic dyes. We used DiO and SP-DiO, an anionic sulfophenyl derivative of DiO, which easily insert into the lipid membrane of EVs and emit fluorescence when excited at

A.

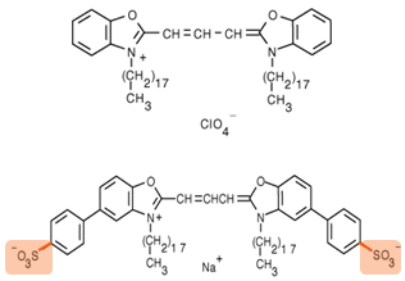

B.

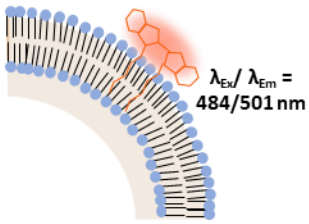

C.

Sample	[EVs] in solution (particles/mL)	[Fluorescent Particles] (particles/mL)	[Fluorescent Particles] corrected for background (particles/mL)	% EVs tagged with DiO
iRBC-derived EVs	7.95×10^{12}	1.4×10^{12}	1.4×10^{12}	17.6
uRBC-derived EVs	8.7×10^{12}	2.1×10^{12}	8.7×10^{12}	24.1
No EVs + DiO	----	4.3×10^{9}	----	----

D.

Sample	[EVs] in solution (particles/mL)	[Fluorescent Particles] (particles/mL)	[Fluorescent Particles] corrected for background (particles/mL)	% EVs tagged with SP-DiO
iRBC-derived EVs	7.95×10^{12}	1.9×10^{12}	1.9×10^{12}	23.7
uRBC-derived EVs	8.7×10^{12}	2.2×10^{12}	2.18×10^{12}	25.1
No EVs + SP-DiO	----	1.6×10^{10}	----	----

Figure 6. Fluorescent tagging of iRBC-EVs and uRBC-EVs for enumeration. A. Lipophilic dye 'DiO' chemical structure (top) and lipophilic dye 'SP-DiO' chemical structure (bottom). SP-DiO is the anionic sulfophenyl derivative of DiO. **B.** Interaction between DiO fluorescent dye and the lipid bilayer of EVs. SP-DiO interacts in the same manner. **C.** Fluorescent particle concentration and total fluorescent labelling efficacy measured by NTA in fluorescent mode (done with the ZetaView) following staining of iRBC-EVs and uRBC-EVs with 500nM DiO (n=2). **D.** Fluorescent particle concentration and total fluorescent labelling efficacy measured by NTA in fluorescence mode (done with the ZetaView) following staining of iRBC-EVs and uRBC-EVs with 500nM SP-DiO (n=2).

a wavelength of 484nm (Figure 6A and B). Since EVs are products of the host cell membrane, we expect them to have a similar membrane composition to RBCs and remain closely related whether they are collected from an uninfected or infected culture. We observed a tagging efficiency of 17.6% of iRBC-EVs and 24.1% of uRBC-EVs with DiO (Figure 5C). Similarly, 23.7% of iRBC-EVs and 25.1% of uRBC-EVs displayed fluorescence when tagged with SP-DiO (Figure 6D). These results show the lipid nature of the vesicles and demonstrate the presence of vesicles in our isolations. Nonetheless, the majority of the particles present in the samples were not successfully tagged, which indicates that the labeling protocol has to be further optimized to reach better labelling efficiency of our particles of interest. Arguably, these results could also denote the presence of microparticles of non-vesicular nature in the EV isolations. Although it is probable

that a small portion of the isolated particles are of non-vesicular nature, we believe we cannot reach such conclusion without optimizing the staining protocol first. Interestingly, when conventional NTA analysis was done on these samples, the quantity of EVs calculated was in the same range as when no dye was added to the EVs, suggesting that the crystal complexes created by the dye were not visible without the fluorescent filter, as was expected, meaning that they do not interfere with EV enumeration when no fluorescence is applied. To further justify our observations, the same lipophilic dyes were tested on the EV suspensions for analysis by flow cytometry (data not shown). The background created by the agglomeration of dye particles and formation of micelles, due to their crystal nature, was too big and made it difficult to find the particles of interest among the noise. Although, we demonstrate the lipid nature of the EVs by fluorescent NTA, the flow cytometry analysis indicates that other lipophilic dyes should be tested to achieve better results.

In conclusion, similar EV subpopulations were released from uninfected RBCs and parasite-infected RBCs. Despite our inability to clearly discern structural differences between samples due to the limitations of the instruments used, we can confirm the vesicular nature of our isolations by fluorescently tagging of the membrane lipid content.

4.3. iRBC-EVs carry host cell markers and parasite-specific markers

Following initial morphological characterization of vesicles isolated from infected and uninfected RBC cultures and underlining of the similarities between the two heterogenous populations, we were interested in finding markers that are differentially expressed in the two EV populations. To further pursue the characterization, we investigated the presence of different host-specific and parasite-specific proteins in iRBC-EVs and uRBC-EVs by means of immunoblotting. We focused our attention on RBC-specific markers band 3 and spectrin due to their abundant presence on the RBC membrane and in the cytoplasm respectively, and because previous studies have demonstrated their presence on RBC-derived EVs (Figure 7A). The value of identifying these host-specific markers is in that they can serve to segregate EVs from other types of similar sized-microparticles and to segregate RBC-derived EVs from EVs of other sources, since band 3 is almost exclusively found in RBCs. Both proteins were found to be carried by iRBC-EVs and

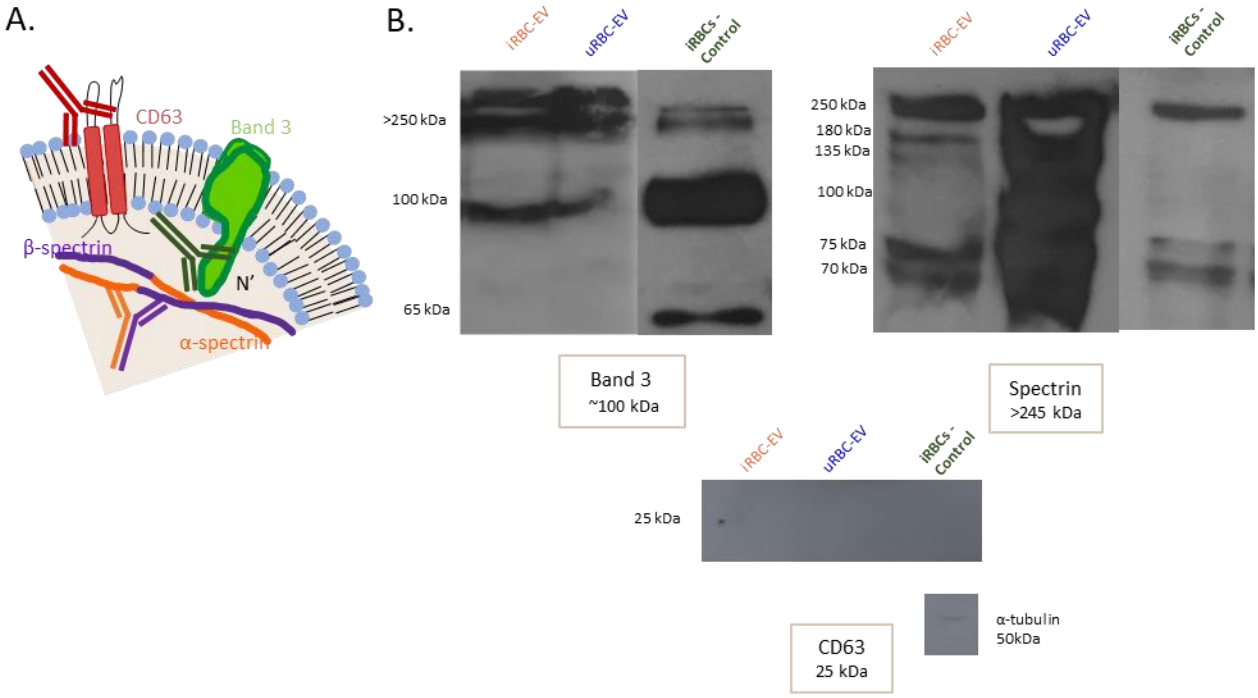

Figure 7. Detection of erythrocyte-specific and EV-specific markers on iRBC-EVs and uRBC-EVs by Western blot. A. Representation of three primary antibodies of interest, anti-band 3 antibody, anti-spectrin antibody and anti-CD63 antibody, and their known targets on EVs. **B.** Immunoblotting analysis for expression of non-parasite specific antigens on iRBC-EVs and uRBC-EVs, i.e. the control EVs. Antigens of interest were erythrocyte-specific band 3 membrane receptor (100kDa), cytoskeletal-specific spectrin (230-250kDa) and exosome-specific marker CD63 (25kDa). The pico chemiluminescent substrate was used for band 3 and spectrin detection and the film was exposed to membrane for 1 hour for EV samples and exposed for 15 minutes for control iRBC lysates. The femto chemiluminescent substrate was used for spectrin and CD63 detection and film was exposed for 10 minutes. Other controls include parasite lysates from an *in vitro* culture as loading and positive controls and α-tubulin from the iRBC control as loading control. The lysis buffer used for protein preparations was RIPA buffer 2 for proteins tested for band 3 expression and RIPA buffer 1 for the proteins used to test for the expression of spectrin and CD63.

uRBC-EVs, using iRBC culture lysates as control (Figure 7B). For band 3, we also identified a heavier band 3 complex of agglomerated proteins migrating at a very high molecular weight, as can also be observed in the control. This was expected as these band 3 complexes also form on the RBC's surface, depending on the cell's activation state instigated as a response to stimuli such as oxidative stress, as a result of normal cell aging and as a consequence of different disease states (91, 92).

For spectrin, a heterodimer formed of an α-subunit of 230kDa and a β-subunit of 250kDa, the full-length subunits were detected at a molecular of approximately 245kDa. A clear separation between the presence of each band was not observed, mainly because the gel did not provide enough resolution at these molecular weights. This same intense band was observed in the iRBC control. In all samples, we also detected the presence of bands migrating at lower molecular weight which are fragments of the spectrin subunits as seen in Figure 7B. Multiple fragments, ranging in size mainly from 80-250kDa but some as small as 20kDa, have been observed using diverse antibodies in RBC ghosts previously which agrees with the bands present in the iRBC control in Figure 7B (93). The two most prevalent fragments observed in the iRBC control were of approx. 75 and 70kDa which were both observed to also be carried by iRBC-EVs and uRBC-EVs. EVs from both sources also carried fragments of 135kDa and 180kDa while a 100kDa fragment was only found in uRBC-EVs. Faint bands of similar weights were seen in the control as well. This goes to show that EVs carry the full-length proteins found in the parent cell and also carry many of the fragments already present in RBCs. Thus, host-specific markers have been found that identify both EV populations, opening the path to further evaluation of other more specific markers.

Since the nature of the EVs isolated from *P. falciparum*-infected RBCs remains uncharacterized, we tested our EV isolations for CD63 expression, a widely-accepted marker for exosomes (Figure 7A). No apparent expression of CD63 in either of our EV populations was detected, even when using the chemiluminescent substrate potent enough to distinguish quantities of protein in the femto range (Figure 7B). This protein was also not detected in the control. This indicates that, even though this protein has been thought to be enriched in exosomes, it is not found on the EVs produced from RBCs. This agrees with previous findings that showed that microvesicles were solely produced by RBCs in circulation. Furthermore, α-tubulin was used as a loading control to confirm the appropriate transfer of the proteins from the gel onto the PVDF membrane which in turns ensures the lack of CD63 expression from all samples was not a result of unsuccessful protein transfer and confirms its absence from RBC membranes.

To detect a potential set of parasite-specific antigens uniquely present on iRBC-EVs, we targeted *P. falciparum*-specific proteins that play various important roles in the parasite's survival as well as proteins expressed at distinct time points of the parasite's life cycle, since timing of EV release is still not fully understood, as we have shown in Figure 1D. We successfully identified several

parasite-specific markers uniquely expressed in iRBC-EVs (Figure 8). Plasmepsin II and histoaspartic protease (HAP), both proteins found in the parasite's digestive vacuole and involved in host cell's hemoglobin degradation, were identified in iRBC-EVs (Figure 8A). Both isoforms at 51 and 37 kDa were identified, with the most abundant expression seen for the 37 kDa isoform. None of these enzymes were detected in the uRBC-EV samples. A housekeeping protein playing the role of a chaperone and previously identified as a stress-related marker, PfGRP78-BiP, was also identified solely in the EVs collected from infected cultures at the correct expected molecular weight of approx.75 kDa with two different antibodies (Figure 8B). In addition to this expected band, for antibody MRA-1246, the anti-PfGRP78-BiP antibody produced in rabbit, small bands of lower molecular weights were observed in both EV samples, at the same weights for both. This suggests this antibody is probably cross-reacting non-specifically with some other proteins present in all RBC-EVs. On the other hand, antibody MRA-1247, the anti-PfGRP78-BiP antibody produced in rat, did not display this cross-reactivity with other smaller proteins but did tag a lower weight protein in the uRBC-EV sample that is not tagged in the iRBC-EV sample. Nevertheless, PfGRP78-BiP is identified to be a parasite-specific marker on EVs as the correct protein was identified solely in iRBC-EVs. We also investigated the presence of components of the parasite's membrane on the surface of EVs. Despite testing 4 different antibodies targeting different epitopes of AMA-1, the apical membrane antigen-1 found on merozoites, only one can confidently identify this protein as a parasite-specific marker (Figure 8D). Antibody MRA-480, targeting AMA-1 and produced in a murine hybridoma cell line, identified a band at the expected weight of 70-80kDa uniquely in iRBC-EVs. The other antibodies demonstrated the presence of the protein of the appropriate size in the uninfected EVs as well or did not tag the protein in any of the samples. Our results corroborate previous findings that have identified this protein on the surface of iRBC-EVs but suggest that there are some epitopes that need to be preferentially tagged to be able to use this protein as a specific iRBC-EV marker. Another membrane protein previously identified on EV's surface by Marti *et al*., EBA-175, a merozoite invasion protein, was not observed to be carried by our iRBC-EVs with either of the antibodies examined (Figure 8C). The absence of this protein was also noted in uRBC-EVs. Lastly, as it has not previously been pursued, we investigated the presence of sexual stage related antigens on the EVs as potential markers (Figure 8E). As expected, most of the targeted proteins with the available antibodies were not observed to be carried by iRBC-EVs. This correlates with the proposition that other studies have put forward; they indicate

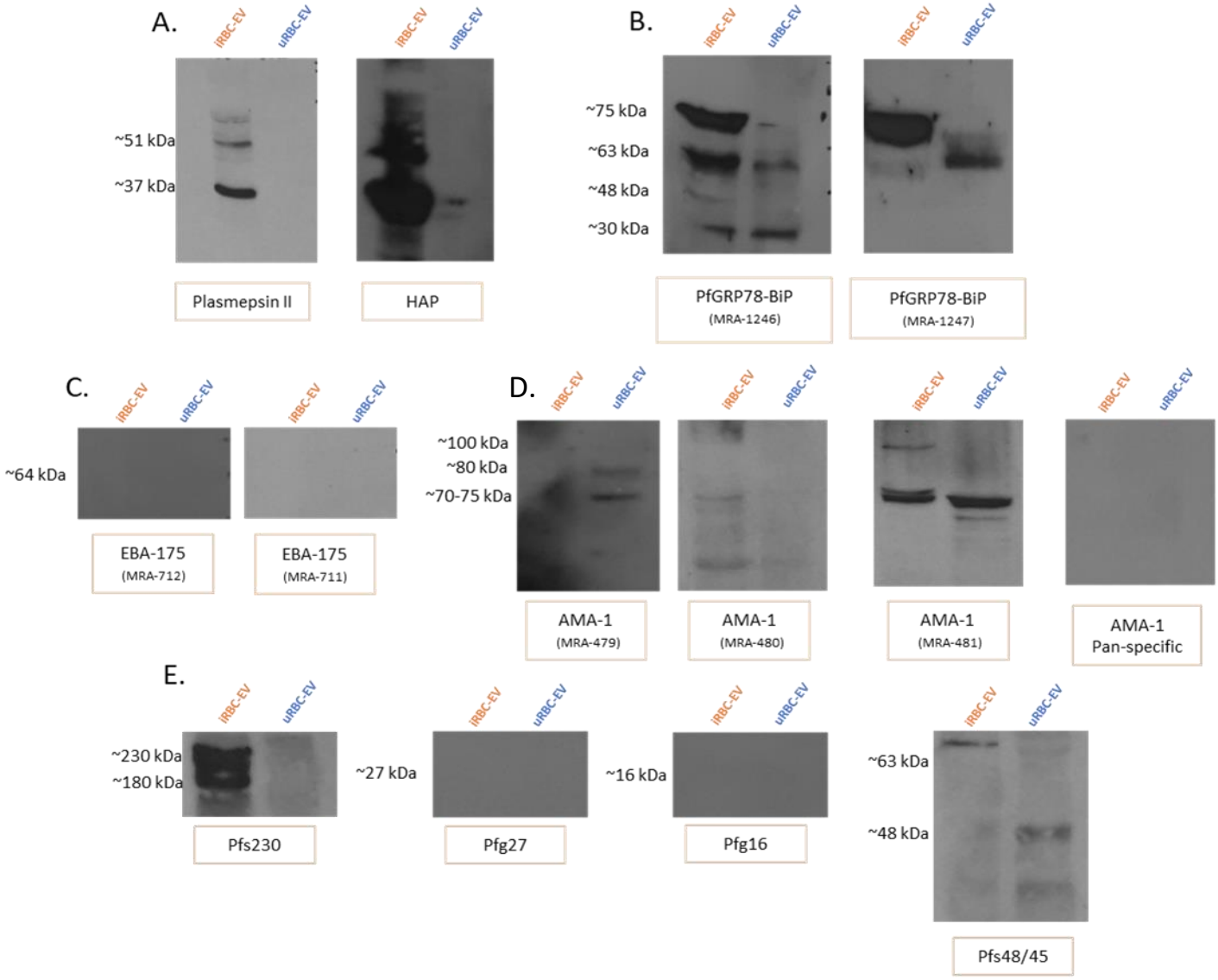

Figure 8. Identification of parasite-specific antigens exclusively carried in iRBC-EVs by Western blot. Immunoblotting analysis for detection of different parasite-specific antigens in iRBC-EVs. Controls include uRBC-EVs as negative controls. Not shown, all iRBC-EVs were also always tested for band 3 marker and were always positive. The lysis buffer used for all protein preparations was RIPA buffer 2 and exposure of film was 1 hour. **A.** Detection of enzymes required by the parasite for hemoglobin degradation inside the digestive vacuole: plasmepsin II and HAP, both visible at 51 and 37kDa. **B.** Detection of chaperone protein PfGRP78-BiP of expected molecular weight of 75-78 kDa with anti-PfGRP78-BiP (MRA-1246) and anti-PfGRP78-BiP (MRA-1247) **C.** Detection of protein required for merozoite invasion: EBA-175, of expected molecular weight of 64 kDa with Anti-EBA 175 (MRA-711) and anti-EBA 175 (MRA-712) **D.** Detection of protein found at the apical membrane in merozoite stage: AMA-1, of expected molecular weight of 70-80 kDa with nti-AMA-1 (MRA-479), anti-AMA-1 (MRA-480), anti-AMA-1 (MRA-481) and Anti-AMA-1 pan-specific **E.** Detetion of proteins necessary for the sexual developmental stages: Pfs230 of 230 kDa, Pfg27 of 27 kDa, Pfs16 of 16 kDa and Pfs48/45 of 48 kDa. Refer to methods for antibody dilutions and specific targets.

that the EVs tend to be produced in earlier stages of the life cycle since most of the proteins targeted in Figure 8E are produced during gametocytogenesis or very late post-infection (94). Surprisingly, Pfs230 was detected at the appropriate weight uniquely in the iRBC-EV sample despite being primarily expressed at the gamete stage, although the production of this protein starts earlier in the life cycle. This highlights our need to better understand the markers and contents of the EVs, as this is key to understand more about the mechanisms used for their secretion and their role within the host.

By immunoblotting, we have validated the presence of common RBC-specific markers carried by iRBC-EVs and uRBC-EVs. Moreover, we can confidently affirm that there is a difference in contents between the EVs collected from the two different sources and that there is a specific set of parasite-specific proteins that can be used as markers to identify each population of EVs. With the antibodies accessible to us at the time of this study, we have identified plasmepsin II, histoaspartic protease, PfGRP78-BiP, AMA-1 and Pfs230 as parasite-specific markers found only on iRBC-EVs and not on uRBC-EVs. These findings also highlight the importance of understanding the role of EVs during a *P. falciparum* infection and the relevance of the parasite-specific materials found in the EVs. Thus, we need to study the EVs' protein profile in greater depth to find the most suitable *P. falciparum*-specific EV markers.

4.4. Fluorescent labelling of band 3 serves as a specific marker for RBC-specific EV identification

After establishing specific markers by Western blot, we wanted to determine whether fluorescent labelling based on these markers is a suitable method for detecting RBC-derived EVs. To do so, iRBC-EVs and uRBC-EVs were incubated with RBC-specific antibodies against band 3 and spectrin and against one exosome-specific marker, CD63. Although the presence of the latter wasn't observed by Western blot, we wanted to test if this detection method was more sensitive and thus more appropriate for low-expression markers. EVs were incubated with a secondary antibody conjugated with a fluorochrome for fluorescent detection. Immunolabelled EVs were first analyzed by fluorescent NTA with the ZetaView for marker expression (Table 2). A small fraction

Table 2. Fluorescent analysis of presence of specific RBC- and EV-specific markers on iRBC-EVs by fluorescent NTA. Fluorescent particle concentration and total fluorescent labelling efficacy measured by NTA in fluorescent mode (ZetaView) following labelling of iRBC-EVs and uRBC-EVs with antigen specific antibodies and anti-mouse AlexaFluor-488 conjugated secondary antibody. Primary antibodies used were anti-band 3 antibody (1:500), anti-spectrin antibody (1:1,000) and anti-CD63 antibody (1:1,000). The secondary antibody was used at 1:1,000 dilution. Controls included are DPBS labelled with both antibodies or with the secondary antibody alone. (n=2 for band 3 and n=1 for spectrin and CD63).

		Anti-BAND 3 Antibody			Anti-Spectrin Antibody			Anti-CD63 Antibody		
Sample	[EVs] in solution (particles/mL)	[Fluorescent Particles] (particles/mL)	[Fluorescent Particles] Background corrected (particles/mL)	% EVs tagged with Antibody	[Fluorescent Particles] (particles/mL)	[Fluorescent Particles] Background corrected (particles/mL)	% EVs tagged with Antibody	[Fluorescent Particles] (particles/mL)	[Fluorescent Particles] Background corrected (particles/mL)	% EVs tagged with Antibody
iRBC-derived EVs	5.6×10^{12}	1.85×10^{11}	1.6×10^{11}	2.86	7.95×10^{10}	0	0	7.2×10^{10}	0	0
uRBC-derived EVs	3.7×10^{12}	4.03×10^{11}	3.78×10^{11}	10.22	6.25×10^{10}	0	0	2.0×10^{12}	1.25×10^{11}	3.38
Only 1°Ab + 2°Ab	----	2.5×10^{10}	----	----	4.32×10^{11}	----	----	7.5×10^{11}	----	----
Only 2°Ab	----	4.1×10^{10}	----	----	4.1×10^{10}	----	----	4.1×10^{10}	----	----

of iRBC-EVs and uRBC-EVs, 2.86% and 10.22% respectively, was positively identified for the band 3 surface marker expression, although at a lower efficiency than expected. No spectrin positive EV populations were identified. The absence of spectrin can be explained by its localization in EVs; being a cytoplasmic protein, the antibody's target is likely not accessible, making spectrin a poor marker for this method. Finally, a CD63 positive population was only observed for the uRBC-EV sample. Taking into account the results from the Western blots that demonstrated the absence of CD63 in iRBC-EVs and uRBC-EVs and combining them with the absence of detection of an iRBC-EV CD63 positive population by fluorescent NTA, it is hard to affirm the presence of CD63 on RBC-EV surfaces and instead is likely attributable to background noise.

In order to confirm that these observations were not a by-product of antibody complexes forming due to the immunolabelling method used and confirm that we in fact segregated specifically labelled EVs, we performed the same experiment with band 3 fluorescent immunolabelling of uRBC-EVs and analyzed the EVs by flow cytometry, a more widely used phenotyping tool (Figure 9A-D). As displayed on a side scatter vs. fluorescent signal dot plot, a second microparticle

population that is FITC positive is found when EVs are labelled for the band 3 surface marker in contrast to unlabelled EVs (Figure 9A). This band 3 positive population has the same side scatter profile as the EV population below, suggesting that immunoblotting and quantification of the heterogenous population was achieved. The presence of this new population is also clearly displayed in the color dot plot that superposes the particle counts for the band 3 positive population, the unlabeled EVs and the DPBS control labeled with both antibodies at the same concentrations than our samples (Figure 9B). After background correction with our DPBS controls, we estimated that 1.05% of the EV population was band 3 positive, which represents 2.3 x 10^7 band 3 positive EVs out of the 2.2 x 10^9 total EVs (Figure 9C). We believe that this fraction might be an underestimation in part due to the high abort rate noted during particle counting. We believe the samples were too concentrated for flow cytometry; thus insufficient dilutions caused the instrument to not be able to adequately discriminate adjacent cells which led to high abort rates. The low immunolabeling efficiency can also be partly explained by issues with the labeling process. Indeed, there is a striking difference in total amount of non-fluorescent particles observed in the dot plots for labeled and unlabeled samples by comparing the particle count in the EV gates of these dot plots. On the other hand, when comparing the control consisting of EVs labelled with the secondary antibody alone to the unlabeled EV sample, the increase in total particle count is not as pronounced. Thus, there is a 100-fold increase in non-fluorescent particle number created solely by the addition of the primary antibody to the samples. The same is observed with the DPBS controls, where a 100-fold increase in particle number is quantified by flow cytometry as a result of the addition of the primary antibody. This is clearly illustrated by the dot plots overlay in which the unlabeled EV population is much smaller than the populations of band 3 positive EVs and of immunolabelled DPBS (Figure 9B). This leads us to believe that the amount of debris introduced into the samples from the primary antibody is interfering with the detection of fluorescent particles and clearly skewing the perceived fraction of particles successfully immunolabelled. The overlay also highlights an overlap between the labeled EVs and the labeled DPBS in the FITC-positive gate, leading us to believe that some complexes of primary and secondary antibodies get formed and are quantified as labelled EVs, indicating that protocol optimization is required. Optimization of primary antibody concentration would be key to increase immunolabelling efficiency, as it can also lead to a reduction of debris introduced to the samples. In this study, primary and secondary antibody titrations were used to find the appropriate concentration required to obtain peak

A.

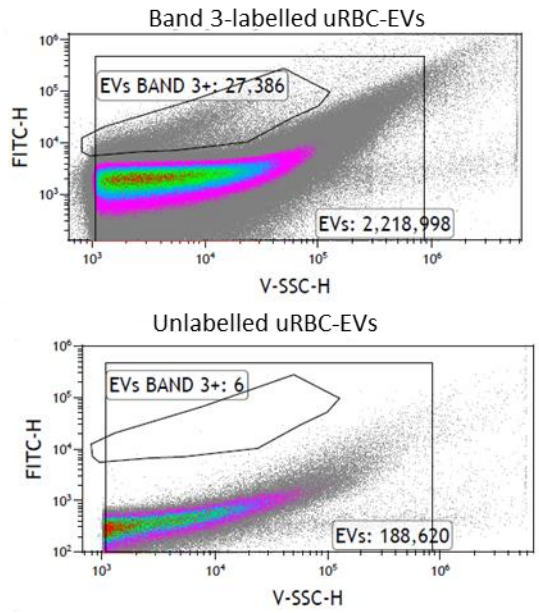

C.

Sample	Fluorescent particle count 1 : 1000 dilution (particles/mL)	Fluorescent particle count PBS-corrected (particles/mL)	Non-fluorescent particle count (particles/mL)
Labelled uRBC-EVs	27 386	2.3×10^7	2.2×10^9
uRBC-EVs labelled with 2nd antibody	1 911	----	3.2×10^8
Unlabelled uRBC-EVs	6	----	1.9×10^8
PBS labelled with antibodies	4 361	----	2.2×10^9
PBS	12	----	8.3×10^7

B.

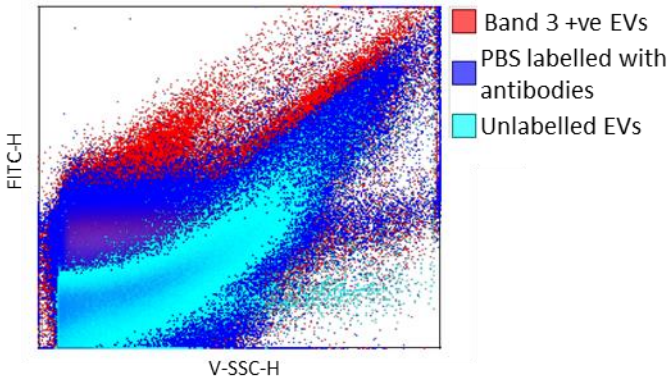

D.

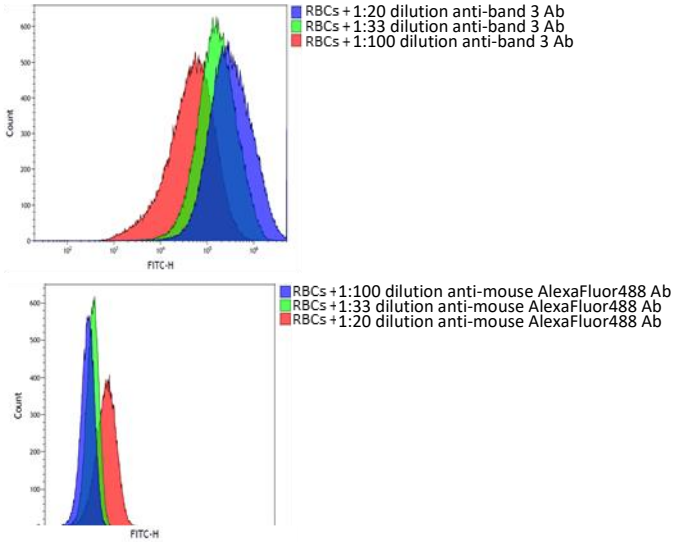

Figure 9. Band 3 positive iRBC-EV subpopulation identification by fluorescence triggered flow cytometry. **A.** Representative flow cytometry plot with gate for band 3 positive EVs (FITC positive particles). Anti-band 3 antibody were used at 1:20 dilution to label 100µl of 1:100 dilution of EV sample (here: uRBC-EV sample tested only). Anti-mouse AlexaFluor-488 conjugated secondary antibody used in the same EV sample at a 1:33 dilution. Top plot: band 3 labelled uRBC-EVs; bottom plot: unlabelled uRBC-EVs serving as negative control. Other controls included DPBS alone and DPBS labelled with both antibodies not shown here. **B.** Overlay of entire microparticle population from flow cytometry plots of labelled EVs, unlabelled EVs and DPBS labelled with both antibodies to highlight the difference in particle distribution between samples. **C.** Summary table of fluorescent particle count and band 3 positive EV count for all samples and controls. The number of total microparticles was also obtained from each sample without fluorescence. **D.** Titrations of primary antibody (anti-band 3 antibody: top graph) and secondary antibody (anti-mouse Alexa-Fluor488-conjugated antibody: bottom graph) tested directly on red blood cells. Looking at optimal antibody concentration, i.e. the highest fluorescent peak.

fluorescence levels and highest labelling efficiency (Figure 9D). We established that the use of a 1:20 dilution of the primary antibody for labeling of the RBC sample resulted in good particle count and that the use of a 1:33 dilution of the secondary antibody for labeling of the RBC sample resulted in the best FITC signal. Further work is needed to pursue analysis of fluorescent tagging of the EVs by flow cytometry. It is worth noting that even though band 3 surface marker expression was solely tested on uRBC-EVs, we expect similar results in iRBC-EVs since band 3 is a host-specific marker and its presence on iRBC-EVs has already been confirmed by Western blotting. Nonetheless, we cannot rule out the possibility of the presence of a band 3 negative EV population from either EV sample as multiple mechanisms of EV biogenesis could be taking place. Indeed, RBC vesiculation does not require band 3 phosphorylation at all times while EVs of endosomal origin would not be expected to carry band 3 on their surface either.

We know band 3 is a good marker for RBC-derived EVs from other particles of different nature present in the media and once a labelling method is properly established it will certainly serve to distinguish EVs out of the background noise that are inherent to these methods. Collectively, these results suggest that there is potential for further phenotyping of larger populations by means of fluorescent immunolabeling and that band 3 can be used to segregate the RBC-EV population from other debris co-isolated with our EV samples.

4.5. Preliminary analysis of RBC-EVs proteomes unveils insufficient levels of sample purification

Following initial morphological characterization of EVs collected from *P. falciparum*-infected cultures and detection of known specific markers, we wanted to look for novel markers. We were interested in further analyzing the proteomic profile of these vesicles by LC-MS/MS to get a deeper understanding of the nature and the cargo of the parasite-specific EVs.

Initially, to determine the best course of action for the protein digestion of our samples, we observed the protein profile by performing a protein separation by SDS-PAGE and Coomassie blue staining (Figure 10A). The separation displays an overwhelming amount of serum albumin in all samples despite the amount of total protein loaded per well and identified albumin as a clear contaminant at 65kDa. This led us to choose an in-gel digestion of our protein samples with trypsin.

The gel was divided in 5 bands and each band was digested and analyzed separately to keep the albumin contamination concentrated in one single gel band and reduce its impact on the analysis of all the proteins.

By means of LC-MS/MS, we conducted a proteomic analysis of iRBC-EVs and of uRBC-EVs as control. We did not identify any parasite-specific proteins. Although the protein composition comparison by Venn diagram indicates that 6 proteins are uniquely found in the iRBC-EV sample, these are proteins that were expected to be shared by both samples since these are RBC-specific proteins and both samples are RBC-derived (Figure 10B). These include actin, previously shown to be an abundantly present protein in RBC-EVs, carbonic anhydrase 2 and peroxiredoxin-2, both also previously found in RBC-EVs and proteasome subunits (α and β) which had not been previously identified in RBC-EVs although they are present in RBCs (Figure 10C). When the peptide threshold is lowered to 80%, 3 other unique proteins are found in the iRBC-EV sample as shown in the table below the red line (Figure 10C). Two of these, glyceraldehyde-3-phosphate dehydrogenase and GTP-binding protein, would also be expected to be found in both EV isolates since they are again RBC-specific proteins. There is one 16 kDa uncharacterized protein that was only identified in the iRBC-EV sample. We cannot speculate on the specific origin of this protein as the full *P. falciparum* genome has not been fully annotated and there are still unidentified proteins, while it has also been previously shown that RBC derived EVs can carry uncharacterized proteins. This further highlights the need for further proteomic profiling of the EVs from both types of RBC cultures. Also, we would expect to see other abundant parasite-specific proteins such as band 3 before identifying uncharacterized proteins in EVs. On the other hand, the only protein identified solely in the uRBC-EV sample is α-S1-casein. This protein is a product of contamination as it is not typically expressed in RBCs and, as a result, it would not be expected to be found on RBC-derived EVs.

Very few RBC-specific proteins were observed in both EV samples compared to previous reports (51, 55, 74, 78). Hemoglobin (α and β subunits), catalase, erythrocyte band 7, carbonic anhydrase 1, L-lactase dehydrogenase (β chain) and gelsolin were found in very low abundance in samples with catalase being the most abundant RBC-specific protein found in the iRBC-EV sample. Expected proteins of high abundance such as band 3 and spectrin, which presence on RBC-EVs is also already confirmed by immunoblotting, were not identified in any of the samples.

Overall, both EV samples display high levels of contamination and no definite conclusions can be drawn from the proteomic study, particularly regarding specific EV or parasite markers. Both samples lacked expected RBC and parasite-specific markers while the uRBC-EV sample even lacked essential RBC-specific proteins found in the other RBC samples (51, 55, 74, 78). They display proteins resulting from contamination during the isolation process and during the protein separation process. Indeed, as shown in the table, many proteins from the work environment such as the different types of keratins and collagens and trypsin were found in relatively high abundance in both EV samples. Less expectedly, numerous serum-related materials were co-isolated with the EVs: serum albumin, complement C3, C4-B and C9, immunoglobulin-λ, vitamin D-binding protein, antithrombin III, lactotransferrin and others. The abundance of albumin, the most abundant protein found by far in both samples, evidently skews the results by masking the presence and reducing the perceived abundance of low-abundance proteins.

Albumin was so abundant that it was found to be in all the bands cut from the gel, i.e. at different sizes (results not shown here). In the case of EVs, due to their size, most of the proteins of interest contained within the EVs would be found at low abundances which makes them prone to go undetected if elevated levels of contamination are seen. It is clear that albumin's ability to associate with RBC membrane proteins and its capacity to form large protein complexes makes it difficult to eliminate this protein through the filtering and centrifugation steps of our protocol. Additional purification steps need to be included in the EV isolation and purification protocol.

A.

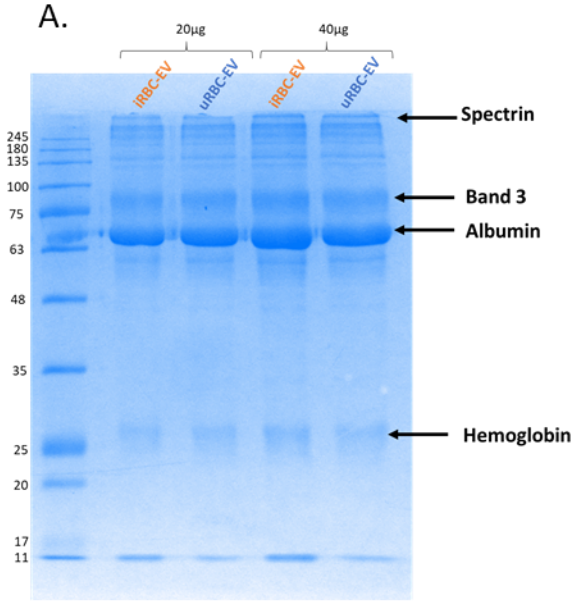

B.

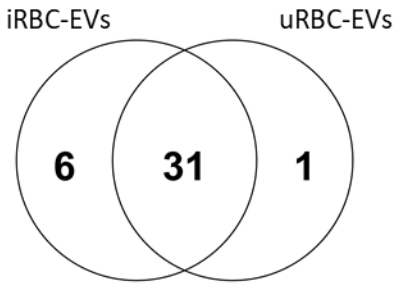

C.

Top protein hits

Protein	Molecular Weight (kDa)	iRBC-EV peptide Count	uRBC-EV peptide Count
Serum albumin	69	65	78
Keratin type II cytoskeletal 1	66	13	22
Catalase	60	9	1
Keratin type I cytoskeletal 9	62	8	8
Keratin type I cytoskeletal 10	59	7	13
Hemoglobin subunit β	16	7	5
Keratin type I cytoskeletal 16	51	7	6
Keratin type II cytoskeletal 2	65	5	10
α-2 macroglobulin	163	5	5
Hemoglobin subunit α	15	5	3
Keratin type II cytoskeletal 5	62	5	5
Complement C3	187	4	7
Serum albumin	69	4	2
Proteasome subunit β type 6	25	4	-
Trypsin	24	3	5
Collagen α-2 (I) chain	129	3	2
Keratin type II cytoskeletal 6	60	3	7
Collagen α-1 (I) chain	139	3	2
Proteasome subunit α	23	3	-
Proteasome subunit α type 5	26	3	-
Peroxiredoxin-2	22	3	-
Vitamin D-binding protein	53	2	5
Antithrombin-III	53	2	1
Lactotransferrin	77	2	2
Complement C4-B	188	2	1
Keratin type II cytoskeleton 6B	60	2	1
Complement component C9	63	2	3
L-lactase dehydrogenase B chain	37	2	2
Gelsolin	83	2	2
retinol-binding protein 4	23	2	2
Actin, cytoplasmic 1	18	2	0
carbonic anhydrase 1	21	2	1
Immunoglobulin lambda variable 2-11	13	2	1
Uncharacterized protein	16	2	-
Carbonic anhydrase 2	29	2	-
Keratin type I cytoskeletal 14	52	1	3
Erythrocyte band 7	32	0	2
alpha-S1-casein	25	-	4
glyceraldehyde-3-phosphate dehydrogenase	36	2	-
GTP-binding nuclear protein Kan	26	2	-
Isoform 5 of outer dense fiber protein 2-like	60	2	-

Figure 10. Profiling of protein content of EVs collected from infected and uninfected RBC cultures. A. Protein content profile of lysed iRBC-EV and uRBC-EV samples separated on SDS-PAGE gel and analyzed by Coomassie blue staining. 20µg and 40µg of protein preparations were loaded onto gel to find the best amount of protein to load on gel for proteomics analysis. The major bands have been associated with proteins previously shown to be carried by EVs. The lysis buffer used for the protein preparation was RIPA buffer 1. **B.** Protein composition comparison between iRBC-EVs and uRBC-EVs following proteomics analysis of samples by LC-MS/MS analysis. The Venn diagram showcases the number of unique proteins found in each sample and the number of proteins shared among the 2 isolates. Data representative of 1 biological replicate. **C.** Most abundant protein hits for iRBC-EVs and uRBC-EVs as measured by the quantity of peptide counts from proteomics analysis. Proteins were ranked by order of abundance in iRBC-EVs. It is important to notice that most proteins are non-specific to the samples studied and are the result of sample contamination. Peptides counts presented in table when peptide threshold is set at 95%. Proteins found below the red line had peptide counts below the 95% threshold but above 80% threshold.

4.6. Density based assays allow further purification of EV isolations from media-derived contaminants

To address the high levels of albumin encountered with the proteomics, we modified our EV isolation protocol to include a density-based separation of the components of concentrated conditioned media by centrifugation before pelleting the EVs by ultracentrifugation. As previously tested on EV isolations from *P. falciparum*-infected cultures, we prepared sucrose gradients ranging from 30% to 50% sucrose, i.e. 1.127 – 1.230 g/cm^3, layered concentrated conditioned media at the top of the gradient and collected each fraction from each sucrose layer of specific density following centrifugation.

We were first interested in comparing the protein profiles of the different samples by Coomassie blue staining (Figure 11A). The protein composition remained similar across samples with no major bands appearing or disappearing. The amount of albumin (~65 kDa) decreases as the density of the layer increases and appears to be notably lower in all samples than the control isolated as per the originally established protocol. The greatest albumin removal was achieved in the densest layers of each gradient tested. We also noted that the decrease in albumin concentration in the sucrose fractions resulted in an increased concentration of other major proteins such as the ones observed at 25 kDa (Hemoglobin subunit), at approx. 85 kDa (likely band 3 since it is expected to be the most abundant RBC protein on RBC-EVs) and a few other high molecular weight proteins. The 40% sucrose fraction from the first gradient seems to be the exception to this observation; although the amount of albumin was reduced, some of the higher weight bands disappeared on the gel, most likely due to failed protein denaturation process. Moreover, when comparing with another protein profile analyzed from iRBC-EV and uRBC-EV isolations from different parasite life stages, even though 4 times greater quantities of samples were loaded onto this gel, there is still a much lower concentration of any proteins other than albumin when compared to the fractions from the gradient (Figure 11D).

To identify the proteins of interest, we performed immunoblots of iRBC-EV and uRBC-EV samples using an antibody specific for albumin to observe the efficacy of albumin removal from EV samples (Figure 11B). We also used a specific antibody for band 3 detection to qualitatively confirm the presence of EVs in each fraction, as this is a host-specific marker for EVs derived from RBCs (Figure 11C). In accordance with the protein profile, a clear decrease in albumin

presence was observed in increasingly denser sucrose fractions. In fact, the band intensity of all fraction remains lower than the intensity of the control sample that was isolated without the additional purification steps. Band intensity was its lowest in the higher density fractions of each of the gradients that was tested, i.e. the 40% and 50% sucrose layers. Nonetheless, the presence of albumin was detected in all the sucrose fractions, suggesting that, while this method reduces substantially the amount of albumin particles co-isolated with EVs at any given density, particularly in the denser fractions, it cannot completely remove the albumin and albumin complexes from the isolations. Moreover, the nature of the isolation does not have an impact on levels of albumin co-isolated with the EVs as the same pattern of albumin removal was seen in both iRBC-EVs and uRBC-EVs, although with a slight lower efficacy for uRBC-EVs.

Band 3 expression (100 kDa) was observed in all fractions from the established density range, affirming the presence of RBC-derived EVs in all fractions, and further confirming the heterogeneity in size and density distribution of the EV isolates (Figure 11C). The highest band 3 expression was observed from the sample collected from the 40% sucrose layer, leading us to believe that a major part of the EV population has a density around 1.176 g/cm^3, which is not far from what other studies have suggested. This is also in the expected range for microvesicles (74). Interestingly, the higher molecular weight band representing band 3 protein aggregates and the lower molecular weight band representing cleaved band 3 proteins are observed across all iRBC-EV fractions, whereas the aggregates are clearly detected in the uRBC-EV samples and the cleaved protein bands at 63 and 45kDa are barely visible. Only the 40% sucrose fraction displays a greater expression of the 100kDa band than the band 3 aggregate band which in turn is the most intense band in all the other fractions.

In agreement with the protein profiles, there is a reduction in total protein concentration in each sample that was isolated using the gradient compared to the controls when protein content was measured by means of a BCA assay (Figure 11E). The reduced presence of albumin in each fraction likely explains these observations. The 35% and 40% sucrose fractions displayed the highest total protein concentrations which is in agreement with the observations from the immunoblots that show much higher band 3 expression in these layers as they probably carry a greater number of EVs. These results lead us to believe that the density of our EVs ranges mainly form 1.151-1.176 g/cm^3.

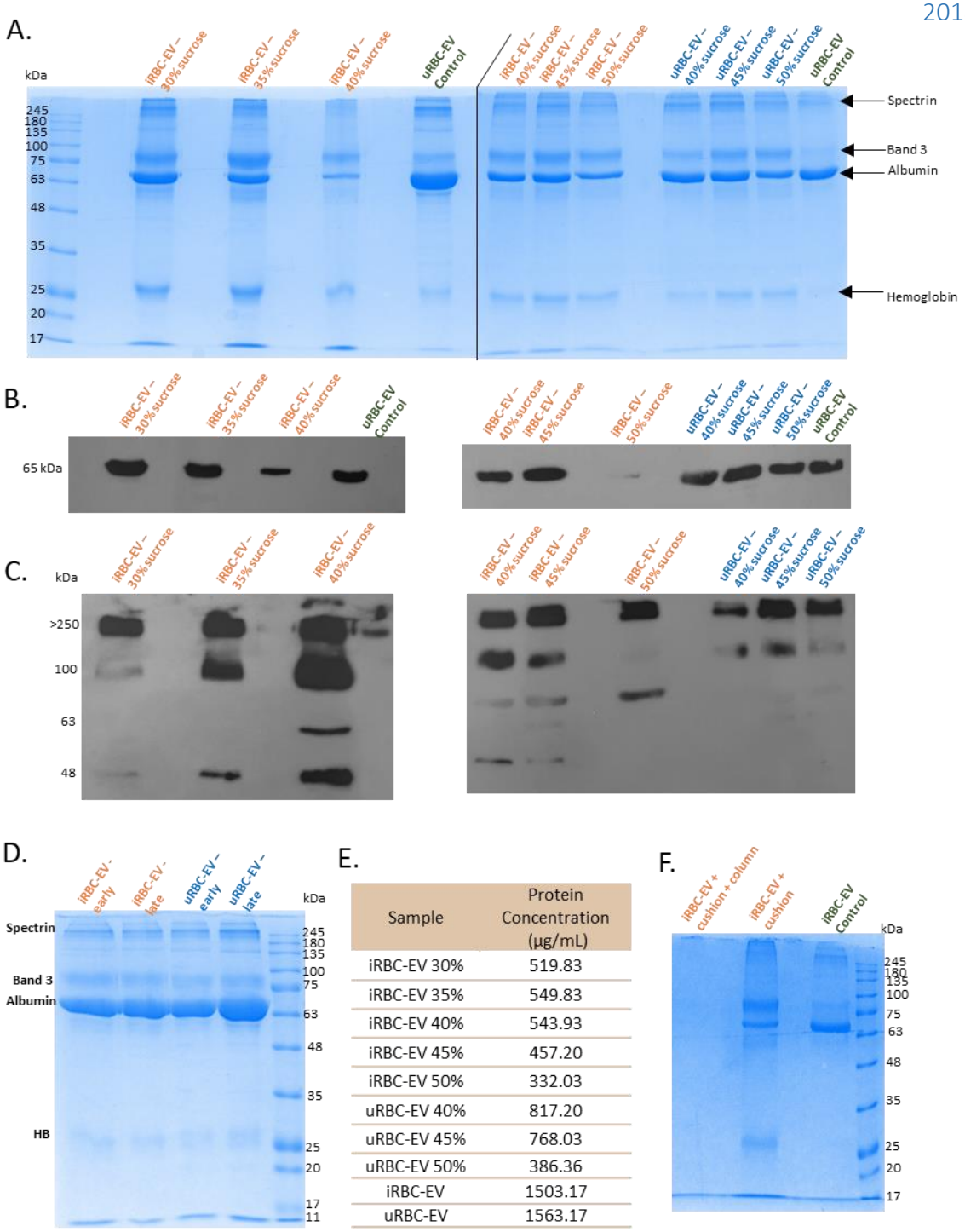

Sample	Protein Concentration (µg/mL)
iRBC-EV 30%	519.83
iRBC-EV 35%	549.83
iRBC-EV 40%	543.93
iRBC-EV 45%	457.20
iRBC-EV 50%	332.03
uRBC-EV 40%	817.20
uRBC-EV 45%	768.03
uRBC-EV 50%	386.36
iRBC-EV	1503.17
uRBC-EV	1563.17

Figure 11. Albumin depletion from EV isolations by fractionation with sucrose gradient to increase EV isolation purity. A. Coomassie blue stain of protein separation on SDS-PAGE gel of EV fractions from each sucrose layer from gradients. First gradient (left of the black line) was composed of 30%-35%-40% sucrose layers and was used to separate contents of iRBC culture media. 5µg of each sample was loaded into gel. The second gradient (right of the black line) was composed of 40%-45%-50% sucrose layers and was used to separate the contents of iRBC culture media and uRBC culture media. 4µg of each sample was loaded into gel. EVs collected from an uninfected culture without a sucrose gradient separation were used as control. The identity of the major bands seen on the gel is indicated on the right. **B.** Analysis of albumin presence (~65 kDa), co-isolated with EVs

from the culture media, in protein preparations from each fraction of the sucrose gradient by Western blot. Membrane was probed with anti-albumin antibody used at 1:10,000 dilution. Film exposure was 10 minutes. EVs collected from an uninfected culture without a sucrose gradient separation were used as control. **C.** Band 3 expression (~100 kDa and >250kDa aggregates) in protein preparations from single fractions from sucrose gradient by Western blot. Membrane was probed with anti-band 3 antibody used at 1:5,000 dilution. Film exposure was 10 minutes. EVs collected from an uninfected culture without a sucrose gradient separation were used as control. **D.** Protein profile of EVs from different life stages analyzed by Coomassie blue stain. Most abundant protein is clearly albumin. 20µg of each sample was loaded into the gel. **E.** Protein content of all sucrose fractions analyzed by BCA assay. Data are presented as a mean of 2 independent experiments except for the 30% and 35% sucrose fractions which were only prepared once. Protein content of previous isolation of EVs from infected and uninfected cultures without the use of a sucrose gradient are added as reference points. **F.** Protein profile of a fraction collected from an EV isolation using a 40% sucrose cushion and this fraction additionally passed through a commercially available albumin depletion column analyzed by Coomassie blue staining. EVs collected from an infected RBC culture without a sucrose gradient separation were used as control.

Since the lowest levels of albumin were also detected in the 40% sucrose fraction, this establishes the ideal separation density required to eliminate serum albumin without losing precious EVs from sample. Therefore, we performed a new EV isolation to test the efficiency of a 40% sucrose cushion instead of a gradient for albumin removal. The protein profile successfully reveals a pronounced removal of albumin and a higher presence of other major bands as seen from the 40% sucrose fractions from the gradients (Figure 11F). However, this protein profile was not seen following the use of a commercially available albumin removal column that uses Cibacron blue dye to interact and bind to albumin to further remove albumin from the iRBC-EV isolation; all proteins were lost. Thus, the albumin depletion kit that uses a chromatography column diluted the protein concentrations further down to the point that subsequent analysis could not detect the proteins of interest or resulted in the removal of EVs from our isolates by simultaneous binding to the column. Thus, it is not a suitable method for albumin removal from our EV samples.

Overall, improved purification of EV isolations was achieved and yielded iRBC-EV samples that were partially depleted of albumin and that displayed greater concentrations of EV proteins as a direct result of the removal of contaminants from the media. Different density layers can potentially be used to reduce albumin contamination, but the 40% sucrose showed the most promise for our purposes, which was also confirmed with the single sucrose cushion assay. Moreover, the separation by sucrose gradients has the potential to be a great method to study the role of each EV subpopulation, unless the interest is placed on whole population in which case, with this method, we lose some EVs from the spectrum to different layers.

5. Discussion

The role of EVs in parasite survival has been linked to parasite-to-host communication resulting in immunomodulation and to parasite-to-parasite communication resulting in gametocytogenesis regulation. Progress in this field is hampered by the lack of suitable methodologies, technology and lack of data reproducibility across publications. With this study, we set out to standardize the methodology used to isolate EVs from *P. falciparum*-infected RBC cultures and to study their morphology and contents. We are looking for differences in iRBC-EVs and uRBC-EVs regarding their cargo and their specific markers that will help us explain their different roles during a malaria infection. We sought to understand the impact of isolation methods on downstream investigation of specific properties uniquely associated with EVs released from RBCs infected by the malaria parasite; we require to comprehend the biological processes regulated by EVs and evaluate the limitations of the available techniques.

5.1. Isolation and characterization methodologies and their limitations

We successfully established a protocol that allowed the isolation of vesicles from *in vitro P. falciparum* RBC cultures. Validation of our isolation method was obtained by means of NTA analysis. The method of isolation we used proved to have a high particle recovery as revealed by NTA analysis but was limited by co-isolation of contaminants. Non-vesicular particles such as proteins and protein complexes such as albumin, demonstrated by the protein profiling of the EV isolations (Figure 10A), are abundantly collected with our protocol for EV collection. Indeed, high speed centrifugations have been associated with increased aggregation of particles and particle fragmentation (95). Since our isolation method includes an overnight ultracentrifugation step, the speed and length of this centrifugation are prone to lead to increased levels of unwanted protein aggregates being simultaneously collected. This indicated that our isolation protocol did not include enough purification steps; the different filtration steps were insufficient to eliminate bigger protein aggregates. We were able to improve our EV yield by combining isolation and purification methods with a density gradient that is generally associated with a low EV recovery. Replacing the last ultracentrifugation by many shorter ultracentrifugation steps using a sucrose gradient yielded purer EV isolations, depleted of albumin, albeit with lower particle concentrations. Thus, as denoted in our study, EV isolation remains the main challenge in the field and a limiting factor

to properly studying the role of EVs. As previously concluded by many groups, a combination of methods is deemed desirable following our study.

Both NTA instruments, the NanoSight and the ZetaView, denoted the presence of heterogenous EV populations in all EV samples, as shown by the size distribution curves. Despite this, we cannot accurately infer the composition and subtypes of EVs present in these populations. Indeed, this remains the biggest challenge for us too, as it would be easier to work with homogenous EV populations. The presence of microvesicles was expected, as RBCs mostly secrete microvesicles at homeostasis. In fact, the EV sizes from our study are in line with the expected sizes for RBC-derived EVs at homeostasis analyzed by other groups (55, 58). Nonetheless, the presence of exosomes cannot be ruled out and would be consistent with Regev-Rudzki *et al.*'s results that, based on size and release pathways, suggested the production of exosome-like vesicles from iRBCs into the environment. Overall, both instruments can be used interchangeably, since they yielded closely related results when looking at particle size and concentration from fresh EV isolations, suggesting the consistency of this visualization technique and the great sensitivity of the CCD camera used by these instruments. On the other hand, flow cytometric analysis for particle enumeration displayed much lower sensitivity, as up to a 10,000-fold decrease in total particle counts were observed in some samples. Although equipped with improved sensitivity compared to conventional flow cytometry thanks to the use of an avalanche photodiode and increased scatter intensity that increase the lower limit of visible particles of this instrument, the CytoFLEX failed to accurately count all the particles in the EV isolations. We conclude that the instrument likely still cannot fully discriminate smaller EVs from the background noise, making this current technology less sensitive than the NTA to study the EV populations produced by RBC cultures.

Moreover, SEM is a superior tool to study the composition of the EV subpopulations and directly measure particle size. We confirmed the observations acquired using NTA and demonstrated the heterogeneity of the EV populations from different fresh isolations by using SEM. Higher magnification revealed the presence of an abundant fraction of particles averaging a size of approx. 100nm for both iRBC-EVs and uRBC-EVs. Subsets of smaller size vesicles and subsets of larger microparticles were observed in both preparations at a similar frequency. EV populations derived from iRBC-EVs and uRBC-EVs show similar EV profiles. These observations are in line with the size distribution profiles determined by NTA, where the majority of the EV population is

concentrated near one specific size of approx. 100nm and where other peaks of smaller and larger sized particles are seen around the main peak. Therefore, not only the average size obtained by NTA with both instruments and the mode and median values match average particle size measured by SEM, the presence of smaller and bigger microparticles was validated by both detection methods. Furthermore, since the average size of EVs determined by SEM is at the upper limit of conventional exosome size and at the lower limit of the expected microvesicle size and without more information on the biogenesis of these particles based on specific markers, again, we cannot comment on the nature of the different subpopulations of EVs from these images. Further studies combining EM methods and labelling strategies have to be employed for better discrimination. Immuno-gold labelling of EVs for electron microscopy analysis and cryo-EM have recently been evaluated for this purpose with success (96, 97). Nonetheless, for morphology, greater magnifications are required to reach the desired level that would allow us to individually image EVs to better analyse their shape. From the images presented in Figure 5, we can only partly infer the shape of the particles. It would seem that the particles display mostly spherical shapes and that the bigger particles exhibit additional non-spherical shapes that we could attribute to the agglomeration of multiple vesicles. We conclude that greater magnification and resolution is required. Although SEM analysis has been performed less frequently on EVs and TEM has been shown to be used to reach better magnifications without compromising image resolution, SEM analysis is more suitable for our purposes. Indeed, SEM analysis yields clearer images of EV surfaces and requires less sample preparation, which has previously been correlated with a decrease in particle size and morphological modifications (96). It is important to reduce the impact on size and morphology since we observed the presence of various EV subpopulations. Indeed, we noted the presence of a small fraction of larger particles, mainly formed as a result of EV clustering, as previously suggested from SEM analysis of exosomes isolated from the media of two different cancer cell lines (98). The group claims this is due mainly to their natural properties regarding their inherent lipid characteristics more so than a consequence of sample preparation. This is not surprising because of the lipid nature exhibited by these lipid bilayer enclosed vesicles. As evidenced by Baj-Krzyworzeka *et al.* from platelet-derived microparticles, EVs possess intrinsic adhesion proteins that allow aggregation (99). Thus, this could be the case in our EV isolations as well. Interestingly, the presence of larger particle complexes can be predicted to be the source of the bias denoted by NTA, particularly with the ZetaView system.

Beyond accurate characterization of the EV isolates, standardization of experiments and optimization of their reproducibility is important to preserve the biological activity of the isolated EVs. Our NTA analysis of isolations that were flash frozen for long-term storage shows the impact on both number and particle size of our isolations and, also, an increase in standard deviation values in NTA measurements, all consistent with previous reports (100, 101). Many groups have associated freeze and thaw cycles with greater damage to the particles, including fragmentation and content leakage, ultimately leading to particle concentration increase and wider size distribution curves as consequence. Although not shown in our results, these observations are consistent with the size distribution curves obtained from the readings with frozen samples with both the NanoSight and the ZetaView and with the particle size and numbers observed with the NanoSight. Furthermore, particle aggregation is promoted in highly concentrated EV suspensions, where interactions between particles are heightened (100), and as indicated by our concentration values from NTA, our EV isolations are highly concentrated. As mentioned earlier, high speed centrifugation is also associated with increased aggregation of particles meaning that both the isolation and the storage methods are promoting particle aggregation (95). Subpopulations of bigger particle complexes, either formed of multiple EVs or formed of multiple contaminant proteins, can be identified by NTA, explaining the shift in size distribution profile and mean size in the frozen EV preparations analyzed with the ZetaView. This has shown to be prevented with the addition of trehalose to the PBS suspension of EVs before ultracentrifugation and storage at -80ºC, i.e. flash freezing, of the isolated microparticles (100, 102). This sugar is known for its capacity to stabilize proteins and has been used as a cryoprotectant for long-term preservation of drugs (100, 103). In one study, these same properties allowed maximum recovery of EVs from pancreatic beta-cells and were shown to stimulate cytokine secretion from the recipient cells to a greater extent than the EVs preserved without trehalose, indicating greater maintenance of the EVs' biological activity (100). Interestingly, to conserve integrity and stability, some groups also add protease inhibitors to the EV suspensions before storage (101, 104). Therefore, the freezing of the EV suspensions in saline solution alone cannot guarantee intact conservation of morphology and activity and has to be optimized through additions to the storage solution for consistent results.

As demonstrated many times over, the nature of the vesicles is dependent on the cell of origin, which leads us to believe that the parasite's stage in the asexual life cycle in the RBCs could direct

changes in morphology and composition of the vesicles. Our study highlights the importance of understanding the impact of this timely release as we have observed a lower peak of the EV population size distribution for EVs collected at early stages of the cycle, denoting the increased release of smaller vesicles, possibly more exosomes at this stage. Our findings agree with the observations from Regev-Rudzki *et al.* who identified vesicles of ~70nm in diameter by ATM released from the parasite's early stages, pointing at a major presence of EVs of smaller size secreted during these time points (75). They also concur with Mantel *et al.* that demonstrated by TEM and NTA the release of a greater number of vesicles ranging from 100-150nm in diameter from the parasite's late stages (74). We went further and tested the presence of stage-specific markers by immunoblotting analysis. Various proteins associated with the asexual parasite stages were identified in iRBC-EVs whereas proteins expressed in the parasite during the sexual stages were absent from iRBC-EVs except from Pfs230, indicating that the proteins carried in EVs are also stage-specific. Thus, even though our results and previously published studies do not reach a consensus regarding the impact of the parasite's life cycle on EV release or in dictating cargo contents, there remains no doubt that *P. falciparum* tailors its EV secretion to fit with its needs at different life stages.

The parasite's life cycle is not the only time-dependent variable that can impact our EV isolations. In fact, another drawback from our *in vitro* study of EV release regards the age of the RBCs. During prolonged storage, RBCs increase their microparticle release (77). One study has shown a 20-fold increase in EV secretion following 50 days of RBC storage at 4ºC in a preservative solution supplemented with sodium, adenine, glucose and mannitol (77). Multiple groups have also identified discrepancies in the protein profiles from RBC-derived microparticles isolated at different ages of the RBCs (77, 105, 106). One other variable noted is the impact of the donor on RBC-EV release, where the number of EVs secreted varies between donors (77). Therefore, we cannot know if these variables have impacted the EV concentrations we have observed in our samples. It will be important to take all these into consideration when optimizing EV isolation protocols.

Overall, the use of all these methods for characterization of EV populations did not yield any noticeable differential characteristics between iRBC-EVs and uRBC-EVs. The SEM analysis shows structurally similar particles of close size ranges and the NTA only showed a slight

difference in average particle size and total particle counts in the iRBC-EVs from the values obtained for uRBC-EVs. These techniques cannot be used to distinguish EVs from different sources studied here, we need more targeted studies. Thus, from our experiments, the nature of EVs remains an unanswered question. Indeed, from our data regarding structural morphology and size distribution we still cannot infer the presence of each subtype of EVs in our isolated populations. Without studying the biogenesis pathways of these EVs, we cannot further interpret our results. These studies can be achieved by attempting to identify unique membrane proteins, the presence of established markers unique to microvesicles or to exosomes, such as the presence of endosomal markers for the latter, and better understanding the lipid composition of the EVs' membranes. For instance, Regev-Rudzki *et al*. studied the role of a protein, PfPTP2, derived from the parasite's Maurer's clefts in EV release which is a required first step into better understanding the pathways of production and secretion of the EVs (75). Similarities between these vesicles carrying proteins associated with Maurer's cleft and late endosomes have been identified, providing more insight into the process of biogenesis. Due to their lipid nature, observed by agglomeration with the SEM analysis, further understanding of the organization of the lipid membrane of iRBC-EVs and uRBC-EVs would be essential to unravel the release and production mechanisms of the vesicles. As lipids associated with lipid rafts have previously been identified in higher proportions on the EV membranes, this will become an interesting avenue (51).

Broadly, methods of isolation and methods of storage can impact downstream events such as cargo packaging and their roles. Perfecting the isolation and storage methods is critical to obtain intact EV isolations that allow the study of the morphology and the identification of reliable markers on the surface or within the EVs as we have attempted throughout the study.

5.2. The use of markers for EV detection and discrimination of iRBC-EVs and uRBC-EVs

We provide evidence that fluorescent labelling of EVs is an appropriate tool for detection of RBC-EVs based on specific phenotypical characteristics. This is the first step into differentiating subpopulations within heterogenous EV isolations as the ones that are derived from our cultures. Our study focused on membrane composition as we targeted lipids and the most prevalent transmembrane protein found on the EV's lipid bilayer by distinct labelling methods and analyzed

the labeled EVs by different means. Despite their abundance, low EV labelling efficiency was observed both by fluorescent NTA and flow cytometry. As analyzed by NTA, the use of lipophilic dyes on EV preparations effectively tagged approx. a quarter of the total EVs, regardless of their origin, due to issues with the staining protocol. By flow cytometry, EVs stained with these lipophilic dyes could not adequately be identified, possibly due to the low fluorescence emitted from the dye. Moreover, a lower portion of band 3 positive EVs was detected by fluorescent NTA for EV populations of both origins than were detected with fluorescent dyes by the same method. In accordance with this observation, only a small fraction of EVs were also observed to be positive for the presence of band 3 by flow cytometry; about 1% of EVs were successfully labelled and identified with band 3 by this procedure. In fact, EVs are known to be dim particles in comparison to full size cells, partly owing to their low light scattering properties and fluorescence intensity due to their size. Being nano-sized particles, the number of copies of specific markers expressed on EVs and the lower number of binding sites due to the smaller membrane surface compared to a cell, both constitute a major limitation to this study. Indeed, it was determined in a previous study that for a protein present at a copy number of 1×10^5 on the cell of origin, only about 10 copies of this protein will be present on the derived EVs (107). Greater labelling was achieved with lipophilic dyes due to the lipid nature of these vesicles whereas band 3 is a more specific marker present at much lower abundance on the EV surface. Besides, antibody detection of the EVs required the use of a primary and secondary antibody, which further complicates specific band 3 tagging as more interactions are required in order to obtain a fluorescent signal. A directly coupled primary antibody with a bright fluorophore may help in this matter, which we are currently studying as a potential alternative.

Despite these challenges, higher labelling efficiency was predicted on the basis of the results obtained by immunoblot analysis of band 3 expression on the EVs' surface that had led us to postulate this protein as a potential EV marker. In all the EV samples and in the RBC control, we identified band 3 expression at the expected molecular weight of 100kDa. Interestingly, we also observed the presence of a >250kDa band carried by EVs and the infected host RBCs, which agrees with previous findings. Malaria parasites are known for activating band 3 phosphorylation processes, as the resulting protein aggregation leads to membrane destabilization that is essential to the parasite's survival within the host (108, 109). Phosphorylation of band 3 increases from the

ring stage to the schizont stage, subsequently leading to microvasculature adhesion and parasite egress. In turn, this leads to the release of microparticles that carry band 3 and band 3 aggregates as RBC-EVs tend to contain proteins targeted for removal (108-110). Since *P. falciparum*'s life stage seems to play a role in band 3 aggregation on the RBC's membrane, we need to carry additional investigations on the stage-specific composition of EVs as was suggested earlier by the NTA analysis that showed differences in EV numbers and sizes depending on the stage of origin of the vesicles. It would be interesting to quantify the amounts of band 3 carried by each EV population and compare it to the amounts present in infected RBCs and uninfected RBCs by measuring band intensity in Western blots and compare the abundance of the individual band 3 protein monomers and aggregates in these EVs. Based on the predicted role of band 3 in the parasite's life cycle, we would expect to see increasing aggregation of this membrane protein in EVs isolated at the later life stages. Nevertheless, band 3 is not a suitable marker to differentiate vesicles from an infected or uninfected culture and serves a better purpose as a marker of RBC-specific EVs to distinguish them from protein complexes and other contaminants that we have shown to be present in our EV isolations.

From our results, attaining the desired level of detection still remains a challenge and we conclude that there is room for optimization of fluorescent labelling methods for membrane lipids and proteins. For instance, other dyes have been linked to greater brightness levels for small particle staining, namely PKH26 (111, 112). Indeed, dyes known for their higher brightness levels are of interest as they can compensate for the lack of surface antigens on EVs. Other successful labelling strategies adequate for flow cytometry have used Annexin V, targeting phosphatidylserine on the EV surface, calcein-AM, CFSE and PKH67 (74, 97, 113, 114). Overall, the use of lipophilic dyes as an EV labelling strategy has been supported by many studies (111, 115, 116). The use of primary antibodies directly conjugated to fluorochromes such as AlexaFluor 488, FITC, PE or biotin, is also recommended. Greater purification levels of the isolated EV samples will equally allow us to attain more consistent labelling efficiencies, which can be initially addressed by albumin removal. Greater labelling efficiency can be achieved by improving the purification methods of labelled vesicles to limit the background noise created by dye or antibody complexes observed with both detection methods, i.e. NTA in fluorescent mode and fluorescence triggered flow cytometry. Some groups remove the excess dye by means of centrifugation with a sucrose gradient, which in our

case would also remove the albumin that precipitates alongside the EVs, or opt for labelling of the cell from which the EVs will originate (111, 112). Thus, from our data, we note that antibody and lipid dye concentrations have to be further optimized as they can result in an increase of background noise when not appropriately diluted or result in insufficient staining when too diluted. Also, due to the lower abundance of antigens on the EVs, labelling concentrations used for the parent cells cannot be used as reference. As a point of comparison, 500nM of DiO and SP-DiO were used for staining EVs in our experiments, whereas a final concentration of 5nM was used for staining with DiD, a lipid dye similar in nature to DiO and its derivative tested here, for flow cytometric analysis of EVs in another study (117). There is a clear discrepancy in dye concentrations across experiments that requires further analysis.

Moreover, since band 3 is a transmembrane protein, using it as a labelling marker can result in unwanted tagging of membrane fragments from damaged EVs or fragments resulting from the disruption of the RBC membrane integrity during the isolation process at any of the centrifugation steps. Therefore, the use of band 3 or other EV membrane markers can yield false positive readings by identifying small particles that are not vesicles, and subsequently overestimate the amount of microparticles expressing the marker of interest. Therefore, we need more reliable markers that will identify intact EVs. The use of anti-spectrin antibodies can be used for more targeted recognition of EVs. Although we observed no positive expression of spectrin by fluorescent NTA on either EV type, we believe this marker could be more appropriate for obtaining accurate EV counts as it would only identify fully intact vesicles. These observations are the result of a lack of labelling protocol for internal markers, as no prior permeabilization step was performed to allow better binding of the specific anti-spectrin antibody to the cytoplasmic proteins. The presence of spectrin was shown by immunoblotting analysis of both iRBC-EVs and uRBC-EVs, indicating that spectrin is carried by the vesicles of RBC origin and has the potential to be targeted for EV identification by fluorescent means.

Using fluorescent NTA we showed the absence of the exosome-specific marker CD63 on iRBC-EVs and uRBC-EVs. Since differentiating each vesicle type remains a challenge, we sought to explore some known EV-specific markers as well. Tetraspanins, also transmembrane proteins as band 3, have the potential to serve as a marker for exosomes, although they have been seen to be expressed on microvesicle membranes as well albeit at lower concentrations, and have the

potential to aid with distinguishing the subpopulations present in the heterogenous EV isolations. These observations correlate with the previous conjecture that the major component of the EV populations isolated from iRBCs and uRBCs are microvesicles of a range of sizes and not exosomes which are the specific target of this antibody. Nevertheless, no expression of CD63 was observed by Western blot analysis, pointing towards the possibility that vesicles do not actually carry this protein and that the very low signals seen by fluorescent NTA was likely due to false positive labelling or background noise. From the literature, it remains unclear if RBCs carry CD63. Indeed, lymphocyte subpopulations, granulocytes, monocytes, macrophages, activated platelets and endothelial cells are known for expressing CD63 but only a few past studies have confirmed the presence of CD63 on exosomes derived from RBCs (118, 119). As previously discussed, EV marker profiles are derived from their cell of origin, meaning that it is important to first establish the presence of a marker on the host RBC surface before looking for these on EVs released from the cells. It is also important to note that the parasite extensively modifies its host cell's membrane to fit its own purposes. Therefore, markers normally present on RBCs at homeostasis might not be present following *P. falciparum* infection, as they might be removed to make place for other more essential parasite proteins needed on the membrane to escape for e.g. the immune system. This could also provide an explanation as to why only uRBC-EVs were shown to express very low levels of CD63 whereas iRBC-EVs do not.

So far, all the markers we have successfully singled out for phenotype-based EV identification and enumeration have potential as RBC-specific markers. Of greater interest and importance for further studies is the exploration of parasite-specific markers to effectively discriminate iRBC-EVs from uRBC-EVs. Indeed, the majority of EVs collected from iRBC cultures are still released from the uRBCs as only 5-10% of the RBCs are infected with *P. falciparum*. Developing tools to study EVs of parasite origin is necessary to further our understanding of the molecular heterogeneity and specific cargo that lead to their specific downstream functions in host-pathogen interactions. Indeed, from Western blot analysis, we provide alternative targets for intact EV identification. Plasmepsin II and HAP have shown potential as parasite-specific markers. Furthermore, these soluble proteins, derived from the parasite's digestive vacuole, are found inside the EVs, making them great candidates for intact vesicle identification (120). Further experiments should assess their use for fluorescent labelling of EVs when combined with a secondary antibody conjugated

to a fluorochrome. We have found additional soluble proteins uniquely carried by iRBC-EVs such as AMA-1, chaperone PfGRP78-BiP and sexual stage specific Pfs230, the two latter not previously studied by other groups. Surprisingly, erythrocyte binding antigen EBA-175, previously identified by Mantel *et al.*, was not shown to not be carried by our iRBC-EV isolations (74). Mantel *et al*. demonstrate that EBA-175 is only peripherally associated with the released EVs, which might justify their absence in some isolates, particularly following freezing storage that has been shown to damage the membrane integrity of the stored vesicles.

Our study of differences between iRBC-EVs and uRBC-EVs has progressed but remains nonetheless incomplete. Differences in content were established by immunoblotting but we haven't identified any proteins with roles of importance in EV production and release. We have identified *P. falciparum*-derived enzymes that play important survival roles for detoxification of their immediate environment but we do not know how their incorporation into EVs and their trafficking would be beneficial to the parasites, or if even these enzymes are voluntarily packaged in the EVs. As they are required for the parasite's survival within the RBCs, this might be part of a strategy that seeks to benefit the entire parasite population. As for the identified chaperone, PfGRP78-BiP, it is known that it is a key element for the stress response of the malaria parasite as it is involved in the unfolded protein response pathway (121). Since it has been proposed time after time that EVs are mainly produced as a response to changes in the environment, it would be fitting to find components of the stress response pathways integrated in the parasite-derived EVs. Also, another study has shown the importance of the interaction between chaperones and miRNA to catalyze the packaging of the latter in exosomes (122). This could be another explanation for the presence of this chaperone within the EVs. As for AMA-1, since this protein is mainly associated with merozoites, the positive expression of this protein in our EV isolations could also indicate the co-isolation of merozoites with our EVs, meaning that this protein might actually not be found within EVs (74). We need to dig deeper in order to understand the importance of the EVs for parasite survival and understand the role of key factors in the maintenance of cell to cell communication within the host. Interfering with the mechanisms of biogenesis and EV cargo selection will allow us to study more specifically the different functions of the EVs and the elements they are trafficking. To fine-tune our understanding of parasite-specific cargo loading in future studies, we also want to produce enriched iRBC cultures to focus our analysis on the vesicles

released by the infected cells by introducing another density gradient, an Easycoll gradient as presented in the methods section, to our isolation methods that will remove uRBCs from the infected cultures. All our studies will be improved by implementing this method as it will increase the percentage of iRBC-EVs collected from the supernatants and reduce the number of uRBC-EVs collected from the infected cultures to yield results that are more representative of the EVs derived principally from parasite-infected RBCs. Following proteomics analysis, we want to sequence the miRNA contents of the vesicles. As we have been experiencing issues with obtaining clean miRNA isolations from the EV preparations, we have not been able to demonstrate any differences in this area yet. However, we understand the importance of these players in pathway regulation in cells and we want to investigate their relevance in control of communication through EVs between parasites as well. As demonstrated by Mantel *et al*., miRNAs could hold the key into understanding a few of the triggers for immunomodulation, which we believe could also be the case for gametocytogenesis, although it has not yet been established by any groups (123).

5.3. Fluorescence triggered flow cytometry

In search of sensitive and reproducible characterization methods, we have shown that fluorescence triggered flow cytometry can be used for fluorescence-based detection of EVs. This method can be used for particle enumeration based on specific EV characteristics and has been improved to identify microparticles below the detection limit of conventional flow cytometry. This tool is shown to have the capacity to quantitatively and qualitatively detect EVs. This method was initially performed for detection of viruses by Marie *et al.* and was subsequently adapted for use for detection of EVs where it has shown great promise, as equally evidenced in our study (97, 111, 124).

Here, our instrument of choice was the CytoFLEX, which uses this new technology. The enhancement in sensitivity seen with this instrument is due to the replacement of traditional side scatter (SSC) used for the light scattering parameter for particle detection, with a fluorescence parameter; SSC is performed with the violet laser of wavelength of 405nm (125). In conventional flow cytometry, only approx. 1% of the EVs labelled for specific markers and only particles >200nm in size tend to be detected due to the limitations of using the light scattering properties of EVs (118, 126). This has now been challenged by the use of fluorescence triggered flow cytometry.

Nonetheless, the labelling efficiency against band 3 was observed to be in the same range as what is expected from conventional flow cytometry. Although, our results corroborate the use of this advanced mode of detection and phenotyping of EVs with band 3 expression, we have not reached the desired levels of detection that have already been reported by other groups using other EV markers (97, 113, 127). Indeed, in a specific study aiming at identifying phosphatidylserine carrying EVs, the superior sensitivity of the fluorescence triggered detection was confirmed, as the latter technique identified 50 times more Annexin V positive microparticles than measurements obtained by conventional light scattering methods (97). Other groups have noted the same trend with fluorescence triggering and detected a significantly higher amount of labelled EVs derived from sources such as platelet free plasma (113, 127). We thus believe that the low success of EV identification by this improved method can be partly explained by the lack of proper antibody concentrations tested and the challenge of using a combination of antibodies (primary and secondary antibodies). The simple addition of primary antibody against band 3 to our preparations lead to an increase in total particle counts. Apart from demonstrating the need for better antibodies adapted for flow cytometry analysis, these observations testify to the instrument's increased sensitivity for nano-sized particles. It highlights the importance of appropriate labelling of EVs to properly discriminate them from the noise and debris that are skewing the analysis, and the necessity to employ the appropriate negative controls for accurate analysis. Indeed, the introduction of non-vesicular particles and increase in perceived background noise are also in part responsible for the low labelling efficiency. Our data also suggests some of the subjectivity surrounding the use of an instrument so close to its detection limits for particle size, as EV counts can be affected by the fluorescence threshold initially decided upon with the controls. In our case, a great volume of particles was observed in the DPBS control alone, consisting mostly of electronic noise. Drawing the line between background and small EVs of interest thus remains the biggest uncertainty attached to the use of this instrument.

Interestingly, the heterogeneity in the EV population is consistent throughout the characterization methods used as demonstrated by the range of particle sizes yielded by both NTA and flow cytometry. Nevertheless, we denoted a clear discrepancy between particle concentration determined by NTA and flow cytometry. This can be explained by the limitations of each method. Indeed, NTA has previously been associated with overestimation of EV counts, as it cannot

distinguish EVs from non-vesicular particles and will thus include the latter in the final count, although this method is notably less biased than other dynamic light scattering methods since it directly visualizes single particles (128). On the other hand, due to their size, microparticles exhibit a low refractive index that is associated with underestimation of particle sizes by flow cytometric analysis (129). In turn, this can potentially lead to underestimating total particle count if these particles that are perceived to be smaller in size and is perceived to be background noise. Additionally, the flow cytometer cannot efficiently discriminate larger microparticles from aggregated microparticles, which are a common by-product of the isolation method of choice in this study, as revealed by SEM, additionally contributing to the underestimation of total EV particles (130). Finally, the 'swarming' effect inherent to flow cytometry is also associated with underestimation of particles in solution as multiple microvesicles can be mistaken for an individual event if the laser beam reaches these microparticles at the same moment. Thus, the differences in the way these instruments operate, and their limitations are emphasized in our study during EV enumeration. The impact of the flow cytometer's limitations underline the importance of bead calibration for flow cytometry, as they are required to infer particle size from refractive index values more accurately and will be further explored by our group (97).

Our findings support the use of fluorescence triggered flow cytometry to assess the properties of the population as a whole and presents this new flow cytometry alternative as a robust tool for EV characterization. As opposed to NTA that can determine actual individual particle sizes, the flow cytometer looks at average size of the population and is more reliable for phenotypic studies. Indeed, it allows the specific targeting of populations based on specific markers, which is not possible using NTA technology. With further optimization, the different EV subpopulations could be easily segregated by means of flow cytometry based on differential marker expression. In the same line of thought, imaging flow cytometry, a new powerful alternative instrument, has also been the subject of an increasing number of studies in the EV field and in the context of a malaria infection (131). This instrument combines the fluorescent set up and the speed of analysis of a conventional flow cytometer with the use of a CCD camera, as used in instruments meant for NTA, to replace the photomultiplier tubes currently used in flow cytometers (131). The latter uses the same advanced technology to image the EVs that allows detection of particles below the diffraction limit.

5.4. Adverse effects of albumin co-isolation and other contaminants on proteomics studies

Our proteomic analysis of the EV isolations provided the rationale for additional purification methods for our EV isolation process. As pointed out previously, the proteomics study revealed high levels of albumin contamination within our preparations that visibly misrepresent the composition of the EV proteome. Albumin-derived components were also identified as sources of contamination such as IgG. In fact, contaminants from serum that were not well cleared out of the packed RBCs used for culturing could be identified in the proteomic analysis of our samples. These proteins are not found within the EVs; albumin likely adheres to the lipid-rich EV membranes, as it is known to associate with the RBC membrane. Other proteins, such as IgG and complement factors such as C3, are also often associated with the RBC membrane (132). They can co-precipitate after prolonged ultracentrifugation with our EVs of interest but as they are linked to the RBC membrane, they could equally be commonly found on the membranes of vesicles produced through budding off from the RBC membrane. Therefore, their presence should still be expected in future studies as they are potentially being carried on the surface of the EVs derived from RBCs, indicating they are part of the EVs extended proteome. Other large particles such as lipoproteins have also been shown to be co-isolated (112). Protein contamination is one of the drawbacks of differential centrifugation-based isolation techniques and is commonly experienced (88, 112). Cvjetkovic *et al.* noted that ultracentrifugations exceeding 4 hours will consistently lead to the co-isolation of proteins with the EVs (88). We run our last ultracentrifugation step overnight, for approximately 12 hours which can definitely be expected to lead to co-isolation of unwanted materials with the EVs. For this reason, we have applied a sucrose density gradient to reduce the amount of possible contaminants. Based on previous findings, human serum albumin was collected from iodixanol fractions of 1.02-1.07g/cm^3 (133). Separation of the EVs was achieved when the EVs were collected from a fraction density of 1.18g/cm^3 (133).Our results agree with those observations, since we successfully removed a considerable amount of albumin based on density differences. Our immunoblot assays for band 3 expression clearly indicate the presence of EVs derived from infected and uninfected RBCs at a density of 1.151-1.76 g/cm^3 and we find an inverse correlation between albumin abundance and fraction density based on anti-albumin detection. We also saw a reduction in total protein concentration using a BCA assay, likely reflecting the

reduction of albumin in the isolates. Albumin depletion will allow us to repeat the proteome analysis once the purification methods have been fully established to obtain unbiased and reproducible data. The removal of a significant fraction of highly abundant albumin has great implications on the detection of low abundant peptides of analogous mass. In fact, due to this 'shrouding' effect, the latter are masked during the analysis (134). Indeed, this became evident by Coomassie blue staining following separation of the proteins, where the presence of dimer albumin band correlated with a visible increase in presence of other bands of higher molecular weights on the gel. We can expand our analysis and infer the amounts of albumin present in each sucrose fraction from the band intensity, which we can use to quantify the efficiency albumin removal. By column chromatography, we showed unsuccessful sample purification and complete loss of proteins from our EV sample. Although further testing is needed, we infer that the protocol followed led to the dilution of the protein concentration in the sample to levels that could no longer be detected by our BCA assay. Due to albumin's nature, this protein will be binding to the EVs, arising the possibility that EVs are being lost by remaining bound to the column through their association to albumin, as we do not know how strong is the bond that links albumin to the EVs.

As a consequence of protein contamination, little overlap in proteome profiles was observed in our EV samples and other publications. Our iRBC-EV and uRBC-EV isolations were not shown to carry two of the most abundantly found proteins on RBCs and on RBC-derived EVs: band 3 and spectrin. RBC-EVs notably lack almost all RBC integral and cytoskeletal proteins except for band 3 and spectrin. Thus, the inconsistency of our data and the disparities between iRBC-EVs and uRBC-EVs regarding the presence of RBC-specific proteins show that our isolation method was not fully optimized when the samples were analysed. Interestingly, a few protein hits in the iRBC-EV sample correspond to observations by Mantel *et al.*, who have provided the most comprehensive proteomic study of EVs collected from *P. falciparum*-infected RBCs. These proteins were hemoglobin, catalase and carbonic anhydrases (74). Interestingly, the presence of peroxiredoxin is in line with reports of RBC-derived EVs carrying oxidized membrane proteins (74). We also observed other sources of contamination due to gel handling. Despite this drawback, in-gel denaturation of the proteins has been shown to increase the detection of proteins present at low abundance, which we had expected in the case of parasite-derived proteins. Therefore, this is not something we are looking to change, since it is not as disruptive for data analysis than highly abundant proteins such as albumin. On the other hand, it has been shown that protein extraction

procedures can modify the amount of proteins detected by MS and can help differentiate integral membrane proteins from proteins that are simply associated with RBC membranes (132).

We also believe that a more detailed study of the parasite stage-specific EV proteome has the potential to reflect processes occurring within the infected RBCs as part of the parasite's life cycle. Other methods can be combined with our isolation methods to further increase the purity of the EV isolations, including size exclusion chromatography and immunoaffinity-based methods (112, 135).

Lastly, of increasing interest to complement proteomics results is the possibility to address the metabolomics of the secreted EVs to study the changes in the metabolite composition of the EV's cargo as a consequence of the pathways taking place in the RBC following malaria parasite invasion. It will paint a better picture of the dynamics of EV release and uptake.

In summary, our findings shed light on the challenges that still need to be resolved for accurate study of EVs and their roles in *P. falciparum* survival within the human host. Moreover, our study lays the foundations necessary to pursue more in-depth studies on the nature of the parasite-derived components sorted into the vesicles and their molecular functions. EVs are critical for achieving trafficking of information and successful communication and we need to better understand the machinery used by the host cells and the parasites to produce them, sort the appropriate cargo and release them. They are a key advantage for parasites in maintaining infection of the human host as it maximizes the chances of transmission to the mosquito vector and thus represent an interesting target. Lastly, we present a comprehensive analysis of many currently used techniques in the EV field and apply them in the context of a malaria *in vitro* infection. The strength of this study lies in its combined used of different techniques to acquire data, since the establishment of methodologies remains controversial in this field.

6. Conclusion

To reach the Millennium development goals of reducing malaria incidence and mortality by 90% by 2030, particularly in the wake of increasing antimalarial resistance, will require a more comprehensive grasp of *P. falciparum*'s invasion and survival mechanisms within humans. Novel insights on the dynamic secretion of host-cell derived soluble factors known as extracellular vesicles can provide new opportunities to disrupt the parasite's life cycle. These new players are used as vehicles of cell to cell communication by which the malaria parasite exchanges valuable information and cues to regulate their survival. With this study, we sought to confirm previous findings and expand upon established knowledge. We hypothesized that the EV population produced during *P. falciparum* infection of RBCs differs in content from the EVs shed by RBCs at homeostasis to include parasite-specific information to allow communication between parasites within the host. Our data shows almost no morphological differences as a result of the cell of origin from which the EVs were released. Besides a slight decrease in average particle size observed from the iRBC-EVs, particle concentration, population heterogeneity and the almost spherical structures were maintained across EV samples as effectively observed by means of SEM analysis and by using two instruments designed to carry NTA analysis, the NanoSight and the ZetaView. However, our study provides evidence for content differences observed by Western blot. Indeed, some parasite-specific enzymes and proteins were identified to be carried solely by iRBC-EVs. As expected, we also observed an overlap in contents in all RBC-derived EVs, identifying RBC-specific markers band 3 and spectrin. Further cargo investigation was hampered by the insufficient purification levels achieved from our isolation method. We are currently in the process of optimizing albumin removal by means of a sucrose gradient to eliminate a major contaminant of our EV isolations. This will allow us to carry on more detailed studies and find unique contents in iRBC-EVs.

To achieve these goals, it was important to use a variety of techniques and tools to compare their ability to produce consistent and reproducible analyses, now one of the long-term aims in this field, since findings are limited by available technologies. We report minor differences in NTA performed with the NanoSight and the ZetaView, principally regarding the instruments' innate bias for small subpopulations of large microparticles. While NTA better illustrates the EV population distribution as a whole, SEM allows single molecule readouts and more detailed

morphological studies that complement the NTA results, despite the low magnifications used. Phenotypical studies, by means of surface protein expression and lipid membrane composition, were achieved at low efficiency by fluorescent NTA and fluorescence triggered flow cytometry. Although not fully optimized, these technologies are necessary to develop tools such as universal fluorescent markers to facilitate EV detection and subpopulation discrimination. We place a particular interest in fluorescence triggered flow cytometry, a newly introduced tool with increased sensitivity for small particles compared to conventional flow cytometry, due to its high-throughput and individual particle readouts. Western blotting was key to find initial markers and differences between EV populations from infected and uninfected RBCs. As part of our future directions, we want to employ more refined technologies to accommodate our need for larger scale studies that encompass the complete contents of the EVs to understand their mechanisms of action, such as proteomics and microRNA sequencing studies, that are underway in our laboratory. Our results suggest that, moving forward, analysis of EV populations requires the combinatorial use of various methods. They also highlight the primordial need to standardize the procedures for isolation and purification to produce consistent results. The impact of the use of non-standardized EV isolation procedures on result interpretation needs to be reduced to enhance our understanding of the key signals contained in the vesicles to fulfill their specific downstream regulatory roles.

Evidently still at the early stages of exploration and standardization, future studies should focus on establishing specific links between the presence of individual EV contents and their downstream functions. Understanding the molecular basis of these key signals and understanding where they fit in different pathways used to successfully maintain their proliferation within the human host is key. Indeed, it is essential to establish a robust causal relationship between EVs and the pathways they are known to regulate such as gametocytogenesis. This could yield new approaches to halting the mechanisms of gametocyte production and stop transmission of the disease back to the mosquito vector. Thus, in-depth profiling of EV contents can elucidate the potential of EVs as new drug targets.

7. References

1. WHO. 2016. Malaria: fact sheet. In *10/01/2016*.
2. Garcia, L. S. 2010. Malaria. *Clinics in laboratory medicine* 30: 93-129.
3. CDC. Malaria - Biology.
4. Gilson, P. R., S. A. Chisholm, B. S. Crabb, and T. F. de Koning-Ward. 2017. Host cell remodelling in malaria parasites: a new pool of potential drug targets. *Int J Parasitol* 47: 119-127.
5. Baruch, D. I., B. L. Pasloske, H. B. Singh, X. Bi, X. C. Ma, M. Feldman, T. F. Taraschi, and R. J. Howard. 1995. Cloning the P. falciparum gene encoding PfEMP1, a malarial variant antigen and adherence receptor on the surface of parasitized human erythrocytes. *Cell* 82: 77-87.
6. Chen, Q., V. Fernandez, A. Sundstrom, M. Schlichtherle, S. Datta, P. Hagblom, and M. Wahlgren. 1998. Developmental selection of var gene expression in Plasmodium falciparum. *Nature* 394: 392-395.
7. Su, X. Z., V. M. Heatwole, S. P. Wertheimer, F. Guinet, J. A. Herrfeldt, D. S. Peterson, J. A. Ravetch, and T. E. Wellems. 1995. The large diverse gene family var encodes proteins involved in cytoadherence and antigenic variation of Plasmodium falciparum-infected erythrocytes. *Cell* 82: 89-100.
8. J., N. F. a. W. N. 2007. Artemisinin-Based Combination Treatment of Falciparum Malaria. *Am. J. Trop. Med. Hyg.* 77: 181-192.
9. Spjeldnaes, A. O., A. Y. Kitua, and B. Blomberg. 2014. Education and knowledge helps combating malaria, but not degedege: a cross-sectional study in Rufiji, Tanzania. *Malar J* 13: 200.
10. Sauerwein, R. W., and T. L. Richie. 2015. Malaria vaccines getting close to clinical reality. *Vaccine* 33: 7423-7424.
11. Thera, M. A., and C. V. Plowe. 2012. Vaccines for malaria: how close are we? *Annual review of medicine* 63: 345-357.
12. Langhorne, J., F. M. Ndungu, A.-M. Sponaas, and K. Marsh. 2008. Immunity to malaria: more questions than answers. *Nature immunology* 9: 725-732.
13. Carter, R., and L. H. Miller. 1979. Evidence for environmental modulation of gametocytogenesis in Plasmodium falciparum in continuous culture. *Bull World Health Organ* 57 Suppl 1: 37-52.
14. Smalley, M. E., and J. Brown. 1981. Plasmodium falciparum gametocytogenesis stimulated by lymphocytes and serum from infected Gambian children. *Trans R Soc Trop Med Hyg* 75: 316-317.
15. Sinden, R. E. 1983. The cell biology of sexual development in plasmodium. *Parasitology* 86 (Pt 4): 7-28.
16. Duffy, S., S. Loganathan, J. P. Holleran, and V. M. Avery. 2016. Large-scale production of Plasmodium falciparum gametocytes for malaria drug discovery. *Nat. Protocols* 11: 976-992.
17. Roncales, M., J. Vidal-Mas, D. Leroy, and E. Herreros. 2012. Comparison and Optimization of Different Methods for the In Vitro Production of Plasmodium falciparum Gametocytes. *Journal of parasitology research* 2012: 927148.
18. Buckling, A., L. C. Ranford-Cartwright, A. Miles, and A. F. Read. 1999. Chloroquine increases Plasmodium falciparum gametocytogenesis in vitro. *Parasitology* 118 (Pt 4): 339-346.
19. Bruce, M. C., P. Alano, S. Duthie, and R. Carter. 1990. Commitment of the malaria parasite Plasmodium falciparum to sexual and asexual development. *Parasitology* 100 Pt 2: 191-200.
20. Trager, W., G. S. Gill, C. Lawrence, and R. L. Nagel. 1999. Plasmodium falciparum: enhanced gametocyte formation in vitro in reticulocyte-rich blood. *Experimental parasitology* 91: 115-118.
21. Schneweis, S., W. A. Maier, and H. M. Seitz. 1991. Haemolysis of infected erythrocytes--a trigger for formation of Plasmodium falciparum gametocytes? *Parasitology research* 77: 458-460.
22. Baker, D. A. 2010. Malaria gametocytogenesis. *Mol Biochem Parasitol* 172: 57-65.

23. Hall, N., M. Karras, J. D. Raine, J. M. Carlton, T. W. Kooij, M. Berriman, L. Florens, C. S. Janssen, A. Pain, G. K. Christophides, K. James, K. Rutherford, B. Harris, D. Harris, C. Churcher, M. A. Quail, D. Ormond, J. Doggett, H. E. Trueman, J. Mendoza, S. L. Bidwell, M. A. Rajandream, D. J. Carucci, J. R. Yates, 3rd, F. C. Kafatos, C. J. Janse, B. Barrell, C. M. Turner, A. P. Waters, and R. E. Sinden. 2005. A comprehensive survey of the Plasmodium life cycle by genomic, transcriptomic, and proteomic analyses. *Science (New York, N.Y.)* 307: 82-86.
24. Young, J. A., Q. L. Fivelman, P. L. Blair, P. de la Vega, K. G. Le Roch, Y. Zhou, D. J. Carucci, D. A. Baker, and E. A. Winzeler. 2005. The Plasmodium falciparum sexual development transcriptome: a microarray analysis using ontology-based pattern identification. *Mol Biochem Parasitol* 143: 67-79.
25. Kafsack, B. F., N. Rovira-Graells, T. G. Clark, C. Bancells, V. M. Crowley, S. G. Campino, A. E. Williams, L. G. Drought, D. P. Kwiatkowski, D. A. Baker, A. Cortes, and M. Llinas. 2014. A transcriptional switch underlies commitment to sexual development in malaria parasites. *Nature* 507: 248-252.
26. Yuda, M., S. Iwanaga, I. Kaneko, and T. Kato. 2015. Global transcriptional repression: An initial and essential step for Plasmodium sexual development. *Proc Natl Acad Sci U S A* 112: 12824-12829.
27. Brockelman, C. R. 1982. Conditions favoring gametocytogenesis in the continuous culture of Plasmodium falciparum. *The Journal of protozoology* 29: 454-458.
28. Graves, P. M., R. Carter, and K. M. McNeill. 1984. Gametocyte production in cloned lines of Plasmodium falciparum. *Am J Trop Med Hyg* 33: 1045-1050.
29. Williams, J. L. 1999. Stimulation of Plasmodium falciparum gametocytogenesis by conditioned medium from parasite cultures. *Am J Trop Med Hyg* 60: 7-13.
30. Dyer, M., and K. P. Day. 2003. Regulation of the rate of asexual growth and commitment to sexual development by diffusible factors from in vitro cultures of Plasmodium falciparum. *Am J Trop Med Hyg* 68: 403-409.
31. Fivelman, Q. L., L. McRobert, S. Sharp, C. J. Taylor, M. Saeed, C. A. Swales, C. J. Sutherland, and D. A. Baker. 2007. Improved synchronous production of Plasmodium falciparum gametocytes in vitro. *Mol Biochem Parasitol* 154: 119-123.
32. Couper, K. N., T. Barnes, J. C. Hafalla, V. Combes, B. Ryffel, T. Secher, G. E. Grau, E. M. Riley, and J. B. de Souza. 2010. Parasite-derived plasma microparticles contribute significantly to malaria infection-induced inflammation through potent macrophage stimulation. *PLoS Pathog* 6: e1000744.
33. Martin-Jaular, L., E. S. Nakayasu, M. Ferrer, I. C. Almeida, and H. A. Del Portillo. 2011. Exosomes from Plasmodium yoelii-infected reticulocytes protect mice from lethal infections. *PLoS One* 6: e26588.
34. Nantakomol, D., A. M. Dondorp, S. Krudsood, R. Udomsangpetch, K. Pattanapanyasat, V. Combes, G. E. Grau, N. J. White, P. Viriyavejakul, N. P. Day, and K. Chotivanich. 2011. Circulating red cell-derived microparticles in human malaria. *J Infect Dis* 203: 700-706.
35. Campos, F. M., B. S. Franklin, A. Teixeira-Carvalho, A. L. Filho, S. C. de Paula, C. J. Fontes, C. F. Brito, and L. H. Carvalho. 2010. Augmented plasma microparticles during acute Plasmodium vivax infection. *Malar J* 9: 327.
36. Faille, D., V. Combes, A. J. Mitchell, A. Fontaine, I. Juhan-Vague, M. C. Alessi, G. Chimini, T. Fusai, and G. E. Grau. 2009. Platelet microparticles: a new player in malaria parasite cytoadherence to human brain endothelium. *FASEB journal : official publication of the Federation of American Societies for Experimental Biology* 23: 3449-3458.
37. Pankoui Mfonkeu, J. B., I. Gouado, H. Fotso Kuate, O. Zambou, P. H. Amvam Zollo, G. E. Grau, and V. Combes. 2010. Elevated cell-specific microparticles are a biological marker for cerebral dysfunctions in human severe malaria. *PLoS One* 5: e13415.

38. Combes, V., N. Coltel, M. Alibert, M. van Eck, C. Raymond, I. Juhan-Vague, G. E. Grau, and G. Chimini. 2005. ABCA1 gene deletion protects against cerebral malaria: potential pathogenic role of microparticles in neuropathology. *Am J Pathol* 166: 295-302.
39. Marcilla, A., L. Martin-Jaular, M. Trelis, A. de Menezes-Neto, A. Osuna, D. Bernal, C. Fernandez-Becerra, I. C. Almeida, and H. A. Del Portillo. 2014. Extracellular vesicles in parasitic diseases. *Journal of extracellular vesicles* 3: 25040.
40. Johnstone, R. M., M. Adam, J. R. Hammond, L. Orr, and C. Turbide. 1987. Vesicle formation during reticulocyte maturation. Association of plasma membrane activities with released vesicles (exosomes). *The Journal of biological chemistry* 262: 9412-9420.
41. Yanez-Mo, M., P. R. Siljander, Z. Andreu, A. B. Zavec, F. E. Borras, E. I. Buzas, K. Buzas, E. Casal, F. Cappello, J. Carvalho, E. Colas, A. Cordeiro-da Silva, S. Fais, J. M. Falcon-Perez, I. M. Ghobrial, B. Giebel, M. Gimona, M. Graner, I. Gursel, M. Gursel, N. H. Heegaard, A. Hendrix, P. Kierulf, K. Kokubun, M. Kosanovic, V. Kralj-Iglic, E. M. Kramer-Albers, S. Laitinen, C. Lasser, T. Lener, E. Ligeti, A. Line, G. Lipps, A. Llorente, J. Lotvall, M. Mancek-Keber, A. Marcilla, M. Mittelbrunn, I. Nazarenko, E. N. Nolte-'t Hoen, T. A. Nyman, L. O'Driscoll, M. Olivan, C. Oliveira, E. Pallinger, H. A. Del Portillo, J. Reventos, M. Rigau, E. Rohde, M. Sammar, F. Sanchez-Madrid, N. Santarem, K. Schallmoser, M. S. Ostenfeld, W. Stoorvogel, R. Stukelj, S. G. Van der Grein, M. H. Vasconcelos, M. H. Wauben, and O. De Wever. 2015. Biological properties of extracellular vesicles and their physiological functions. *Journal of extracellular vesicles* 4: 27066.
42. Tauro, B. J., D. W. Greening, R. A. Mathias, S. Mathivanan, H. Ji, and R. J. Simpson. 2013. Two distinct populations of exosomes are released from LIM1863 colon carcinoma cell-derived organoids. *Molecular & cellular proteomics : MCP* 12: 587-598.
43. Pallet, N., I. Sirois, C. Bell, L. A. Hanafi, K. Hamelin, M. Dieude, C. Rondeau, P. Thibault, M. Desjardins, and M. J. Hebert. 2013. A comprehensive characterization of membrane vesicles released by autophagic human endothelial cells. *Proteomics* 13: 1108-1120.
44. Buzas, E. I., C. Gardiner, C. Lee, and Z. J. Smith. 2016. Single particle analysis: Methods for detection of platelet extracellular vesicles in suspension (excluding flow cytometry). *Platelets*: 1-7.
45. Vallhov, H., C. Gutzeit, S. M. Johansson, N. Nagy, M. Paul, Q. Li, S. Friend, T. C. George, E. Klein, A. Scheynius, and S. Gabrielsson. 2011. Exosomes containing glycoprotein 350 released by EBV-transformed B cells selectively target B cells through CD21 and block EBV infection in vitro. *J Immunol* 186: 73-82.
46. Zhang, Z. G., and M. Chopp. 2016. Exosomes in stroke pathogenesis and therapy. *J Clin Invest* 126: 1190-1197.
47. Jiang, X. C., and J. Q. Gao. 2017. Exosomes as novel bio-carriers for gene and drug delivery. *International journal of pharmaceutics* 521: 167-175.
48. Silverman, J. M., and N. E. Reiner. 2011. Exosomes and other microvesicles in infection biology: organelles with unanticipated phenotypes. *Cellular microbiology* 13: 1-9.
49. Pegtel, D. M., K. Cosmopoulos, D. A. Thorley-Lawson, M. A. van Eijndhoven, E. S. Hopmans, J. L. Lindenberg, T. D. de Gruijl, T. Wurdinger, and J. M. Middeldorp. 2010. Functional delivery of viral miRNAs via exosomes. *Proc Natl Acad Sci U S A* 107: 6328-6333.
50. Gong, J., R. Jaiswal, J. M. Mathys, V. Combes, G. E. Grau, and M. Bebawy. 2012. Microparticles and their emerging role in cancer multidrug resistance. *Cancer treatment reviews* 38: 226-234.
51. Tissot, J.-D., G. Canellini, O. Rubin, A. Angelillo-Scherrer, J. Delobel, M. Prudent, and N. Lion. 2013. Blood microvesicles: From proteomics to physiology. *Translational Proteomics* 1: 38-52.
52. Harisa, G. I., M. M. Badran, and F. K. Alanazi. 2017. Erythrocyte nanovesicles: Biogenesis, biological roles and therapeutic approach: Erythrocyte nanovesicles. *Saudi pharmaceutical journal : SPJ : the official publication of the Saudi Pharmaceutical Society* 25: 8-17.

53. Lutz, H. U., and A. Bogdanova. 2013. Mechanisms tagging senescent red blood cells for clearance in healthy humans. *Frontiers in physiology* 4: 387.
54. Föller, M., M. Huber Stephan, and F. Lang. 2008. Erythrocyte programmed cell death. *IUBMB Life* 60: 661-668.
55. Nguyen, D. B., T. B. Ly, M. C. Wesseling, M. Hittinger, A. Torge, A. Devitt, Y. Perrie, and I. Bernhardt. 2016. Characterization of Microvesicles Released from Human Red Blood Cells. *Cellular physiology and biochemistry : international journal of experimental cellular physiology, biochemistry, and pharmacology* 38: 1085-1099.
56. Kuo, W. P., J. C. Tigges, V. Toxavidis, and I. Ghiran. 2017. Red Blood Cells: A Source of Extracellular Vesicles. *Methods Mol Biol* 1660: 15-22.
57. Allan, D., and P. Thomas. 1981. Ca²⁺-induced biochemical changes in human erythrocytes and their relation to microvesiculation. *Biochemical Journal* 198: 433.
58. Lutz, H. U., S. C. Liu, and J. Palek. 1977. Release of spectrin-free vesicles from human erythrocytes during ATP depletion. I. Characterization of spectrin-free vesicles. *The Journal of cell biology* 73: 548-560.
59. Werre, J. M., F. L. Willekens, F. H. Bosch, L. D. de Haans, S. G. van der Vegt, A. G. van den Bos, and G. J. Bosman. 2004. The red cell revisited--matters of life and death. *Cellular and molecular biology (Noisy-le-Grand, France)* 50: 139-145.
60. Straat, M., M. E. van Hezel, A. Boing, A. Tuip-De Boer, N. Weber, R. Nieuwland, R. van Bruggen, and N. P. Juffermans. 2016. Monocyte-mediated activation of endothelial cells occurs only after binding to extracellular vesicles from red blood cell products, a process mediated by beta-integrin. *Transfusion* 56: 3012-3020.
61. Alaarg, A., R. Schiffelers, W. van Solinge, and R. Van Wijk. 2013. Red blood cell vesiculation in hereditary hemolytic anemia. *Frontiers in physiology* 4.
62. Camus, S. M., J. A. De Moraes, P. Bonnin, P. Abbyad, S. Le Jeune, F. Lionnet, L. Loufrani, L. Grimaud, J.-C. Lambry, D. Charue, L. Kiger, J.-M. Renard, C. Larroque, H. Le Clésiau, A. Tedgui, P. Bruneval, C. Barja-Fidalgo, A. Alexandrou, P.-L. Tharaux, C. M. Boulanger, and O. P. Blanc-Brude. 2015. Circulating cell membrane microparticles transfer heme to endothelial cells and trigger vasoocclusions in sickle cell disease. *Blood* 125: 3805.
63. Twu, O., N. de Miguel, G. Lustig, G. C. Stevens, A. A. Vashisht, J. A. Wohlschlegel, and P. J. Johnson. 2013. Trichomonas vaginalis exosomes deliver cargo to host cells and mediate hostratioparasite interactions. *PLoS Pathog* 9: e1003482.
64. Deolindo, P., I. Evans-Osses, and M. I. Ramirez. 2013. Microvesicles and exosomes as vehicles between protozoan and host cell communication. *Biochemical Society transactions* 41: 252-257.
65. Marcilla, A., M. Trelis, A. Cortes, J. Sotillo, F. Cantalapiedra, M. T. Minguez, M. L. Valero, M. M. Sanchez del Pino, C. Munoz-Antoli, R. Toledo, and D. Bernal. 2012. Extracellular vesicles from parasitic helminths contain specific excretory/secretory proteins and are internalized in intestinal host cells. *PLoS One* 7: e45974.
66. Buck, A. H., G. Coakley, F. Simbari, H. J. McSorley, J. F. Quintana, T. Le Bihan, S. Kumar, C. Abreu-Goodger, M. Lear, Y. Harcus, A. Ceroni, S. A. Babayan, M. Blaxter, A. Ivens, and R. M. Maizels. 2014. Exosomes secreted by nematode parasites transfer small RNAs to mammalian cells and modulate innate immunity. *Nat Commun* 5: 5488.
67. Coakley, G., R. M. Maizels, and A. H. Buck. 2015. Exosomes and Other Extracellular Vesicles: The New Communicators in Parasite Infections. *Trends Parasitol* 31: 477-489.
68. Geiger, A., C. Hirtz, T. Becue, E. Bellard, D. Centeno, D. Gargani, M. Rossignol, G. Cuny, and J. B. Peltier. 2010. Exocytosis and protein secretion in Trypanosoma. *BMC microbiology* 10: 20.
69. Goncalves, M. F., E. S. Umezawa, A. M. Katzin, W. de Souza, M. J. Alves, B. Zingales, and W. Colli. 1991. Trypanosoma cruzi: shedding of surface antigens as membrane vesicles. *Experimental parasitology* 72: 43-53.

70. Bayer-Santos, E., C. Aguilar-Bonavides, S. P. Rodrigues, E. M. Cordero, A. F. Marques, A. Varela-Ramirez, H. Choi, N. Yoshida, J. F. da Silveira, and I. C. Almeida. 2013. Proteomic analysis of Trypanosoma cruzi secretome: characterization of two populations of extracellular vesicles and soluble proteins. *Journal of proteome research* 12: 883-897.
71. Cestari, I., E. Ansa-Addo, P. Deolindo, J. M. Inal, and M. I. Ramirez. 2012. Trypanosoma cruzi immune evasion mediated by host cell-derived microvesicles. *J Immunol* 188: 1942-1952.
72. Halle, M., M. A. Gomez, M. Stuible, H. Shimizu, W. R. McMaster, M. Olivier, and M. L. Tremblay. 2009. The Leishmania surface protease GP63 cleaves multiple intracellular proteins and actively participates in p38 mitogen-activated protein kinase inactivation. *The Journal of biological chemistry* 284: 6893-6908.
73. Silverman, J. M., J. Clos, E. Horakova, A. Y. Wang, M. Wiesgigl, I. Kelly, M. A. Lynn, W. R. McMaster, L. J. Foster, M. K. Levings, and N. E. Reiner. 2010. Leishmania exosomes modulate innate and adaptive immune responses through effects on monocytes and dendritic cells. *J Immunol* 185: 5011-5022.
74. Mantel, P. Y., A. N. Hoang, I. Goldowitz, D. Potashnikova, B. Hamza, I. Vorobjev, I. Ghiran, M. Toner, D. Irimia, A. R. Ivanov, N. Barteneva, and M. Marti. 2013. Malaria-infected erythrocyte-derived microvesicles mediate cellular communication within the parasite population and with the host immune system. *Cell Host Microbe* 13: 521-534.
75. Regev-Rudzki, N., D. W. Wilson, T. G. Carvalho, X. Sisquella, B. M. Coleman, M. Rug, D. Bursac, F. Angrisano, M. Gee, A. F. Hill, J. Baum, and A. F. Cowman. 2013. Cell-cell communication between malaria-infected red blood cells via exosome-like vesicles. *Cell* 153: 1120-1133.
76. Sisquella, X., Y. Ofir-Birin, M. A. Pimentel, L. Cheng, P. Abou Karam, N. G. Sampaio, J. S. Penington, D. Connolly, T. Giladi, B. J. Scicluna, R. A. Sharples, A. Waltmann, D. Avni, E. Schwartz, L. Schofield, Z. Porat, D. S. Hansen, A. T. Papenfuss, E. M. Eriksson, M. Gerlic, A. F. Hill, A. G. Bowie, and N. Regev-Rudzki. 2017. Malaria parasite DNA-harbouring vesicles activate cytosolic immune sensors. *Nat Commun* 8: 1985.
77. Rubin, O., D. Crettaz, G. Canellini, J. D. Tissot, and N. Lion. 2008. Microparticles in stored red blood cells: an approach using flow cytometry and proteomic tools. *Vox sanguinis* 95: 288-297.
78. Abdi, A., L. Yu, D. Goulding, M. K. Rono, P. Bejon, J. Choudhary, and J. Rayner. 2017. Proteomic analysis of extracellular vesicles from a Plasmodium falciparum Kenyan clinical isolate defines a core parasite secretome. *Wellcome open research* 2: 50.
79. Antwi-Baffour, S., J. K. Adjei, F. Agyemang-Yeboah, M. Annani-Akollor, R. Kyeremeh, G. A. Asare, and B. Gyan. 2016. Proteomic analysis of microparticles isolated from malaria positive blood samples. *Proteome science* 15: 5.
80. Kamm, R. C., and A. G. Smith. 1972. Nucleic acid concentrations in normal human plasma. *Clinical chemistry* 18: 519-522.
81. Kosaka, N., Y. Yoshioka, K. Hagiwara, N. Tominaga, T. Katsuda, and T. Ochiya. 2013. Trash or Treasure: extracellular microRNAs and cell-to-cell communication. *Frontiers in genetics* 4: 173.
82. Valadi, H., K. Ekstrom, A. Bossios, M. Sjostrand, J. J. Lee, and J. O. Lotvall. 2007. Exosome-mediated transfer of mRNAs and microRNAs is a novel mechanism of genetic exchange between cells. *Nature cell biology* 9: 654-659.
83. Azzouzi, I., H. Moest, B. Wollscheid, M. Schmugge, J. J. M. Eekels, and O. Speer. 2015. Deep sequencing and proteomic analysis of the microRNA-induced silencing complex in human red blood cells. *Experimental hematology* 43: 382-392.
84. Taylor, D. D., and S. Shah. 2015. Methods of isolating extracellular vesicles impact down-stream analyses of their cargoes. *Methods (San Diego, Calif.)* 87: 3-10.
85. Xu, R., D. W. Greening, A. Rai, H. Ji, and R. J. Simpson. 2015. Highly-purified exosomes and shed microvesicles isolated from the human colon cancer cell line LIM1863 by sequential

centrifugal ultrafiltration are biochemically and functionally distinct. *Methods (San Diego, Calif.)* 87: 11-25.

86. Kowal, J., G. Arras, M. Colombo, M. Jouve, J. P. Morath, B. Primdal-Bengtson, F. Dingli, D. Loew, M. Tkach, and C. Théry. 2016. Proteomic comparison defines novel markers to characterize heterogeneous populations of extracellular vesicle subtypes. *Proceedings of the National Academy of Sciences* 113: E968.
87. Witwer, K. W., E. I. Buzas, L. T. Bemis, A. Bora, C. Lasser, J. Lotvall, E. N. Nolte-'t Hoen, M. G. Piper, S. Sivaraman, J. Skog, C. Thery, M. H. Wauben, and F. Hochberg. 2013. Standardization of sample collection, isolation and analysis methods in extracellular vesicle research. *Journal of extracellular vesicles* 2.
88. Cvjetkovic, A., J. Lotvall, and C. Lasser. 2014. The influence of rotor type and centrifugation time on the yield and purity of extracellular vesicles. *Journal of extracellular vesicles* 3.
89. Linares, R., S. Tan, C. Gounou, N. Arraud, and A. R. Brisson. 2015. High-speed centrifugation induces aggregation of extracellular vesicles. *Journal of extracellular vesicles* 4: 29509.
90. Momen-Heravi, F., L. Balaj, S. Alian, A. J. Trachtenberg, F. H. Hochberg, J. Skog, and W. P. Kuo. 2012. Impact of biofluid viscosity on size and sedimentation efficiency of the isolated microvesicles. *Frontiers in physiology* 3: 162.
91. Schluter, K., and D. Drenckhahn. 1986. Co-clustering of denatured hemoglobin with band 3: its role in binding of autoantibodies against band 3 to abnormal and aged erythrocytes. *Proc Natl Acad Sci U S A* 83: 6137-6141.
92. Low, P. S., S. M. Waugh, K. Zinke, and D. Drenckhahn. 1985. The role of hemoglobin denaturation and band 3 clustering in red blood cell aging. *Science (New York, N.Y.)* 227: 531-533.
93. Ciana, A., C. Achilli, and G. Minetti. 2017. *Spectrin and Other Membrane-Skeletal Components in Human Red Blood Cells of Different Age*.
94. Baker, D. A. 2010. Malaria gametocytogenesis. *Molecular and Biochemical Parasitology* 172: 57-65.
95. Linares, R., S. Tan, C. Gounou, N. Arraud, and A. R. Brisson. 2015. High-speed centrifugation induces aggregation of extracellular vesicles. *Journal of extracellular vesicles* 4: 10.3402/jev.v3404.29509.
96. Momen-Heravi, F., L. Balaj, S. Alian, J. Tigges, V. Toxavidis, M. Ericsson, R. J. Distel, A. R. Ivanov, J. Skog, and W. P. Kuo. 2012. Alternative methods for characterization of extracellular vesicles. *Frontiers in physiology* 3: 354.
97. Arraud, N., C. Gounou, R. Linares, and A. R. Brisson. 2015. A simple flow cytometry method improves the detection of phosphatidylserine-exposing extracellular vesicles. *Journal of thrombosis and haemostasis : JTH* 13: 237-247.
98. Wu, Y., W. Deng, and D. J. Klinke, 2nd. 2015. Exosomes: improved methods to characterize their morphology, RNA content, and surface protein biomarkers. *The Analyst* 140: 6631-6642.
99. Baj-Krzyworzeka, M., M. Majka, D. Pratico, J. Ratajczak, G. Vilaire, J. Kijowski, R. Reca, A. Janowska-Wieczorek, and M. Z. Ratajczak. 2002. Platelet-derived microparticles stimulate proliferation, survival, adhesion, and chemotaxis of hematopoietic cells. *Experimental hematology* 30: 450-459.
100. Bosch, S., L. de Beaurepaire, M. Allard, M. Mosser, C. Heichette, D. Chretien, D. Jegou, and J. M. Bach. 2016. Trehalose prevents aggregation of exosomes and cryodamage. *Sci Rep* 6: 36162.
101. Zhou, H., P. S. Yuen, T. Pisitkun, P. A. Gonzales, H. Yasuda, J. W. Dear, P. Gross, M. A. Knepper, and R. A. Star. 2006. Collection, storage, preservation, and normalization of human urinary exosomes for biomarker discovery. *Kidney international* 69: 1471-1476.
102. Beranger, F., C. Crozet, A. Goldsborough, and S. Lehmann. 2008. Trehalose impairs aggregation of PrPSc molecules and protects prion-infected cells against oxidative damage. *Biochemical and biophysical research communications* 374: 44-48.

103. Jain, N. K., and I. Roy. 2009. Effect of trehalose on protein structure. *Protein science : a publication of the Protein Society* 18: 24-36.
104. Jayachandran, M., V. M. Miller, J. A. Heit, and W. G. Owen. 2012. Methodology for isolation, identification and characterization of microvesicles in peripheral blood. *Journal of immunological methods* 375: 207-214.
105. Kriebardis, A. G., M. H. Antonelou, K. E. Stamoulis, E. Economou-Petersen, L. H. Margaritis, and I. S. Papassideri. 2007. Storage-dependent remodeling of the red blood cell membrane is associated with increased immunoglobulin G binding, lipid raft rearrangement, and caspase activation. *Transfusion* 47: 1212-1220.
106. Bosman, G. J., and M. M. Kay. 1988. Erythrocyte aging: a comparison of model systems for simulating cellular aging in vitro. *Blood cells* 14: 19-46.
107. Nolan, J. P. 2015. Flow Cytometry of Extracellular Vesicles: Potential, Pitfalls, and Prospects. *Current protocols in cytometry* 73: 13.14.11-16.
108. Winograd, E., J. G. Prudhomme, and I. W. Sherman. 2005. Band 3 clustering promotes the exposure of neoantigens in Plasmodium falciparum-infected erythrocytes. *Mol Biochem Parasitol* 142: 98-105.
109. Kesely, K. R., A. Pantaleo, F. M. Turrini, P. Olupot-Olupot, and P. S. Low. 2016. Inhibition of an Erythrocyte Tyrosine Kinase with Imatinib Prevents Plasmodium falciparum Egress and Terminates Parasitemia. *PLoS One* 11: e0164895.
110. Willekens, F. L., J. M. Werre, Y. A. Groenen-Dopp, B. Roerdinkholder-Stoelwinder, B. de Pauw, and G. J. Bosman. 2008. Erythrocyte vesiculation: a self-protective mechanism? *British journal of haematology* 141: 549-556.
111. van der Vlist, E. J., E. N. Nolte-'t Hoen, W. Stoorvogel, G. J. Arkesteijn, and M. H. Wauben. 2012. Fluorescent labeling of nano-sized vesicles released by cells and subsequent quantitative and qualitative analysis by high-resolution flow cytometry. *Nat Protoc* 7: 1311-1326.
112. Franquesa, M., M. J. Hoogduijn, E. Ripoll, F. Luk, M. Salih, M. G. Betjes, J. Torras, C. C. Baan, J. M. Grinyo, and A. M. Merino. 2014. Update on controls for isolation and quantification methodology of extracellular vesicles derived from adipose tissue mesenchymal stem cells. *Front Immunol* 5: 525.
113. Arraud, N., C. Gounou, D. Turpin, and A. R. Brisson. 2016. Fluorescence triggering: A general strategy for enumerating and phenotyping extracellular vesicles by flow cytometry. *Cytometry. Part A : the journal of the International Society for Analytical Cytology* 89: 184-195.
114. de Rond, L., E. van der Pol, C. M. Hau, Z. Varga, A. Sturk, T. G. van Leeuwen, R. Nieuwland, and F. A. W. Coumans. 2018. Comparison of Generic Fluorescent Markers for Detection of Extracellular Vesicles by Flow Cytometry. *Clinical chemistry* 64: 680-689.
115. Erdbrugger, U., C. K. Rudy, M. E. Etter, K. A. Dryden, M. Yeager, A. L. Klibanov, and J. Lannigan. 2014. Imaging flow cytometry elucidates limitations of microparticle analysis by conventional flow cytometry. *Cytometry. Part A : the journal of the International Society for Analytical Cytology* 85: 756-770.
116. Nolte-'t Hoen, E. N., E. J. van der Vlist, M. Aalberts, H. C. Mertens, B. J. Bosch, W. Bartelink, E. Mastrobattista, E. V. van Gaal, W. Stoorvogel, G. J. Arkesteijn, and M. H. Wauben. 2012. Quantitative and qualitative flow cytometric analysis of nanosized cell-derived membrane vesicles. *Nanomedicine : nanotechnology, biology, and medicine* 8: 712-720.
117. Ter-Ovanesyan, D., E. J. K. Kowal, A. Regev, G. M. Church, and E. Cocucci. 2017. Imaging of Isolated Extracellular Vesicles Using Fluorescence Microscopy. In *Extracellular Vesicles: Methods and Protocols*. W. P. Kuo, and S. Jia, eds. Springer New York, New York, NY. 233-241.
118. Almizraq, R. J., J. Seghatchian, J. L. Holovati, and J. P. Acker. 2017. Extracellular vesicle characteristics in stored red blood cell concentrates are influenced by the method of detection. *Transfusion and Apheresis Science* 56: 254-260.

119. Pugholm, L. H., #xe6, R. k, #xf8, E. K. L. ndergaard, A. L. S. Revenfeld, #xf8, M. M. rgensen, #xf8, ller, and K. Varming. 2016. Phenotyping of Leukocytes and Leukocyte-Derived Extracellular Vesicles. *Journal of Immunology Research* 2016: 12.
120. Banerjee, R., J. Liu, W. Beatty, L. Pelosof, M. Klemba, and D. E. Goldberg. 2002. Four plasmepsins are active in the Plasmodium falciparum food vacuole, including a protease with an active-site histidine. *Proceedings of the National Academy of Sciences* 99: 990.
121. Shonhai, A. 2010. Plasmodial heat shock proteins: targets for chemotherapy. *FEMS Immunology & Medical Microbiology* 58: 61-74.
122. Mentkowski, K. I., J. D. Snitzer, S. Rusnak, and J. K. Lang. 2018. Therapeutic Potential of Engineered Extracellular Vesicles. *The AAPS Journal* 20: 50.
123. Mantel, P. Y., D. Hjelmqvist, M. Walch, S. Kharoubi-Hess, S. Nilsson, D. Ravel, M. Ribeiro, C. Gruring, S. Ma, P. Padmanabhan, A. Trachtenberg, J. Ankarklev, N. M. Brancucci, C. Huttenhower, M. T. Duraisingh, I. Ghiran, W. P. Kuo, L. Filgueira, R. Martinelli, and M. Marti. 2016. Infected erythrocyte-derived extracellular vesicles alter vascular function via regulatory Ago2-miRNA complexes in malaria. *Nat Commun* 7: 12727.
124. Marie, D., C. P. D. Brussaard, R. Thyrhaug, G. Bratbak, and D. Vaulot. 1999. Enumeration of marine viruses in culture and natural samples by flow cytometry. *Applied and environmental microbiology* 65: 45-52.
125. Beckman Coulter Inc: CytoFLEX.
126. Arraud, N., R. Linares, S. Tan, C. Gounou, J. M. Pasquet, S. Mornet, and A. R. Brisson. 2014. Extracellular vesicles from blood plasma: determination of their morphology, size, phenotype and concentration. *Journal of thrombosis and haemostasis : JTH* 12: 614-627.
127. Xiong, Z., T. B. Oriss, J. P. Cavaretta, M. R. Rosengart, and J. S. Lee. 2012. Red cell microparticle enumeration: validation of a flow cytometric approach. *Vox sanguinis* 103: 42-48.
128. Dragovic, R. A., C. Gardiner, A. S. Brooks, D. S. Tannetta, D. J. Ferguson, P. Hole, B. Carr, C. W. Redman, A. L. Harris, P. J. Dobson, P. Harrison, and I. L. Sargent. 2011. Sizing and phenotyping of cellular vesicles using Nanoparticle Tracking Analysis. *Nanomedicine : nanotechnology, biology, and medicine* 7: 780-788.
129. Kastelowitz, N., and H. Yin. 2014. Exosomes and microvesicles: identification and targeting by particle size and lipid chemical probes. *Chembiochem : a European journal of chemical biology* 15: 923-928.
130. Jy, W., L. L. Horstman, J. J. Jimenez, Y. S. Ahn, E. Biro, R. Nieuwland, A. Sturk, F. Dignat-George, F. Sabatier, L. Camoin-Jau, J. Sampol, B. Hugel, F. Zobairi, J. M. Freyssinet, S. Nomura, A. S. Shet, N. S. Key, and R. P. Hebbel. 2004. Measuring circulating cell-derived microparticles. *Journal of thrombosis and haemostasis : JTH* 2: 1842-1851.
131. Ofir-Birin, Y., P. Abou Karam, A. Rudik, T. Giladi, Z. Porat, and N. Regev-Rudzki. 2018. Monitoring Extracellular Vesicle Cargo Active Uptake by Imaging Flow Cytometry. *Front Immunol* 9: 1011.
132. Pasini, E. M., M. Kirkegaard, P. Mortensen, H. U. Lutz, A. W. Thomas, and M. Mann. 2006. In-depth analysis of the membrane and cytosolic proteome of red blood cells. *Blood* 108: 791.
133. Buschmann, D., B. Kirchner, S. Hermann, M. Marte, C. Wurmser, F. Brandes, S. Kotschote, M. Bonin, O. K. Steinlein, M. W. Pfaffl, G. Schelling, and M. Reithmair. 2018. Evaluation of serum extracellular vesicle isolation methods for profiling miRNAs by next-generation sequencing. *Journal of extracellular vesicles* 7: 1481321.
134. Hodge, K., S. T. Have, L. Hutton, and A. I. Lamond. 2013. Cleaning up the masses: exclusion lists to reduce contamination with HPLC-MS/MS. *Journal of proteomics* 88: 92-103.
135. Pietrowska, M., S. Funk, M. Gawin, L. Marczak, A. Abramowicz, P. Widlak, and T. Whiteside. 2017. Isolation of Exosomes for the Purpose of Protein Cargo Analysis with the Use of Mass Spectrometry. *Methods Mol Biol* 1654: 291-307.

136. Raposo, G., and W. Stoorvogel. 2013. Extracellular vesicles: exosomes, microvesicles, and friends. *The Journal of cell biology* 200: 373-383.